CHARACTERIZING PROTEIN DYNAMICS OF PROTEIN-LIGAND INTERACTIONS BY HYDROGEN-DEUTERIUM EXCHANGE MASS SPECTROMETRY

DIANA RESETCA

A THESIS SUBMITTED TO
THE FACULTY OF GRADUATE STUDIES
IN PARTIAL FULFILLMENT OF THE REQUIREMENTS
FOR THE DEGREE OF
MASTER OF SCIENCE

GRADUATE PROGRAM IN CHEMISTRY
YORK UNIVERSITY
TORONTO, ONTARIO

August 2014

Abstract

The study of protein-ligand and protein-protein interactions is of paramount importance to the understanding of their biological function. Whereas this area of research has been largely dominated by conventional structural biology techniques, such as NMR and X-ray crystallography, an emerging methodology that relies on the implementation of hydrogen deuterium exchange (HDX) powered by MS-based analysis holds the potential to greatly expand on our ability to probe the protein dynamics of fundamental biological processes. In this work, the entire HDX workflow for site-specific analysis of protein dynamics was integrated onto a concerted microfluidic device and applied to the interrogation of the dynamic changes that accompany protein-ligand interactions. This application is described for two model systems: the binding of glutathione (GSH) by Glutathione-S-Transferase (GST), and the binding of three novel salicylic acid-based inhibitors of Signal Transducer and Activator of Transcription 3 (STAT3) to its SH2 domain. This work extends the application of time-resolved electrospray ionization mass spectrometry (TRESI-MS) HDX to the study of protein ligand interaction dynamics and ligand-binding site mapping.

Acknowledgments

I would like to thank my mentor Dr. Derek J. Wilson for his valuable advice, thorough feedback and ample opportunity to thrive as a research scientist in his laboratory! Thank you for believing in me and for supporting me above and beyond the scope of my projects. I find the expertise and knowledge I mastered while working under your supervision to be exceptional and indispensible.

I would also like to thank our collaborators Dr. Patrick T. Gunning and Sina Haftchenary for developing and providing the STAT3 inhibitors. I would like to also thank Dr. Rob C. Laister for generously providing the STAT3 cDNA.

I would like to thank my graduate committee, Dr. Gerald F. Audette and Dr. Mark A. Bayfield, for all the valuable comments, suggestions, and encouragement they provided throughout my training.

I would like acknowledge the help of all the past and present members of the Wilson Group with whom I have the pleasure of working along with: Dr. Tamanna Rob, Dr. Yanfang Liang, Peter Liuni, Shaolong Zhu, John van Nostrand, Preet Kamal, Crisitna Lento, and Nick Zinck. I would like to thank you for your help and support with all the aspects of the MS world during the course of my studies. You helped create a truly vibrant and dynamic environment with a lot of fruitful discussions and unforgettable memories.

Finally, I would like to thank my parents and my fiancé Anton Neschadim for their unconditional love, support, patience and encouragement to persevere!

List of Publications

1. **Resetca, D**. and D. J. Wilson (2013). "Characterizing rapid, activity-linked conformational transitions in proteins via sub-second hydrogen deuterium exchange mass spectrometry." FEBS J 280(22): 5616-5625.

2. Eiring, A.M., Page, B.G., Kraft, I.L., Mason, C.C., Vellore, N.M., R**esetca, D.**, Zabriskie, M.S., Zhang, T.Y., Khorashad, J.S., Engar, A.J., Reynolds, K.R., Anderson, D.J., Senina, A., Pomicter, A.D., Arpin, C.C., Ahmad, S., Heaton, W.L., Tantravahi, S., Moriggl, R., Wilson, D.J., Baron, R., O'Hare, T., Gunning, P.T., and Deininger, M.W. (2014). "Combined STAT3 and BCR-ABL1 Inhibition Induces Synthetic Lethality in Therapy-Resistant Chronic Myeloid Leukemia" Leukemia. DIO: 10.1038/leu.2014.245.

Table of Contents

Abbreviations

ATP – Adenosine Triphosphate
Cbp – Csk-Binding Protein
CD – Circular Dichroism
CID – Collision Induced Dissociation
CNS – Central Nervous System
COSY – Correlation Spectroscopy
CPMG – Carr-Purcell-Meiboom-Gill
Csk – C-terminal Src
Da – Dalton
DAHP – 3-Deoxy-D-
-Arabinoheptulosonate 7-
-Phosphate Synthase
DMSO – Dimethyl Sulfoxide
DNA – Deoxyribonucleic Acid
DSSP – Dictionary of Protein
Secondary Structure
ECD – Electron Capture Dissociation
ESI – Electrospray Ionization
ETD – Electron Transfer Dissociation
FRET – Förster Resonance
Energy Transfer
GSH – Glutathione
GSK3β - Glycogen Synthase
Kinase 3β
GST – Glutathione-S-Transferase
HDX – Hydrogen Deuterium Exchange
HPLC – High Performance
Liquid Chromatography
HTS – High-throughput Screen
IDP – Intrinsically Disordered Protein
IMS – Ion-Mobility Spectrometry
kDa – Kilo Dalton
LC – Liquid Chromatography
MALDI – Matrix-Assisted Laser
Desorption Ionization
MBP – Maltose-Binding Protein
MDa – Mega Dalton
MS – Mass Spectrometry
MWCO – Molecular Weight Cut-Off
NMR – Nuclear Magnetic Resonance
NOE – Nuclear Overhauser Effect
NOESY – Nuclear Overhauser
Effect Spectroscopy
PDB – Protein Data Bank
PDLA – Poly-DL-Alanine
PMMA – Polymethyl Methacrylate
pNPA – para-Nitrophenyl Acetate
PTFE – Polytetrafluoroethylene
Q-TOF – Quadrupole Time of Flight
QSAR – Quantitative Structure-Activity
Relationship
SAR – Structure Activity Relationship
SDS-PAGE – Sodium Dodecyl
Sulfate Polyacrylamide Gel
Electrophoresis
SEM – Standard Error of the Mean
SH2 – Src Homology 2
STAT3 – Signal Transducer and
Activator of transcription 3
TRESI-MS – Time-Resolved
Electrospray Ionization
Mass Spectrometry
TROSY – Transverse Relaxation
Optimized Spectroscopy
UV – Ultra Violet

List of Tables

List of Figures

Chapter 1

1 Introduction

A version of this chapter was published in FEBS Journal:

Resetca, D. and D. J. Wilson (2013). "Characterizing rapid, activity-linked conformational transitions in proteins via sub-second hydrogen deuterium exchange mass spectrometry." FEBS J 280(22): 5616-5625.

1.1 Summary

This review outlines the application of Time-Resolved ElectroSpray Ionization Mass Spectrometry (TRESI-MS) and hydrogen-deuterium exchange (HDX) to study rapid, activity-linked conformational transitions in proteins. The method is implemented on a microfluidic chip, which incorporates a capillary mixer for sub-second HDX labeling, a microreactor for rapid protein digestion, and on-chip electrospray. By combining short HDX labeling pulses with rapid digestion, this approach can provide a detailed characterization of the structural transitions that occur during protein folding, ligand binding, post-translational modification, and catalytic turnover in enzymes. This broad spectrum of applications in areas largely inaccessible to conventional techniques makes microfluidics-enabled TRESI-MS/HDX a unique and powerful approach for investigating the fundamental dynamic basis of protein function.

1.2 Characterizing Protein Dynamics

1.2.1 Current Analytical Techniques for the Characterization of Protein Dynamics

Molecular dynamics play a fundamental role in ensuring proper protein function, from protein folding to enzyme catalysis to the more complex protein-protein interactions. The study of protein conformational ensembles, and how they evolve and shift upon interaction with other molecules, has helped rationalize the concepts of allosteric regulation, induced-fit binding and conformer selection. The examination of protein dynamics has contributed to the understanding of many aspects of basic protein function that cannot be explained using static, ground state representations of proteins. The latter merely capture the start and end results of a process, rather than the complex pathway of a series of fluctuations from equilibrium and conformer selection steps that the protein navigates through. Observation of protein dynamic changes necessitates the use of bioanalytical techniques that are capable of capturing and dissecting the broadest range of conformational transitions across the entire energetic landscape accessible to the protein. Thus, the most robust technique should permit the probing of large conformational ensembles of both stable, ground states, as well as sparsely populated, excited and transition states, with high structural resolution. One rapidly advancing technique that has the potential to greatly satisfy these criteria is structural mass spectrometry.

Conventional structural biology techniques, like X-ray crystallography and structural NMR, have greatly advanced our understanding of protein structures, protein

interactions and catalysis using static representations of typically low energy state conformers, but are generally ill-suited to the study of transient intermediates and excited species (1-4). Analyzing short-lived intermediates of proteins as they transition between states, whether in protein folding, enzyme catalysis or protein-protein interactions, has proven a major challenge in analytical biochemistry. As a result, there is a substantial gap in our understanding of the dynamic processes that underlie protein-mediated biological function in the cell.

The occurrence of short-lived protein intermediates has been demonstrated by a variety of spectroscopic methods, including circular dichroism (CD) (5,6), fluorescence-based assays (7), and NMR spectroscopy (8,9). These methods have been widely used for the interrogation of changes in protein dynamics, but each approach has a restricted applicability in conducting kinetic experiments that can provide structural and/or mechanistic insights.

Parameters derived through the various analytical techniques have also enabled the application of a vast number of computational tools for the theoretical study of protein dynamics (10). However, current *in silico* simulations are still greatly limited by processing power, where the accuracy of predictions trade off with the complexity of the models and the built-in parameters (11,12).

1.2.2 Analysis of Protein Dynamics by CD

Circular dichroism is an analytical technique with some utility in the study of protein secondary structure composition. Optically active chromophores, such as peptide bonds, posses an intrinsic ability to differentially absorb left and right circularly polarized light when placed in the plane polarised environment. Thus, regular secondary structure

features such as α-helices and β-sheets can be evaluated and differentiated in the far UV region (180-240 nm) as a characteristic elliptical polarization. CD spectroscopy is a useful method for monitoring protein unfolding, or melting, allowing one to discern changes in secondary and tertiary structures of proteins, and, in certain cases, even for examining protein-protein interactions (13,14). However, quantitative structural interpretation of the CD spectra is at best limited to an 'aggregate' measurement of secondary structure and is reliant on calibration to known structures. Additionally, CD spectra yield no site-specific information of protein secondary structure and lack the ability to distinguish multiple, sparsely populated conformational states.

1.2.3 Analysis of Protein Dynamics by FRET

Fluorescence-based methods, particularly Forster Resonance Energy Transfer (FRET), have been widely applied in time-resolved studies of enzyme catalysis and protein-ligand interactions and offer a large sensitivity range (15). The FRET technique typically involves two fluorophores or a fluorophore and quencher, each tagged to a separate analyte. Excitation of the first fluorophore results in a fluorescence emission in the excitation range of the second fluorophore, resulting in its bystander excitation, or, in the case of a quencher, the suppression of fluorescent signal. The efficiency of this energy transfer is inversely proportional to the distance between the two fluorophores. Therefore, this technique is highly applicable to the probing of protein-protein interactions. However, FRET-based experiments provide limited structural insights, usually in the form of single inter-probe distance measurements, whose biological significance is somewhat reduced by the presence of the FRET probes themselves in the protein (16).

1.2.4 Analysis of Dynamics by NMR

From amongst the various spectroscopic techniques applied in analytical biochemistry, NMR spectroscopy has made the largest contribution to studies of protein structure in solution. In application to protein, NMR takes advantage of the presence of paramagnetic nuclei with angular spin momentum in biological macromolecules. In high, static magnetic field, spin energy levels of such nuclei tend to split due to the Zeeman's effect (17). In nuclei with a spin of I = ½, the splitting results in equally spaced energy levels with two possible values for the magnetic quantum number (m = ½ or -½) (18). Application of electromagnetic radiation in the radio frequency range can drive nuclear transitions between the two energy levels. Each nucleus will absorb and resonate at a specific frequency as a function of the local environment. In pulsed NMR, applied as part of the broadband radio frequency pulse, such radio frequency excites the corresponding nuclei to populate the highest energy spin level resulting in the inversion of the nuclear spin. The nuclear magnetization then relaxes back to the ground state, precessing around the magnetic field vector at a specific precession frequency, known as the Larmor frequency, which can be detected by the radio frequency receiver coil of the instrument (17). The Larmor frequency for each nucleus is strongly influenced by the surrounding environment, specifically, shielding by localized magnetic fields of nearby electrons. The diverse chemical environment of each nucleus will cause the frequency at which it resonates to be slightly different, reflected as a shift in the peaks of the NMR spectrum, known as a chemical shift δ (17). This quantity is relative and is independent of the strength of the static magnetic field of the instrument, and different atomic nuclei are influenced by their chemical environment to varying extents. In biological macromolecules, ^{1}H, ^{13}C, and ^{15}N nuclei are readily available to analysis by

NMR, and are either highly abundant naturally or can be enriched for in recombinantly expressed molecules. The relaxation times of the various nuclei are simultaneously detected as a signal image current by the NMR receiver coil in the time domain, which can be Fourier transformed into the frequency domain. The Fourier transformed NMR spectrum enables resolving the individual signals corresponding to each relaxing nucleus. An important characteristic of NMR spectra, which aids in the interpretation of the structure of the analyte molecule, is that the area under curve of each peak is proportional to the number of the nuclei resonating at the same frequency. Another NMR phenomena that is crucial in aiding the interpretation of the analyte molecule structure is scalar coupling between nuclei that are covalently bonded and separated by up to 4 covalent bonds, also known as J-coupling. This coupling effectively results in a splitting of the energy level populated by a particular nucleus, which ultimately translates into additional chemical shifts (J-constant in Hz) and manifests as a multiplet of peaks on the NMR spectrum. The resulting, complex multiplets can be interpreted for each nucleus with respect to its covalent bond assignment. Yet another phenomena, known as the Nuclear Overhauser Effect (NOE), which is a form of dipolar coupling taking place between nuclei that are very close spatially (less than a few Å), is invaluable in interpreting distance constraints in structural analysis of proteins. The NOE NMR experiment, which can be performed in two dimensions, permits the determination of a distance constraint matrix for each excitable nucleus. The introduction of variable delay into the complex pulse sequence also referred to as evolution time permits the generation of two-dimensional spectra, which greatly simplifies the interpretation of highly complex molecular structures compared to a one-dimensional experiment. Most popular multi-dimensional NMR experiments are correlation spectroscopy (COSY),

which relies on scalar J-couplings, and nuclear Overhauser effect spectroscopy (NOESY), which relies on dipolar couplings, with the latter particularly useful for the interpretation of distance constraints in protein structures. Finally, additional significant structural information helpful in the interpretation of protein structures can be derived form heteronuclear NMR experiments, whereby ^{1}H scalar coupling to the ^{13}C and ^{15}N nuclei could be detected and interpreted with respect to structural distance constraints (17,18).

Some of the practical advantages of NMR are that the experiments can be conducted on native proteins in solution and are non-destructive to the analyte. This facilitates the use of NMR for the study of protein dynamics under physiological conditions. Importantly, hydrogen deuterium exchange (HDX) experiments, described in detail in the subsequent sections, can also be analyzed by NMR owing to the fact that deuterium (^{2}H) nuclei are not visible to NMR (17). However, applications of NMR in kinetic studies of transient protein states are generally restricted by the relative insensitivity of the technique (requiring mid- to high-μM concentrations) and the size limit of proteins that can be analyzed (typically, subunit size of less than 70kDa with the use of TROSY) (19). Conducting time-resolved kinetic experiments in real-time with the application of NMR on the sub-second timescale is practically challenging, requiring complex pulse sequences with greatly diminished sensitivity. One methodology that has been developed for real-time NMR studies relies on photo-labile “caged” compounds (20), but the experimental set-up is complex, requires the design and synthesis of “caged” ligands, making the overall approach far from universally applicable.

Recent developments in biophysical NMR methods have allowed some insight into millisecond-timescale conformational dynamics of proteins. In particular, Carr-Purcell-Meiboom-Gill (CPMG) relaxation dispersion allows for the site-specific characterization of the kinetic and thermodynamic properties of nuclei on the microsecond-millisecond timescale as they sample different environments during conformational exchange (21). However, continuous presence of the species/conformational states analyzed throughout the time-window of the relaxation dispersion experiment is needed, and these experiments will thus be typically limited to systems at equilibrium (22). Furthermore, systems exchanging between more than two states are difficult to characterize by CPMG experiments (23).

1.3 Analysis of Protein Dynamics by Mass Spectrometry

1.3.1 Label-Free Analysis of Protein Structure by Mass Spectrometry

The intrinsic analytic capabilities of mass spectrometry are of limited utility on their own in the study of protein structure and dynamics, but can be greatly expanded by a number of complementary methods for probing protein dynamics. One direct method is based on the propensity of more unfolded proteins to acquire more charges in the process of electrospray ionization (24). The resulting distribution of multiply charged ions in the mass spectrum will reflect the extent of protein unfolding, but this information is also limited to the overall three-dimensional packing of the protein.

Ion mobility-mass spectrometry is also emerging as a label-free technique for structural analysis in the gas phase. In this experiment, a weak electrostatic field is applied across the ion drift space, influencing macromolecular ions to separate based on their drift velocities (25). Ions sample different possible geometric orientations as they proceed

through the drift tube, and, in the presence of a neutral background gas, macromolecular ions possessing different sizes and geometries pass through the drift region at different velocities. The results are collisional cross sections that vary with the three-dimensional organization of the ions (26). Therefore, ion mobility spectrometry can provide information on the overall three-dimensional packing of the protein and can easily differentiate between folded and loosely-folded states, but provides no true structural resolution.

1.3.2 Hydrogen-Deuterium Exchange (HDX) for the Analysis of Protein Dynamics

Mass spectrometry with HDX has recently emerged as a powerful tool in structural biology, especially in the context of high-throughput structural proteomics (27). Mass spectrometry offers the capability to conduct millisecond-timescale measurements (28), in addition to high sensitivity, and the potential for direct in-line coupling to a variety of liquid chromatography (LC) and microfluidic devices (29), allowing kinetic experiments to be implemented with ease (30,31). Electrospray ionization (ESI) and matrix-assisted laser desorption/ionization (MALDI) methods enable the analysis of whole proteins of any size, and protein complexes larger than 1 MDa have been successfully analyzed (32,33). HDX experiments in conjunction with MS-based analysis permit simultaneous structural and kinetic analyses, enabling complex protein energy landscapes to be mapped in protein folding and enzyme catalysis (34-36).

The advance that significantly enhanced MS-based analysis of protein dynamics is isotope incorporation by means of HDX (37). This approach has been extensively reviewed (e.g., (38)) and is briefly described below. HDX relies on the ability of hydrogen atoms to undergo exchange with deuterons from solvent (or surrounding gas),

resulting in the incorporation of deuterium at accessible sites of the macromolecule. In solution, HDX is base-catalyzed (though general acid catalysis becomes dominant at pH < 2.6). The rate of HDX at individual sites is dependent on a multitude of factors, including the character of the functional group, accessibility to the exchange reagent, degree of hydrogen bonding of the labile hydrogen, and the nature of deuterium donor that dictates the exchange mechanism (i.e., salt bridge, tautomer, onium ion, flip-flop, and relay mechanisms) (39).

Hydrogen exchange takes place from a hydrogen donor (A-H) to a hydrogen acceptor (B). In biological macromolecules, such as proteins, hydrogen exchange is either driven by strong base OH^- and strong acid $H3O^+$ catalysis. The mechanism of the exchange reaction, as depicted in Fig. 1A, occurs *via* the formation of a collision complex followed by rapid equilibration of the proton across the hydrogen bridge, followed by the dissociation of the new hydrogen-bonded complex (40). The direction of the proton transfer reaction is from a strong acid to a weaker acid, and is determined by the rate constant of the exchange, which is governed by the diffusion limit (k_1). Alternatively, an exchange reaction from a weak acid to a strong base occurs only in a small fraction of productive collisions, is influenced by the environment of the backbone amides in the polyamide chain, and is governed by the exchange rate constant $k = k_1(10^{\Delta pK}/(10^{\Delta pK}+1))$, where k1 is the diffusion-limited collision rate constant and ΔpK is the difference between the pK of the acceptor and the donor (41). Amide hydrogens in the peptide backbone can undergo slower exchange than the polar hydrogens of the side chains or N- and C- termini, which exchange easily. The pK parameter is the rate-determining step in the exchange reaction of backbone amides, which have a high

deprotonation pK value of ~18, much higher than the pK of side-chain exchangeable protons, which is typically less than 13 and is highly reactive with the hydroxyl base at neutral pH. Thus, owing to their slower rate of exchange, backbone amide hydrogens are exceedingly good probes of secondary structure of proteins and are present in every amino acid, but proline (42).

While backbone amide hydrogen exchange can proceed by several mechanisms, under physiological conditions, amide hydrogen exchange proceeds *via* base catalysis (Fig. 1B) as proposed by Berger and coworkers in 1959 based on the proteolysis and ionization results of N-methylacetamide (43). The first step of the exchange reaction is the abstraction of the amide proton by the deuterium hydroxide ion and formation of an imidate anion. Reprotonation of the imidate anion by a deuteron subsequently leads to the completion of exchange transfer reaction. This direct mechanism of amide proton exchange is highly influenced by the particular environment of the peptidic bond in the protein structure. A number of factors affect hydrogen deuterium rate of exchange, with the pH being of paramount importance. Studies of hydrogen deuterium exchange in random coil-like poly-DL-alanine peptide (PDLA) revealed a quantitative dependence of the amide proton exchange rate on the pH (44). Bai *et al*. established the contributions of each of the components on the overall rate of exchange in PDLA in acidic and basic solutions and concluded that the rate of exchange was proportional to the concentration of the acid and base catalysts (45). The overall rate of exchange of free amide in solution, k_{ex}, can be summarized as a sum of the contributions from water- (k_{water}), acid- (k_{H3O}^{+}), and base- (k_{OH}^{-}) catalyzed rate constants ($k_{ex} = k_{water} + k_{H3O}^{+} [H_3O^{+}] + k_{OH}^{-} [OH^{-}]$ or $\log (k_{ex}) = \log (k_{water} + k_{H3O}^{+} [H_3O^{+}] + k_{OH}^{-} [OH^{-}])$) (45-47).

A

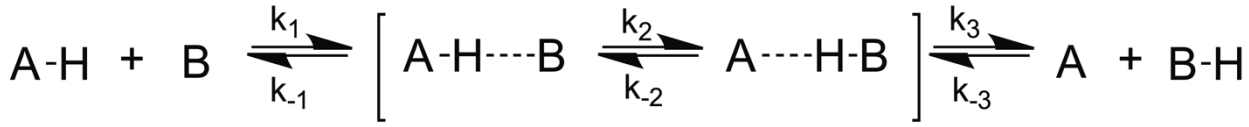

B

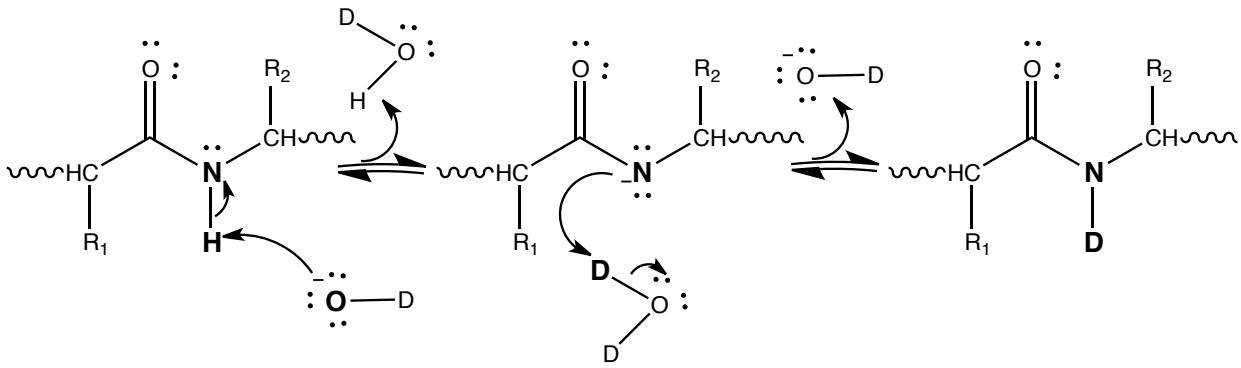

Fig. 1 The Mechanism of Hydrogen Exchange in Proteins. A) Proton transfer in the hydrogen exchange reaction between a hydrogen bond donor (AH) and an acceptor (B). A collision between a hydrogen bond donor and acceptor induces the formation of a hydrogen bridge, governed by the k_1 rate constant (a diffusion-limited process). Equilibration of the proton within the hydrogen bridge is dependent on the rate constant k_2. The release of the newly formed hydrogen complex is dependent on the rate constant k_3. B) Base-catalyzed mechanism of hydrogen deuterium exchange of amide hydrogens in protein backbone. A deuterium hydroxide base attacks the covalently attached hydrogen at the peptide amide position, which leads to the formation of an imidate anion and the subsequent reprotonation of the imidate by D_2O.

Furthermore, base catalysis of amide hydrogens is at least 8 orders of magnitude more effective than acid catalysis (48). The pH profile of the hydrogen exchange, plotted as log (k_{ex}) versus pH, is typically V-shaped, where pH_{min} reflects the point where acid- and base-catalyzed exchanges are equal. Fig. 2 depicts the hydrogen deuterium exchange as a function of pH as determined for backbone and side-chain amide hydrogens, demonstrating that a change in one pH unit is reflective of an approximately 10-fold change in the exchange rate. For backbone amides, pH minimum (pH_{min}) occurs approximately pH 3. Temperature and solvent composition also exert a significant effect on the hydrogen deuterium exchange rates (41,45,49). The temperature parameter can be estimated at different temperatures using the Arrhenius equation, $k(x)_T = k(x)_{T2} \exp(-E_a(x)/R[1/T-1/T_2])$, where x is either base-, acid-, or water-catalyzed reaction, $k(x)_T$ and $k(x)_{T2}$ are the exchange constants at two different temperatures, R is the ideal gas constant, and the activation energies $E_a(x)$ for base-, acid- and water-catalyzed exchanges are 17 kcal/mol, 14 kcal/mol and 19 kcal/mol, respectively (45). Temperature changes mainly affect the k_{ex} by altering the ionization constant of water and thus changing the concentration of the catalyst ($[^-OH]$ for base catalysis) (41,49). Additionally, the diffusion coefficient k_1, describing the number of successful hydrogen-bonded complexes forming, is significantly reduced with decreasing temperature, thus affecting the transfer rate between the proton donor and acceptor in the collision reaction, due to the increased viscosity of the solution, a parameter dependent on the temperature. Organic additives can also affect the effective concentration of the base catalyst in the hydrogen transfer reaction, and do so by depressing the equilibrium constant of water (K_w) or hydroxide ion activity, thus resulting in a shift of pH_{min} (50-52).

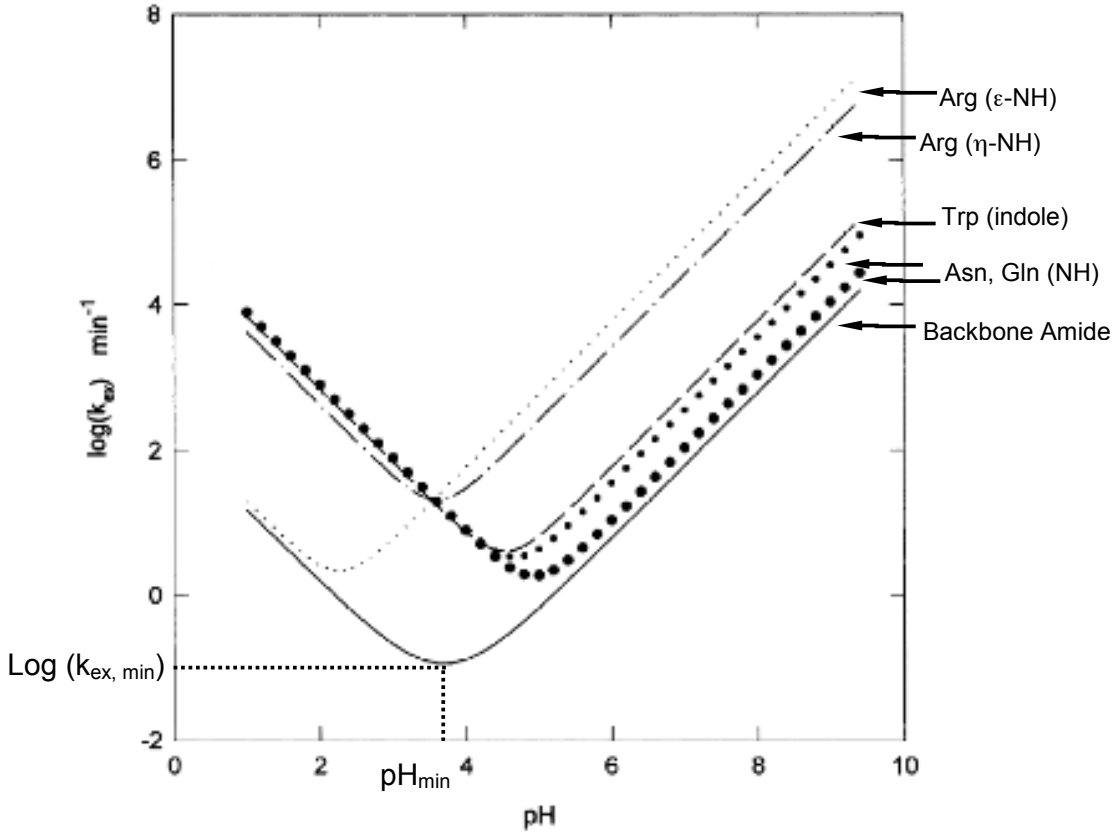

Fig. 2 Plot of log (k_{ex}) versus Solution pH in the Hydrogen Deuterium Exchange Reaction (Adopted from ref. (48)). Hydrogen deuterium exchange profiles for nitrogen-bound hydrogens in unstructured polypeptides plotted as a function of pH, where pH_{min} reflects a point of minimum exchange log ($k_{ex,\ min}$), where k_{acid} equals to k_{base}. The pH_{min} of backbone amides occurs at approximately pH 3.

On average unstructured, fully solvent-exposed amides have been shown to exchange with deuterium with a k_{ex} of $10^1 – 10^3$ s^{-1} (45). Two factors known to affect the exchange rate of backbone amide hydrogens in proteins are solvent accessibility of the region and intermolecular hydrogen bonding. The latter can significantly decrease the rate of the exchange reaction. In proteins, backbone amide hydrogen exchange with the deuterium of the solvent has been proposed to occur either directly in the folded state or first be preceded by partial or global unfolding, known as “breathing”, and then followed by deuterium exchange. The overall, experimentally-observed exchange rate (k_o) can be characterized as a sum of two components, the exchange rate of folded (k_f) and exchange rate of unfolded (k_u) states, $k_o = k_f + k_u$ (46,53). Fig. 3 depicts the current understanding of deuterium exchange in proteins, comprising a two-state model, whereby the exchange occurs in either the folded or partially unfolded species. In the folded-state model (Fig. 3A), the exchange is suggested to be limited by solvent diffusion into the core of the protein and governed by $k_f = \beta k_{ex}$, where k_{ex} is the rate constant of the exchange of the backbone amides in an unstructured polypeptide and β is the probability of backbone amide being exposed to both catalyst and water (54). Thus, hydrogens which are on the protein surface or in proximity to solvent channels are thought to readily exchange in the presence of a catalyst, while buried amide hydrogens exchange as a function of the dynamic solvent accessibility due to hydrogen bond reorganization through short and transient molecular motions. Additionally, Tuchsen and Woodward proposed that amide hydrogens which take part in hydrogen bonding with the solvation shell of the protein primarily exchange at the surface, while the core portion of the protein undergoes exchange by a relay mechanisms from the

surface, as a function of pH (55,56). In the partially unfolded state model (Fig. 3B), exchange rate is $k_u = k_{ex}(k_1/(k_{-1}+k_{ex}))$, and in native proteins is thought to proceed through extended “breathing” motions that result in partial unfolding and refolding events governed by the k_1 and k_{-1} rate constants, respectively, and an intrinsic exchange rate constant in the unfolded state described by k_{ex} (57,58). In general, proteins in their native state are thought to experience very small relative rates of unfolding and refolding, where the rate of the unfolding dynamics is very fast ($k_1 << k_{-1}$), and this is known as the EX2 kinetics (Fig. 3B and C), where the rate limiting step for hydrogen deuterium exchange is governed by the k_{ex}. Additionally, although observed very rarely in proteins, the exchange can proceed *via* EX1 kinetics, where the hydrogen exchange is preceded by a slow, global unfolding compared to refolding ($k_1 >> k_{-1}$) (59). While EX2 kinetics shows a high dependence on the pH and is reflective of the native protein conformation, EX1 kinetics proceed independently of the pH and reflect a cooperative exchange mode that can be facilitated by denaturing conditions. Thus, in backbone amides of proteins, the observed exchange rate constant (k_o) at a steady-state can be described by a composite of both folded and partially-unfolded models, with $k_o = k_{ex}(\beta + k_1/k_{-1})$, where either EX1 or EX2 kinetics or a combination of both can be observed.

The ability of MS to accurately resolve mass shifts associated with the appearance of deuterated species makes this analytical method highly suitable for and efficient in the analysis of HDX experiments. Furthermore, MS enables the measurement of both global as well as site-specific HDX in biological macromolecules.

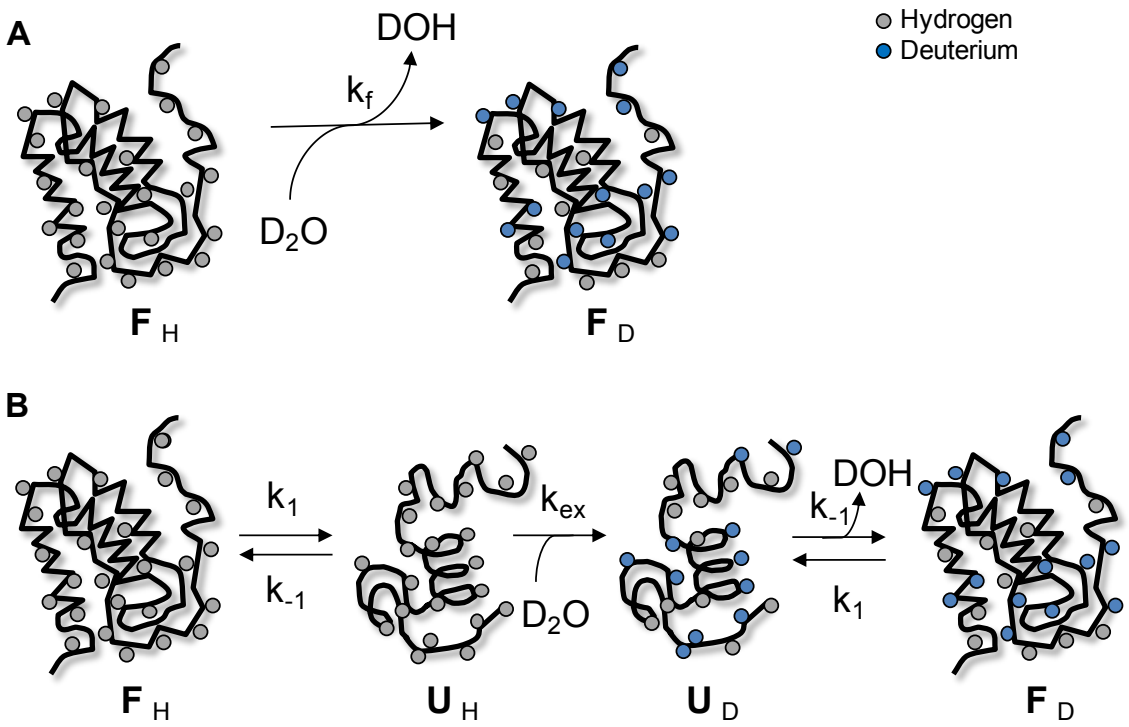

C

EX1 Type of kinetics when $k_1 >> k_{-1}$

EX2 Type of kinetics when $k_1 << k_{-1}$

Fig. 3 Mechanistic Models of Backbone Amide Exchange in Proteins. A) Folded protein backbone amides exchange ($F_H \rightarrow F_D$) with deuterium solvent with the rate constant $k_f = \beta k_{ex}$. B) Local unfolding, "breathing" motions and global unfolding of the protein result in the backbone amide exchange ($F_H \rightarrow U_H \rightarrow U_D \rightarrow F_D$) with deuterium solvent with the rate constant $k_u = k_{ex}(k_1/(k_{-1}+k_{ex}))$. C) Conditions for EX1 and EX2 exchange kinetics.

MS-based HDX measurements can be implemented 'globally' to give information on the overall flexibility of proteins (relevant to protein stability under specific conditions) or 'locally' to distinguish regions exhibiting varying degrees of protection from exchange due to structure. 'Global' measurements are made simply by exposing the protein to D_2O for a variable period of time, followed by online or offline MS analysis to measure the increasing mass associated with deuterium uptake. To achieve spatial resolution (i.e., 'local' measurements), the HDX process can be quenched using low pH conditions (the average minimum rate for HDX occurs at pH ~ 2.6) followed by enzymatic digestion by an acid protease and analysis of differentially-labeled peptides. This is known as a 'bottom-up' workflow. Alternatively, non-ergodic fragmentation techniques such as Electron Capture Dissociation (ECD) can be used to fragment the labeled protein in the gas phase (known as a 'top-down' workflow). Either of these approaches can achieve spatial resolution down to the near-single amino acid level (35,36).

1.3.3 Time-resolved electrospray mass spectrometry with HDX

Time-Resolved ElectroSpray Ionization mass spectrometry (TRESI-MS) allows for the detection of full-length, native proteins in kinetic experiments in which virtually all mass-distinguishable species can be monitored simultaneously (60-62). In the study of enzyme catalysis, TRESI-MS has proven to be a remarkably enabling technology, allowing a nearly universal (in principle) application to the characterization of catalytic reaction intermediates using native enzymes and substrates (60,63). This is a significant improvement over standard spectroscopic techniques that rely on colourigenic (chromogenic) or fluorogenic substrate analogues and methods utilizing radioactive substrates. Applied to protein dynamics, TRESI-MS can, in combination with

HDX, facilitate a structural analysis of the dynamic regions of proteins undergoing conformational changes during biological activity (35,64).

'Time-resolved' experiments employ rapid mixing setups to access short-timescale processes in (bio)chemical reactions, conventionally using NMR. NMR is a particularly powerful means of measuring rapid conformational dynamics, with experimental approaches that include stopped-flow or quench-flow rapid mixing (65,66) or equilibrium methods (e.g., CPMG relaxation dispersion) (67). The primary advantage of NMR-based measurements is that data are (almost) always site specific, which can allow for semi-quantitative analyses of local structural stability. However, NMR has a number of inherent drawbacks that limit applicability to large proteins and dynamics on certain timescales. Lengthy data acquisition times in multidimensional NMR also represent a challenge in the application to time-resolved measurements, particularly in the case of physiological pH HDX, in which exchange processes often go to completion within a few seconds of exposure to D_2O.

1.3.4 Capillary-based Rapid Mixer for Millisecond-Timescale HDX

A number of devices have been developed to couple mass spectrometry with rapid mixing including pulsed-flow, stopped-flow and quench-flow setups (68-70). Wilson and Konermann adapted continuous-flow rapid mixing for MS using a concentric capillary device with an automatically adjustable reaction chamber volume (Fig. 4A) (28). Solutions are supplied to each of the capillaries at the inlet by infusion pumps, generating a continuous laminar flow. One of the key advantages of this apparatus is that the outer capillary can be used as the ion source, resulting in a minimum reaction volume of 0 μL and a dead-time governed exclusively by the mixing volume

(corresponding to approximately 8 nL). The approach requires a custom 'front-end' (usually a straightforward modification of the commercial nanospray source) and the application of a laminar-flow corrected analytical framework to extract accurate rate parameters from the data. A detailed treatment of the theory underlying capillary mixer data analysis can be found in the original publication (28).

TRESI-MS with HDX provides a unique and powerful approach for conducting continuous-flow HDX experiments outside of the constrained time-window accessible to studies employing the conventional adapted LC setup. The capacity of TRESI-MS/HDX to generate short (ms) labeling pulses confers the ability to analyze dynamics in weakly-structured regions of proteins, such as molten globules, random coils and intrinsically disordered domains. For the added capability of measuring site-specific exchange, the labeled products can be subsequently fragmented or digested (29). This is a significant improvement over conventional LC-based methods, which typically achieve minimum labeling times of 1 second at best, with a substantial delay between labeling and analysis (71). In the case of a 'bottom-up' approach, the outlet of the capillary mixer can be coupled to a microfluidic chip that handles subsequent sample processing (Fig. 4B). This includes the introduction of low pH solution for HDX quenching, and proteolysis in a pepsin-functionalized reaction chamber (29,35). Oxidative labeling is a complementary structural method that has also been linked to TRESI (72). This approach involves the covalent attachment of a non-labile label to redox-active amino acid side-chains, eliminating the back-exchange issue, which can occur in HDX. In contrast to HDX, influenced by both hydrogen bonding and solvent access, oxidative labeling efficiency is linked specifically to solvent accessibility and is typically much lower resolution (since it can only be measured at redox active side-chains) (73).

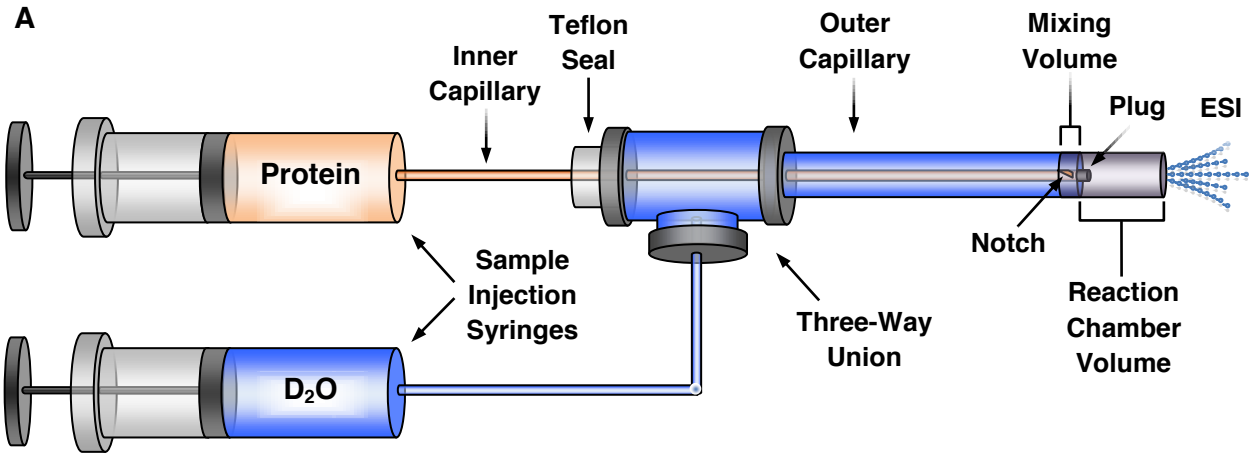
A
Inner Capillary
Teflon Seal
Outer Capillary
Mixing Volume
Plug
ESI
Protein
Notch
Sample Injection Syringes
Three-Way Union
Reaction Chamber Volume
D2O

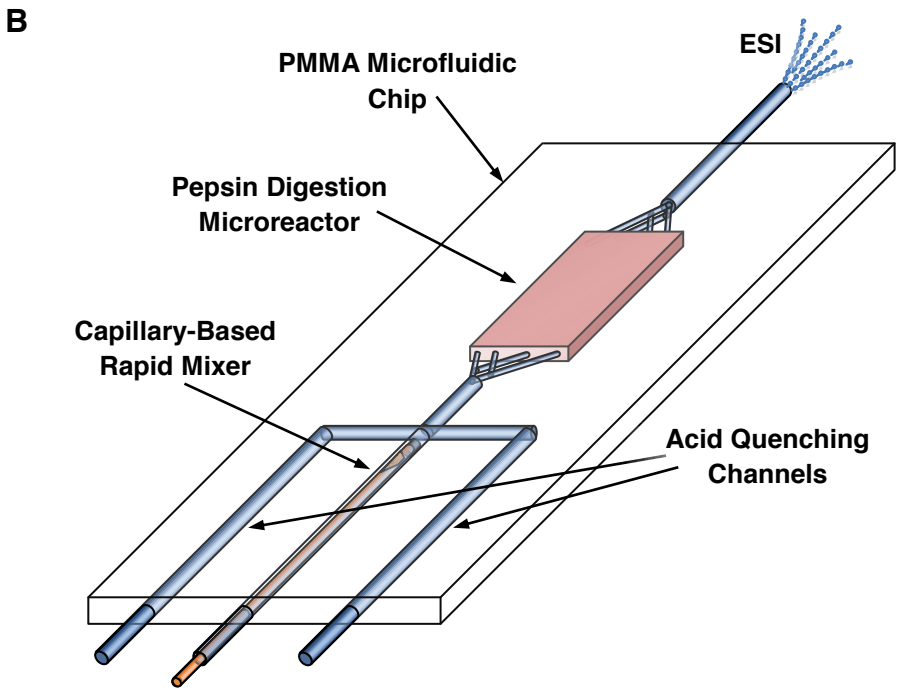
B
ESI
PMMA Microfluidic Chip
Pepsin Digestion Microreactor
Capillary-Based Rapid Mixer
Acid Quenching Channels

Fig. 4 Schematic of the Microfluidic-Based Rapid-Mixing Device for TRESI-MS/HDX Experiments. A) Schematic depiction of a Capillary-based rapid mixer with adjustable reaction chamber volume. An inner fused silica capillary is inserted through an outer metal capillary of larger diameter through a three-way union. Two different solutions, one containing the protein and the second a deuterium donor, are supplied at the inlets of the capillaries by automated Hamilton syringes at rates maintaining laminar flow throughout the apparatus. A small notch, about 2 mm away from the plugged end of the inner capillary, enables the solution from the inner capillary to escape and mix rapidly with the solution in the outer capillary in the inter-capillary space. The region between the notch and the outlet of the apparatus at the end of the outer capillary represents the reaction chamber volume. The outer capillary is used as an ESI source. B) Microfluidic chip for site-specific HDX experiments is diagrammed. The capillary-based rapid mixer is integrated onto the PMMA chip, which is additionally equipped with downstream supply channels for the HDX quenching solution and a further downstream microreactor for proteolytic digestion of HDX-labelled products. The microreactor chamber is filled with an immobilized pepsin bead bed or another protease. The outlet of the microfluidic chip is connected on-line to the ESI.

1.3.5 Global analysis of protein folding using TRESI-MS/HDX

Perhaps the most straightforward application of TRESI-MS/HDX is in the study of protein folding. The first such study was conducted by Pan et al. (74), in which a pulse-labeling approach was used to identify a 'hidden' intermediate in the ubiquitin folding pathway that could only be detected by considering both the HDX and charge-state characteristics simultaneously. This folding intermediate had a 'native-like' most prevalent charge state of 5+, but acquired deuterium in a manner analogous to the unfolded species (Fig. 5A). As the folding reaction progressed, the 5+ peak transitioned from this intermediate to a species that acquired substantially less deuterium, indicating a more folded, native configuration. The authors were thereby able to propose a multistep mechanism for ubiquitin folding (Fig. 5B) and to provide evidence for the common occurrence of folding intermediates, even for small proteins generally assumed to be 'two-state' folders.

The work by Simmons et al. 2004, exemplifies another application of TRESI-MS to the study of protein dynamics on the millisecond timescale (34). The authors have used the online rapid mixing device to monitor the kinetics of hemoglobin denaturation induced by the addition of acetic acid. As early as 9 ms of exposure to acid, changes in the profile of the observed ionic species were detected reflecting the appearance of different hemoglobin unfolding intermediates. The method enabled authors to detect short-lived unfolding intermediates on the sub-second timescale, and determine the order of reaction steps in the different mechanistic pathways of haemoglobin (Hb) denaturation by fitting the kinetic data (34). Different quaternary intermediates could be detected as either having a different subunit composition or losing/retaining the heme

prosthetic group (apo- versus holo- states) (Fig. 6). Various conformational species were observed based on their distinct charge distributions. The time-resolution of the method enabled the authors to construct a complex unfolding reaction landscape for Hb denaturation that involved two subpopulations of Hb tetramers that followed different denaturation pathways in parallel. The added advantage of the structural resolution of ESI-MS over other conventional methods is clearly highlighted here in its ability to simultaneously detect a complex mixture of quaternary and conformational species.

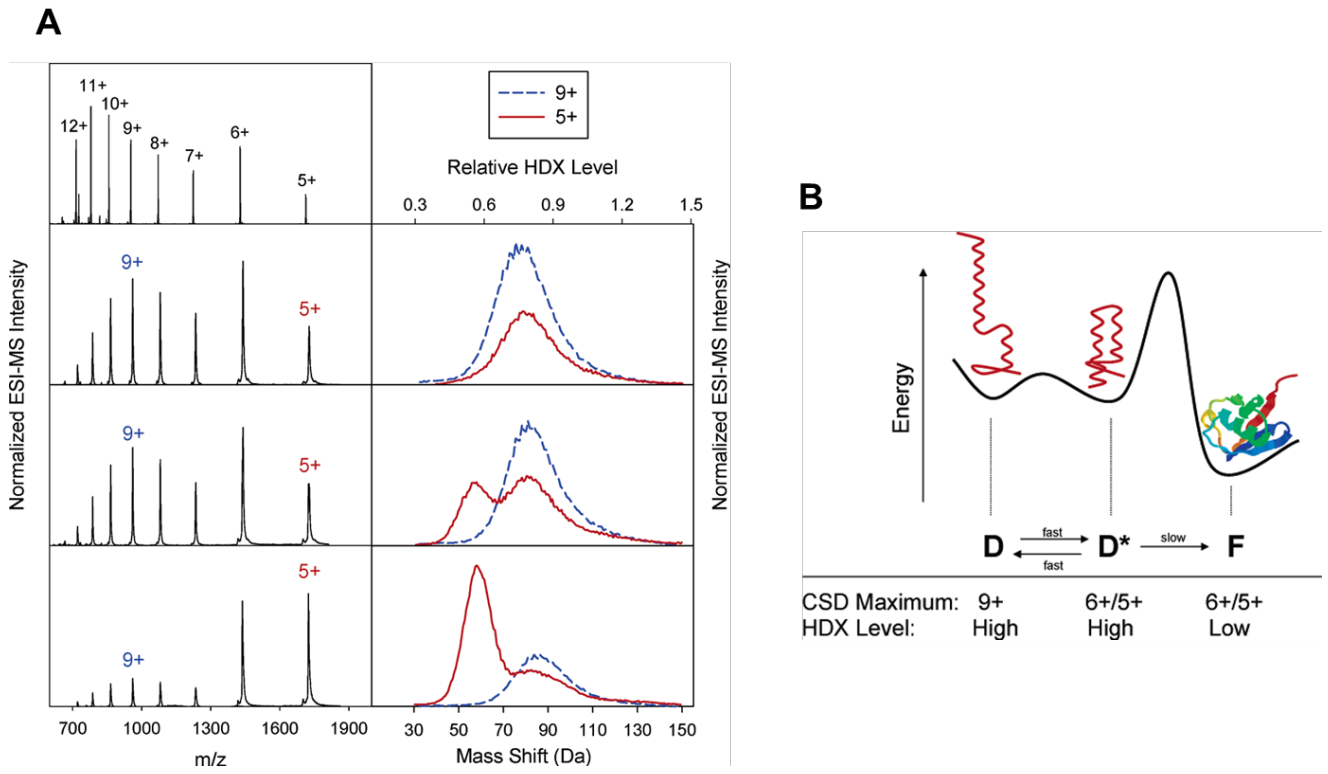

Fig. 5 TRESI-MS/HDX Study of Ubiquitin Folding Using Pulse Labeling. A) Time-resolved mass spectra recorded at 0 ms, 40 ms, 240 ms and 3.3 s by row, top to bottom. Right column is an overlay of the 5+ and 9+ peak mass shifts. B) A schematic depiction of the proposed ubiquitin folding pathway. The intermediate species D* can only be detected by considering both the charge state distribution and HDX. Reprinted with permission from (74). © 2005 American Chemical Society.

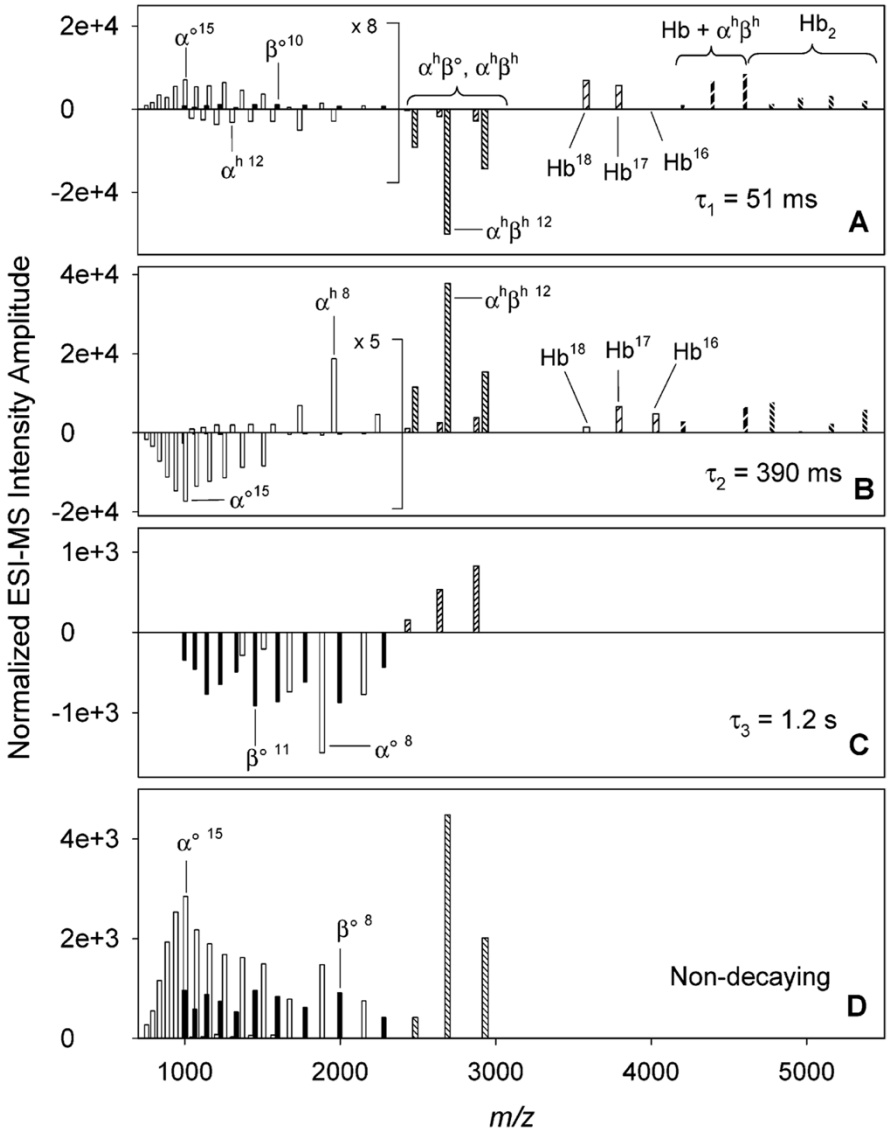

Fig. 6 TRESI-MS Study of the Acid-Induced Denaturation of Hemoglobin. Shown are amplitude spectra for the exponential relaxation times observed during the acid-induced denaturation, obtained by global data analysis by regression of kinetic data. Positive amplitudes correspond to the occurrence of species decay or a lag phase, while negative amplitudes represent species formation. Reprinted with permission from (34).

1.3.6 TRESI-MS/HDX in the study of catalysis-linked dynamics in enzymes

The microfluidics-based rapid mixing device can be successfully applied to the study of conformational fluctuations of proteins under non-equilibrium conditions in the context of TRESI-MS/HDX experiments. This method permits conformational dynamics to be probed in a system that is inaccessible to study by alternative methods, such as relaxation dispersion NMR on the millisecond timescale. Liuni et al. have utilized the rapid mixer to study conformational changes occurring during the catalytic turnover in chymotrypsin (63). The rapid mixing device was used to generate sub-second pulses of HDX labeling in the pre-steady state of chymotrypsin-catalyzed hydrolysis of *para*-nitrophenyl acetate (*p*NPA). In this experimental set-up, D_2O and *p*NPA substrate were supplied simultaneously into the mixing chamber of the device. TRESI-MS permitted the simultaneous detection and quantification of the free enzyme and an acyl-enzyme intermediate, while also allowing the quantification of the rate and amplitude of global HDX that occurred in each of the species (63).

Significantly higher rates of deuterium uptake were detected in the acyl-enzyme intermediate compared to the free enzyme, suggesting that the acyl-enzyme intermediate experienced higher rates of conformational sampling, yet the conformational space sampled by the enzyme and the acyl-enzyme intermediate was similar, as reflected by the comparable amplitudes of HDX observed between the two species (Fig. 7). In this instance, application of TRESI-MS/HDX yielded new mechanistic insights into the understanding of catalysis-linked dynamics, and provided evidence for a new model of conformer selection followed by intensified conformational searching during catalysis. An inherent advantage of MS-based methodology in kinetic

and dynamic studies of catalysis lies in its applicability to nearly any enzyme-substrate system, without the confines of having to use modified or unnatural substrates.

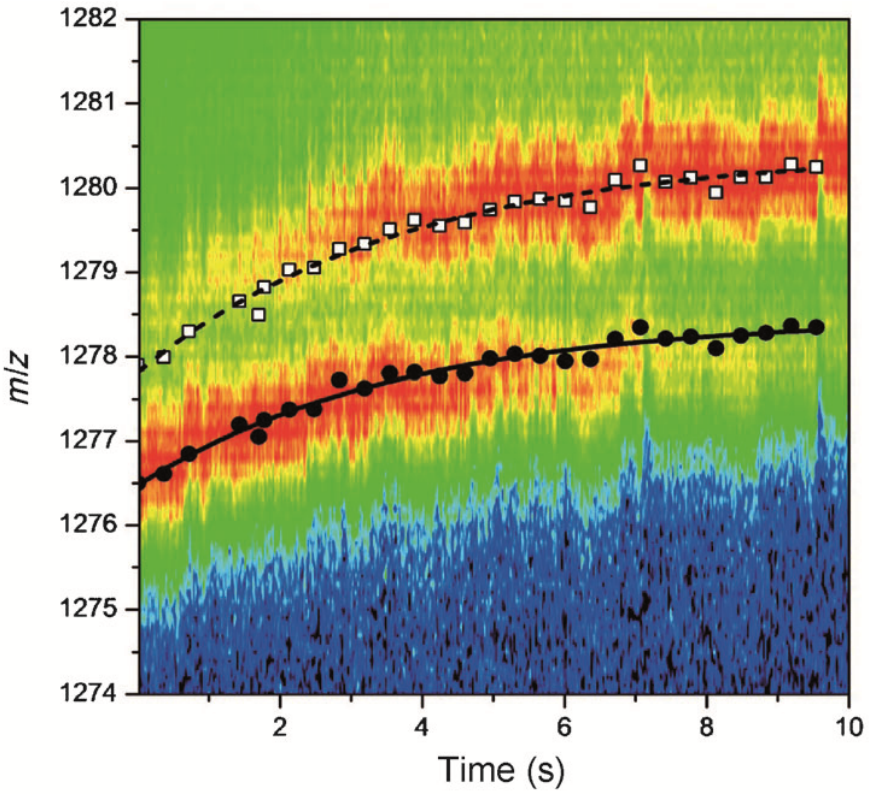

Fig. 7 A Heat Map Describing the Catalysis and HDX of Chymotrypsin Analyzed by TRESI-MS for the 20+ Charge State. The progress of catalysis can be observed as decreasing heat (for free enzyme) or increasing heat (for the acyl-enzyme intermediate). The global HDX kinetics are reflected in the rate of shift to higher m/z. Regression of the HDX kinetics data was achieved by plotting the position of the centroid of the peak for each m/z as a function of time. Filled circles (●) and open squares (□) represent the free protein and acyl-enzyme intermediate, respectively. Significantly higher rates of deuterium uptake were detected in the acyl-enzyme intermediate compared to the free enzyme, suggesting that the acyl-enzyme intermediate experienced higher rates of conformational sampling, yet the conformational space sampled by the enzyme and the acyl-enzyme intermediate was similar, as reflected by the comparable amplitudes of HDX observed between the two species. Reproduced with permission from (63).

1.3.7 Incorporating the HDX Workflow onto a Microfluidic Device for TRESI-MS/HDX Experiments

A greater degree of characterization of conformational dynamics of proteins can be achieved by utilizing microfluidic device-based TRESI-MS/HDX to examine site-specific HDX rates. In order to accomplish this, a 'bottom-up' TRESI-MS/HDX workflow was implemented, which included an HDX quenching step and subsequent protein digestion, prior to ESI-MS. In the device introduced by Rob et al., a capillary-based rapid mixer was incorporated onto a polymethyl methacrylate (PMMA)-based microfluidic chip that was etched with additional supply channels for a quenching solution and a microreactor chamber for enzymatic protein digestion (Fig.4B) (35). Aqueous acetic acid (4% v/v, pH 2.3) was used as an HDX quenching solution, rapidly dropping the rate of exchange and back-exchange to negligible levels. The microreactor chamber for protein digestion was filled with pepsin-agarose cross-linked beads immobilized onto the PMMA surface (29). Pepsin’s broad proteolytic specificity generally provides good sequence coverage, but the experimental set-up is not restricted to the use of pepsin, and could utilize other peptidases active under acidic pH.

1.3.8 Studying protein dynamics in weakly structured regions of intrinsically disordered proteins

This integrated experimental set-up was validated by application to a number of model systems, specifically highlighting the utility of sub-second HDX labeling to the examination of dynamics in weakly structured regions of protein. Utilizing a single 100 ms HDX pulse Rob et al., 2012, were able to derive a crude secondary structure profile of ubiquitin by analyzing deuterium uptake in the pepsin-generated peptide fragments. Similarly, by fitting the kinetics of segment-specific HDX of cytochrome c, the relative

conformational flexibilities of loop regions were determined (Fig. 8). Loop flexibility was expressed as segment-averaged 'protection factors': a ratio of the calculated 'intrinsic' rate of exchange to the observed rate of exchange (which is attenuated by structure) (35). Experimentally-determined protection factors were in good agreement with previously derived or predicted properties of the specific loops and generally agreed with predictions based on the heme prosthetic group negatively impacting the dynamics of the regions it contacts, with those segments in closest contact with the heme group showing the least flexibility.

On the millisecond timescale, backbone amide HDX in strongly hydrogen-bonded secondary structures is negligible. It was therefore possible to judge the extent to which the solution structure deviates from the reported (crystal or NMR) structure by comparing the observed level of exchange to the level expected based on the number of loop residues in the peptide.

In yet another application of microfluidics-enabled 'bottom up' HDX, Rob et al., were able to study a large, rapid change in conformational flexibility associated with substrate binding in the large tetrameric enzyme, DAHP synthase (35). By comparing site-specific HDX kinetics of the free enzyme with the substrate-bound complex, the authors localized the changes in dynamics to a large region centered on the active site. The tetramer interface, however, remained largely unchanged in the presence and absence of substrate, and this was supported by the detection of primarily tetrameric DAHP synthase in the 'native' mass spectrum. Site-specific HDX analyses of DAHP synthase dynamics contributed an important mechanistic insight, suggesting that the residual

tetramer structure in the molten globule-like substrate-free form could be acting as a template for the development of structure upon substrate binding.

One of the most exciting features of TRESI-MS/HDX is the ability to characterize residual structure in intrinsically disordered proteins (75). An example of this is a structural analysis of the neuronal Tau protein, which forms neurofibrillary tangles in Alzheimer's disease. By examining the disordered regions of the Tau protein under native (non-amyloidogenic) and hyperphosphorylated (amyloidogenic) conditions, regions that undergo substantial structural rearrangement during the development of pathogenicity can be identified and characterized. Phosphorylation of the native Tau protein by GSK3β *in vitro* yields an amyloidogenic paired helical filament form (76), and subsequent TRESI-MS/HDX analysis of site-specific exchange rates between the two forms revealed striking differences in the rates of exchange, concentrated in the disordered regions and regions that fold into beta sheet structures in the native protein (manuscript in preparation). This experimental system can yield structural and kinetic insights that could greatly facilitate the development of new Tau aggregation inhibitors, as well as provide a platform for direct chemical library screens aimed at identifying new inhibitors.

Site-specific HDX measurements on the millisecond timescale enabled by the microfluidics-coupled TRESI-MS are proving to be a versatile method for studying conformational dynamics in weakly structured protein regions and in IDPs. This approach is useful in an array of applications, from high-throughput predictions of secondary structure and dynamics to characterization of weak hydrogen bonding networks in flexible protein segments.

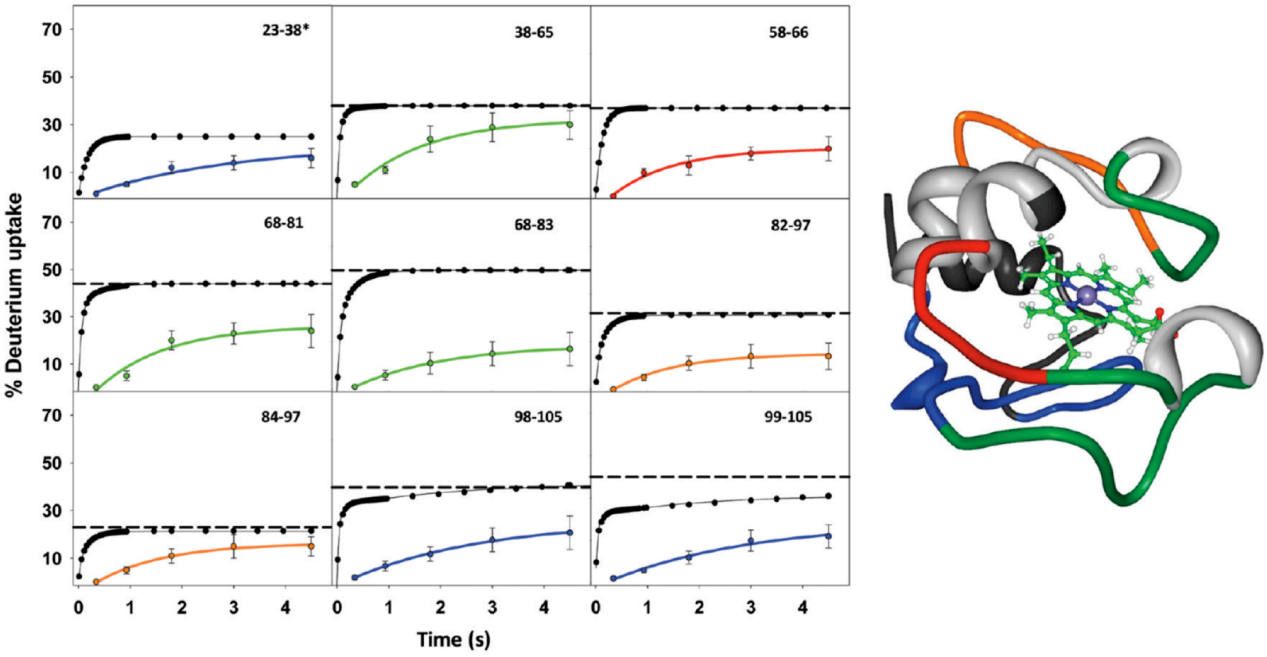

Fig. 8 Analysis of Site-Specific HDX Rates in Weakly Structured Regions of Cytochrome c by Microfluidic Device-Enabled TRESI-MS. By fitting the kinetics of segment-specific HDX of cytochrome c, the relative conformational flexibilities of loop regions were determined. A) Representative kinetic plots of % deuterium exchange as a function of time for 9 peptide fragments of cytochrome c. The loop amide profiles based on the intrinsic rates are shown in black. The dashed line represents 100% exchange of loop amides. The measured profiles are colored by protection factor: blue (strong protection), green (moderate protection), orange (low protection), and red (very low protection). B) Structural representation of cytochrome c loop dynamics based on the time-resolved HDX data. Different loops are mapped onto the solution NMR structure of oxidized horse heart cytochrome c (1AKK) (77) and colored by protection factors as in (A). Structured regions represented by detected peptide fragments are colored light gray. Regions for which no peptides were observed are colored dark gray. Reprinted with permission from (35). © 2012 American Chemical Society.

1.3.9 Interrogating the Dynamics of Protein-Ligand Interactions by HDX MS

The ability of HDX to probe rapid changes in the environment of backbone hydrogen amides with great sensitivity on the timescale of protein “breathing” motions makes it highly useful for probing the conformational dynamics and structural fluctuations in protein-protein and protein-ligand interactions. Probing of site-specific HDX, which is greatly facilitated by MS-based approaches, is ideally suited for sensing and resolving the perturbations in protein structure induced by ligand binding, both local and allosteric. Because ligand binding to a protein typically results in the exclusion of solvent molecules from the protein solvation shell and, in some cases, results in the formation of new hydrogen bonds between the protein and ligand, rapid decreases in deuterium uptake are often observed at the ligand-binding site. In the majority of cases, this clustering of decreases in deuterium uptake observed upon ligand binding can be interpreted to define the ligand-binding site and backbone regions interacting with the ligand. HDX has been applied to the study of protein-ligand interactions and associated dynamics to derive mechanistic insights in a variety of protein-ligand models, explaining ligand binding, catalysis, binding site preference, or allosteric regulation (78-81). Over the years, HDX has proven complimentary, if not indispensible, to other bioanalytical and structural biology techniques when interpreting protein-ligand interactions and the underlying parameters and mechanisms. One such example was the study of Bennett and co-workers, where they employed HDX MS in the characterization of a remote binding site for laulimalide, a new, non-taxane class of microtubule stabilizers, in the β-tubulin protein (82). Following the unsuccessful attempts to resolve the laulimalide

binding site on β-tubulin by NMR and X-ray crystallography, likely owing to the highly dynamic and flexible nature of this protein-ligand pair, it was found by HDX MS to bind to a new site, not previously known to support ligand binding and located outside of the canonical paclitaxel-binding site. Using HDX, the authors were able to show that the laulimalide-binding site is unique in its ability to provide a hydrophobic surface for ligand stabilization that is considerably shallower and less tolerant to significant structure adaptation than other known ligand binding sites on β-tubulin, yet is exposed to the outside surface of the protein, making it difficult to interrogate by other structural techniques.

Another good example of a successful application of HDX MS was a study by Zhang and co-workers, examining the binding of the Bcr-Abl inhibitor, GNF-5, a non-ATP inhibitor binding to the myristoyl pocket of the protein, and a close analog of GNF-2 (83). In this study, the combination of X-ray crystallography and solution NMR was sufficient to define the binding pocket of GNF-2 in Bcr-Abl, but these techniques failed to observe any allosteric changes that this inhibitor class could induce in the ATP-binding pocket of the protein. The authors then applied HDX MS to probe the dynamic perturbations in Bcr-Abl structure induced by the binding of the GNF-5 analog to the myristoyl pocket of the protein, and observed clear, allosteric coupling between the myristoyl pocket and the distal ATP-binding site. This finding ultimately led the authors to uncover the mechanism for synergistic combination of GNF-5 with the ATP-binding site inhibitor, nilotinib. This and other studies highlight both the importance of probing protein conformational dynamics for the full understanding of the mechanistic steps occurring in protein-ligand interactions, and the utility of HDX MS to accomplish this.

1.4 Conclusion and Future Directions

Coupling of ESI-MS to a microfluidic device that enables rapid mixing and provides an adjustable reaction chamber volume extends the reach of HDX analyses to weakly structured regions of proteins. The microfluidic device allows for continuous-flow experiments to be conducted, which greatly broadens the applicability of this methodology. In the study of enzyme kinetics, this device enables pre-steady state measurements to be conducted with ease, offers high selectivity for reaction intermediates, and permits the study of natural substrates and native enzyme-substrate intermediates. In the study of protein dynamics, microfluidics-enabled TRESI-MS/HDX is capable of characterizing conformational changes that occur rapidly and frequently – conditions that are largely inaccessible to conventional techniques – with a spatial resolution of 5 amino acid residues on average.

Currently, site-specific HDX is limited to the analysis of a single structural species or an ensemble of species, which is the major limitation of this approach compared to the great deal of additional information it provides over global HDX experiments. This is because in order to measure site-specific HDX rates of multiple resident structural states, one has to be able to map the detected peptide fragments to the originating species. Proteolytic 'bottom-up' work-up of HDX-labelled proteins is thus intrinsically limited to a study of a single structural species (63). Non-ergodic gas phase fragmentation techniques such as ECD do not suffer from this limitation and are thus potentially highly applicable to the study of multiple resident structural states by time-resolved, site-specific HDX (36,84). However, ECD has its own limitations, particularly low sensitivity and a size limitation (presently around 18kDa) (36).

Ultimately, TRESI-MS provides a powerful alternative for time-resolved studies of protein dynamics, revealing rapid, activity-linked conformational changes that occur in response to ligand binding, allosteric effects or post-translational modification. It is hoped that these new insights will translate into a much-improved understanding of protein function and the nature of pathogenic misfolding and aggregation in the cell.

Chapter 2

2 Epitope Mapping Using Microfluidics-Enabled Millisecond Timescale Hydrogen-Deuterium Exchange

A version of this chapter was submitted for publication as Resetca, D., and Wilson, D.J. “Epitope Mapping Using Microfluidics-Enabled Millisecond Timescale Hydrogen-Deuterium Exchange”.

2.1 Summary

A microfluidic device that integrates a full “bottom-up” workup for mass spectrometry-based hydrogen-deuterium exchange (HDX) epitope mapping is described. The microfluidic device integrates a rapid mixer for millisecond timescale deuterium labelling, an acetic acid supply channel for exchange quenching, and a micro-digestion chamber filled with immobilized pepsin. The rapid mixer provides precise control over the deuterium labelling time. Direct coupling of the device to electrospray ionization mass spectrometry (ESI-MS) enables the workup cycle to be completed in less than 10 seconds, providing a basis for future automation and applications requiring high sample throughput. Furthermore, microfluidic integration of the quenching channel minimizes the confounding effects of back-exchange, which can convolute readouts in conventional HDX set-ups. The glutathione-S-Transferase (GST) epitope for binding to its cofactor, glutathione (GSH), was evaluated as a proof of concept for binding-site mapping using this technique. Significant decreases in dynamics mapped exclusively to the GST active site epitopes that make direct contact with GSH via backbone hydrogen bonding. Capturing the evolution of dynamics in accommodating ligands is a highly predictive approach to characterizing ligand binding sites.

2.2 Introduction

Hydrogen-deuterium exchange (HDX) Mass Spectrometry (MS), first introduced during the early 1990s for probing conformational changes in proteins (24,37), has recently experienced significant resurgence in interest paralleled by major technological advances. A major driver has been a move away from static representations of proteins towards dynamic ensembles that help better understand and predict biological processes and interactions (85,86). In addition to the relative ease of implementation, HDX offers substantial advantages over other methodologies, enabling the characterization of rapid conformational transitions and the interrogation of native structures in solution (87).

Recently, microfluidic sample processing was introduced as a key enabling technology for HDX experiments (35,63,88). Microfluidics allows for controlled, short labelling pulses to be implemented reproducibly and for minimization of the confounding effects of back-exchange (in which the deuterium label is lost during subsequent sample handling steps). Integration of HDX workflows onto a microfluidic device greatly facilitates sample workup and extends HDX to site-specific measurements with up to a single amino acid resolution, ultimately allowing dynamic protein structures to be constructed. We have demonstrated a number of applications for a microfluidic device adapted for a ‘bottom-up’ HDX workflow ranging from interrogating enzyme active site dynamic (35), evaluating allosteric effects (88), or characterizing the flexibility/rigidity of native structural ensembles of proteins (89). Here we present the applications of this device to the investigation of protein-ligand interactions and identification of ligand binding sites.

To improve on conventional liquid chromatography-coupled HDX (LC-HDX) methodologies (90), which suffer from the inability to implement sub-second timescale deuterium labelling pulses and increased back-exchange, a microfluidic device was developed to conduct HDX experiments. This microfluidic device integrates a millisecond timescale capillary-based mixer (28), an HDX quenching channel, and a proteolytic digestion chamber for on-chip 'bottom-up' sample workup. Directly coupled to the electrospray ionization mass spectrometer (ESI-MS), this experimental set-up enables time-resolved HDX experiments (TRESI-MS/HDX) to be implemented in continuous mode.

Two different approaches, 'top-down' and 'bottom-up' workups, have been developed for the site-specific analysis of HDX labelling of proteins. 'Top-down' approaches can be implemented by a variety of non-ergodic fragmentation methods that preserve deuterium label position, such as Electron Transfer Dissociation (ETD) (91) or Electron Capture Dissociation (ECD) (92). While these methods provide high spatial resolution (up to a single amino acid), they are currently limited to the analysis of HDX on small proteins (up to ~17kDa) (36). 'Bottom-up' workups use enzymatic proteolysis of the analyte protein, with acid proteases (most commonly pepsin) being the enzymes of choice to generate labelled protein fragments (93). Digestion is carried out a pH ~2.3, corresponding to the pH minimum of the HDX reaction, to ensure that exchange is quenched. 'Bottom-up' workups typically yield a spatial resolution of several amino acids (79).

Site-specific deuterium incorporation into the protein backbone can be interpreted with respect to the solvent accessibility of backbone amides and the degree of their

involvement in hydrogen bonding (87). Lack of exchange (or lowering exchange rates) could reflect limited solvent accessibility or the presence of hydrogen-bonded amides. Since ligand binding can have a dramatic effect on both of these factors, HDX is highly useful in predicting ligand binding sites and the accompanying dynamic changes within the protein. Binding sites are typically identified as pronounced, localized decreases in exchange induced by solvent exclusion and/or formation of hydrogen bonds between the backbone amides and the ligand molecule. In some cases, decreased (or increased) exchange is observed far from the actual binding site, resulting from allosteric structural rearrangements associated with ligand binding. These allosteric effects can convolute binding site mapping somewhat, but ultimately structurally-contiguous regions exhibiting pronounced changes in HDX (i.e. HDX hotspots) are a good indicator of ligand binding sites (94,95).

In this study, we investigated the performance of the microfluidic device in the context of epitope mapping using the 26kDa isozyme of Glutathione-S-Transferase (GST) from *Schistosoma japonicum* (an infectious zoonotic parasite with a broad mammalian host range) (96). GST catalyzes the detoxification of a variety of xenobiotic substrates by conjugating them with a small, abundant tripeptide – a reduced (sulfhydryl) form of γ-glutathione (GSH). GST is active as a dimer (97). It binds its substrates via the H-site of the catalytic domain in its C-terminal domain, while stably binding GSH as a cofactor in the G-site, a well-defined binding pocket, localized to its N-terminal domain (98). Here, we have interrogated the dynamics of apo-GST as well as that of GST stably complexed with the GSH cofactor as a model system for protein-ligand interactions. In the process, we have also evaluated the ability of time-resolved, site-specific HDX labelling to map protein-ligand interactions.

2.3 Experimental

2.3.1 Materials

Recombinant Glutathione-S-Transferase (>90% purity, GST from *Schistosoma japonicum*) produced in *E.coli* was purchased in lyophilized form from GenScript (Piscataway, NJ). Deuterium oxide (D2O – 99.99%), ammonium acetate (99.99%), acetic acid (99.7%), pepsin agarose beads, and reduced L-glutathione (γ-GSH) were purchased form Sigma Aldrich (St. Louis, MO). Dialysis cassettes (2.5kDa MWCO) were purchased from Fisher Scientific (Ottawa, ON). Metal capillaries (O.D. 355 µm, I.D. 177 µm and O.D. 400 µm, I.D. 254 µm) and PTFE tubing (O.D. 1/16”, I.D. 400 µm and O.D. 1/16”, I.D. 360 µm) were purchased from McMaster-CARR (Aurora, OH). Upchurch PEEK fittings 1/16” and PEEK MicroTEE were purchased from IDEX (Oak Harbor, WA). Poly-methyl-methacrylate (PMMA) blocks (8.9 cm × 3.8 cm × 0.6 cm) for production of the microfluidic device were purchased form Professional Plastics (Orchard Park, NY). Ultrapure water was generated in-house using a Millipore Milli-Q Advantage A10 system (Billerica, MA).

2.3.2 Microfluidic Device Fabrication

The microfluidic device for HDX workup was produced as described previously (30). The microfluidic device is illustrated in Fig. 9. Briefly, standard PMMA block (8.9 cm × 3.8 cm × 0.6 cm) was laser-ablated to incorporate two input channels for introduction of reactants, a proteolytic digestion chamber and a third output channel using the VersaLaser™ engraver (Universal Laser, Scottsdale, AZ). The first channel was utilized for embedding the rapid-mixing device (28) (for D2O labelling). The second channel was used for the supply of quenching solution (5% acetic acid pH 2.4). A proteolytic-

digestion chamber for pepsin-agarose beads (average diameter 20-50 μm) was edged in a rectangular shape (30 mm × 5 mm × 0.05 mm). The output channel feeds directly into the MS. A blank PMMA block was used as a cover to seal the device, lined with a silicon-rubber gasket for liquid-tight seal. A custom-build pressure-clamp was used to secure the device seal (LAC Machine & Tooling Limited, Toronto, ON). Metal capillaries were melted into the etched PMMA chip in order to connect the supply syringes to the device and provide an outlet for direct coupling to MS. Reactants were supplied into the device with gas-tight Harvard syringes through PTFE tubing using automated infusion pumps (Harvard, Holliston, MA).

2.3.3 HDX Measurements

HDX experiments were carried out in triplicate on GST alone or GST pre-incubated with GSH. Reconstituted GST protein was dialyzed overnight into 100 mM ammonium acetate buffer (pH 7.5). Lyophilized reduced GSH was reconstituted as a 10mM solution in deionized water, and was pre-incubated with GST (80 μM) for 2 hours on ice prior to HDX experiments (final GSH concentration of 400 μM, 1:5 molar ratio). The microfluidic device was directly coupled to the front-end of a modified QStar Elite hybrid quadrupole time-of-flight (Q-TOF) mass spectrometer (AB Sciex, Framingham, MA). GST solutions were infused through a polyamide-coated glass capillary into the rapid mixing device at a flow rate of 1 μL min^{-1}. Deuterium was supplied through outer metal capillary at a flow rate of 3 μL min^{-1}. The resulting maximum labelling was 75%. Deuteration pulse length was controlled by the withdrawal of the inner capillary and was calculated by measuring the position of the inner capillary in reference to the outer capillary of the rapid mixing device. 5% acetic acid solution for quenching was supplied through the secondary channel at a flow rate of 15 μL min^{-1}.

2.3.4 Mass Spectrometry

ESI-MS HDX experiments were performed on a QStar Elite Q-TOF instrument. A bypass switch was introduced to simulate the presence of a commercial source. Acquisition was carried out in a positive ion mode, with an electrospray voltage of +4700 V to +4900 V, 60 V declustering potential and 250 V focusing potential. Spectra were acquired over the range of 300-1600 m/z with a scanning rate of 1 s^{-1}.

2.3.5 Analysis

All spectra analyses were performed on the mMass software, version 5.5 (99). Deuterium incorporation was computed utilizing an in-house developed software. HDX data was fit using single exponential non-linear regression and normalized in SigmaPlot (Systat Software, San Jose, CA). All protein structures were rendered using PyMOL (The PyMOL Molecular Graphics System, Version 1.5.0.4 Schrödinger, LLC.).

2.4 Results and Discussion

2.4.1 Microfluidic HDX-MS Device for Characterization of Protein Dynamics

Millisecond-timescale HDX kinetics of protein-ligand complexation were interrogated using TRESI-MS/HDX on the microfluidic device shown in Fig. 9. The device comprises a capillary-based rapid-mixer and a quenching channel supplying acetic acid, both embedded into the PMMA chip, as well as etched channels for reagent supply that converge into an etched proteolytic digestion chamber. The digestion chamber is filled with pepsin that has been immobilized onto agarose beads. This integrated, continuous-flow set-up is directly coupled to the electrospray emitter and permits the complete ‘bottom-up’ workup to be performed on the device. The capabilities of the device for

characterizing ligand binding were evaluated via a well-studied interaction between GST with its natural cofactor γ-GSH. GSH complexes with GST in a defined binding pocket at the active site (Kd of $3.5x10^{-5}$M) (100), forming a complex that is stable in the absence of substrates. With GSH acting as a cofactor, this comprises an ideal system for the investigation of a natural enzyme-substrate type of protein-ligand binding interaction as it eliminates the need for substrate analogues or synthetic inhibitors to stabilize the protein-ligand complex.

The rapid mixer occupies one of the channels of the device and consists of an inner polyamide-glass capillary that has been sealed, notched 2 mm away from the plug, and inserted into a metal outer capillary (Fig. 9). A three-way union permits the integration of the inner capillary into the outer capillary, while connecting the outer capillary to the PTFE tubing that supplies the deuterated water. In the current set-up, GST alone, or pre-incubated with GSH, was flowed into the rapid-mixer through the inner capillary, entering through the notch into the mixing chamber (the volume between the inner and outer capillaries around the notch region), where it was exposed to the deuterated water supplied through the outer capillary. After mixing, the solution was passed into a reaction region whose volume was controlled by the position of the inner capillary within the outer capillary, resulting in variable reaction times.

HDX was rapidly quenched with the supply of 5% acetic acid through a separate channel, connecting downstream of the mixing chamber. It was previously determined that this quenching step lowers the pH of the reaction to approximately 2.6, which, combined with an exceedingly short (~4 s) residence time in the device, virtually prevents back-exchange (35). The protein unfolds during this step, facilitating

proteolysis by pepsin (whose activity maximum is at pH 2) in the subsequent chamber. Acidified GST was digested by pepsin immobilized onto agarose beads that fill the protein digestion chamber (Fig. 9). The resulting digest was continuously electrosprayed directly into the mass spectrometer for analysis.

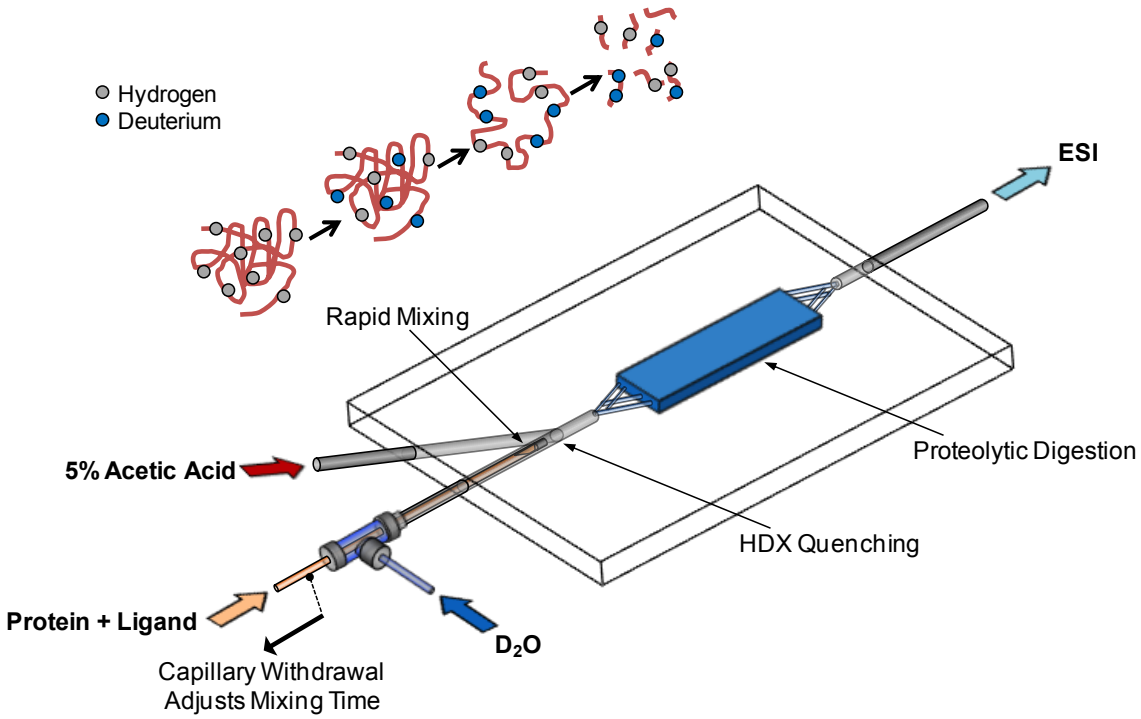

Fig. 9 Microfluidic Device for Millisecond Timescale Continuous Labelling HDX Integrating Complete 'Bottom-up' Workup. The device comprises a capillary-based rapid-mixer and a quenching channel supplying acetic acid, both embedded into the PMMA chip. The chip harbors etched channels for reagent supply that converge into an etched proteolytic digestion chamber, which is filled with pepsin agarose beads. The rapid mixer occupies the central input channel of the device and consists of an inner polyamide-glass capillary that has been sealed, notched 2 mm away from the plug, and inserted into a metal outer capillary. A three-way union permits the integration of the inner capillary into the outer capillary, and connects the outer capillary to the PTFE tubing that supplies the deuterated water. The protein solution enters the device through the inner capillary of the mixer. Following the deuterium labeling pulse, the solution mixes with the acetic acid quencher, and then passes through the proteolytic digestion chamber. The resulting peptide mixture is injected directly into MS for analysis.

Individual peptides were identified from raw MS spectra and theoretical and actual isotopic distributions were calculated for each observed fragment (101). Representative spectra of peptides mapping to the GSH binding site of GST are shown in Fig. 10A, demonstrating significant changes in HDX as a result of GSH complexation. Fig. 10A shows non-deuterated GST spectra, as well as spectra of GST, with or without complexed GSH, treated with a D_2O labelling pulse of 2.02 s. Isotopic distributions for each labelling time-point were computed for all observed peptic peptides to derive percent deuterium uptake. The complete HDX kinetics are depicted for representative peptides in Fig. 10B, demonstrating a clear decrease in deuterium uptake by the holo-GST-GSH complex as opposed to the apoenzyme. Table 1 lists the percent deuterium uptake calculated for all off the peptic peptides identified in the study, for the apo-GST and GST-GSH complex. Fig. 11 is a heat map representation of deuterium uptake of the GST apo- (Fig. 11A) and holoenzyme (Fig. 11B), as derived from triplicate HDX measurements, modelled onto the crystal structure of the protein (1GTA for apoenzyme and 1M9A for holoenzyme, where GST was docked in place of a GSH analogue) (102). Comparison of deuterium uptake between the structures reveals that significant HDX changes are confined to the active site of the protein.

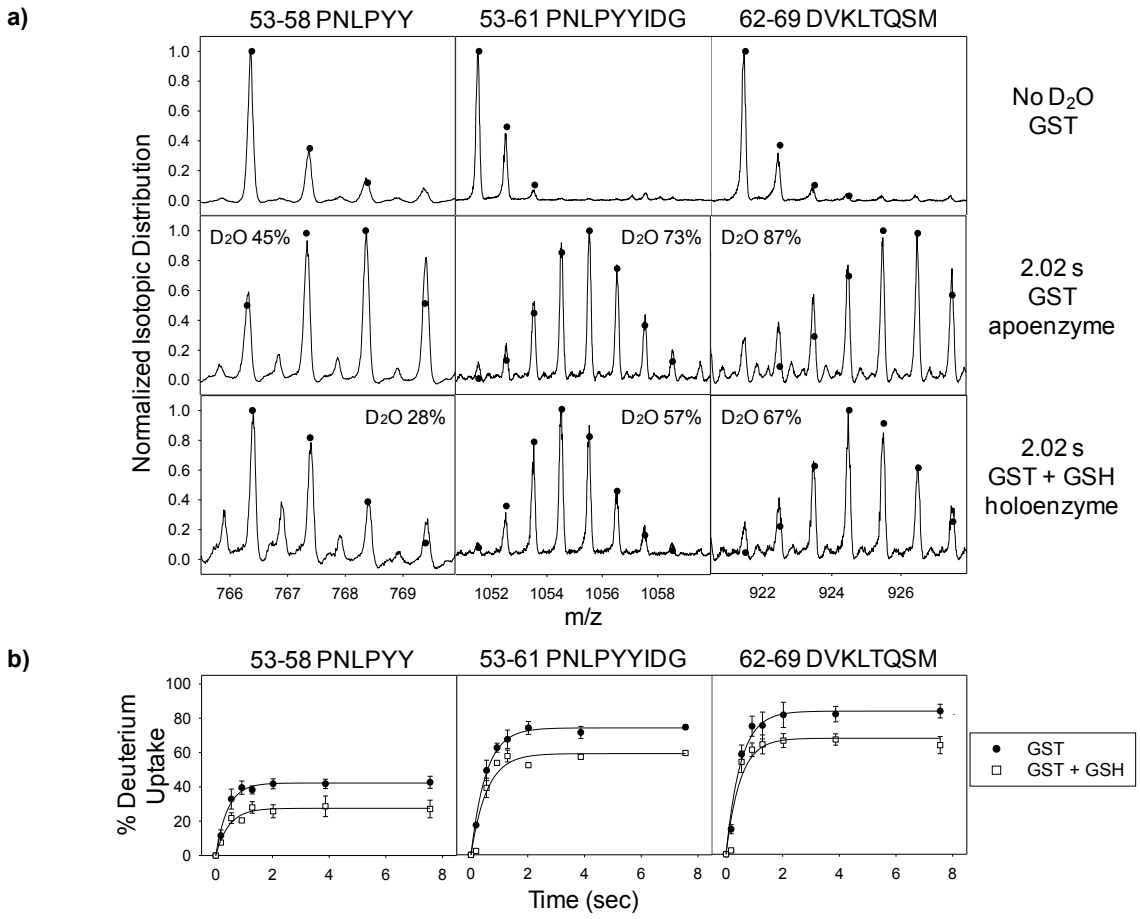

Fig. 10 Analysis of Site-Specific HDX in GST-GSH Ligand Binding. A) Representative spectra of peptides mapping to the GSH binding site of GST for non-deuterated GST (top row), GST labeled by a 2.02 s HDX pulse (middle row), and GST complexed with GSH labeled by a 2.02 s HDX pulse (bottom row). Raw spectra depict the observed shifts in isotopic distribution following HDX. Percent deuterium uptake is shown for each spectrum. B) Normalized HDX kinetic plots of representative peptides mapping to the GSH binding site of GST derived for the GST apoenzyme (closed circles) or GST-GSH holoenzyme (open squares).

Peptic Peptide	Sequence	Observed Amplitude (GST)	Std. Error	Observed Amplitude (1:5 GST:GSH)	Std. Error
MSPILGY/(W)	1-7	67.9	0.9	71.2	4.4
(Y)/WKIKGLVQPTRL/(L)	8-19	83.1	2.3	83.8	5.7
(L)/VQPTRLL/(L)	14-20	89.6	2.4	96.8	6.7
(E)/YLEE/(K)	23-26	99.9	2.7	95.2	6.7
(K)WRNKKFELG(L)	41-49	88.1	1.5	81.2	4.0
(F)/ELGLE/(F)	47-51	62.1	2.6	58.4	2.9
(F)/PNLPYY/(I)	53-58	42.2	1.1	27.5	1.2
(Y)/YIDGDVK(L)	58-64	81.7	5.9	79.7	5.8
(F)/PNLPYYIDG(D)	53-61	74.2	1.3	59.2	4.2
(Y)/IDGDVK(L)	59-64	51.1	1.2	49.3	2.8
(G)DVKLTQSM(A)	62-69	84.0	2.9	68.1	5.0
(A)/IIRY/(I)	71-74	32.8	2.3	31.9	3.5
(K)ERAEIS(M)	88-93	84.3	4.4	84.6	3.1
(R)AEISMLE/(G)	90-96	73.3	2.8	70.3	5.2
(L)/EGAVL/(D)	96-100	65.0	1.8	63.8	3.9
(Y)/GVSRIAYS(K)	105-112	94.3	2.4	96.7	5.5
(D)FETL/(K)	115-118	81.9	1.7	83.2	4.7
(V)DFLS(K)	121-124	77.4	2.9	78.0	5.5
(D)FLSKLPE/(M)	122-128	69.1	3.1	67.2	5.0
LSKLPEM/(L)	123-129	86.4	0.9	78.1	2.1
(F)/EDRLC(H)	134-138	87.0	3.6	91.7	6.1
(L)/NGDHVTHPDF/(M)	144-153	84.2	2.8	88.8	6.5
(Y)/MDPMCLDAFPKLVCF/(K)	165-179	70.0	1.1	68.8	7.1
(F)/KKRIEAIPQIDKY/(L)	180-192	56.2	1.6	60.5	3.7
(Y)/IAWPLQG(W)	199-205	68.8	1.5	75.3	2.7
(G)WQATFGGGDHPPKSDL/(V)	206-221	68.5	1.4	66.2	3.9
(L)/VPRGSPGIHRD	222-232	79.5	5.4	73.8	4.0

Table 1. Site-Specific Deuterium Uptake by GST and GST-GSH Complex. Calculated percent deuterium uptake is shown for each peptic peptide that was identified in the analysis of GST and GST-GSH complex (each experiment was repeated three times; corresponding SEM is shown).

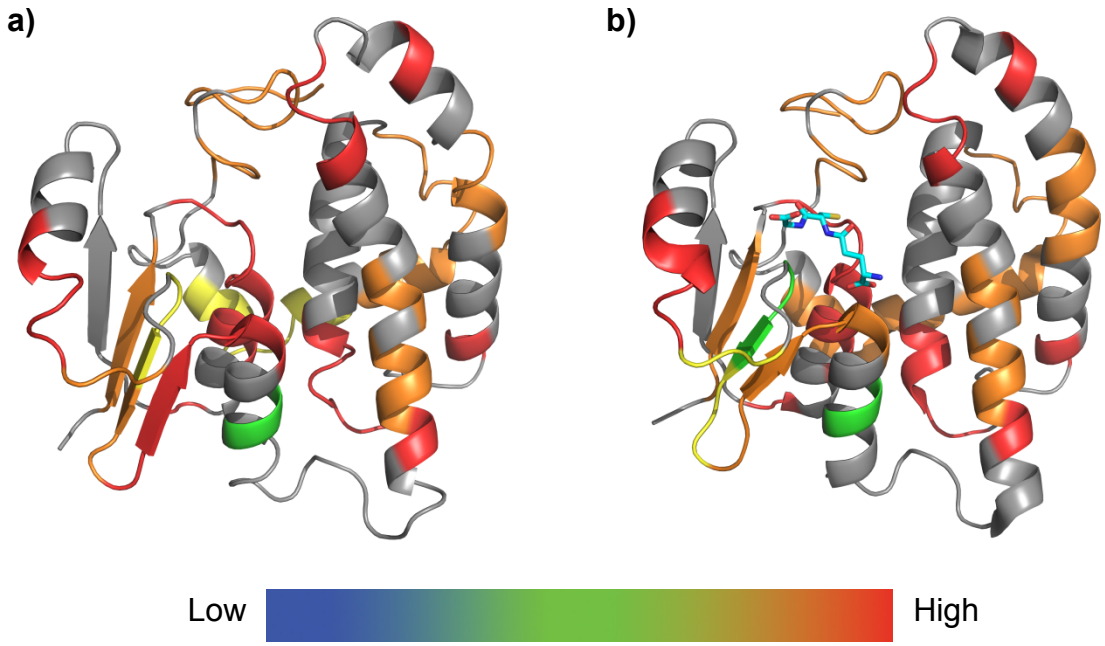

Fig. 11 Average Deuterium Uptake in Mapped onto the Crystal Structure of A) GST apoenzyme (PDB ID#1GTA) and B) GST complexed with GSH (modelled with GSH based on PDB ID#1M9A). GSH molecule is depicted as a stick representation coloured by element. Low (blue shading) represents 0-20% deuterium uptake, followed by green (20-40%), yellow (40-60%), orange (60-80%), and then high (red shading) representing 80-100% deuterium uptake.

2.4.2 Device Performance

A number of criteria are considered in assessing the performance of a microfluidic device for site-specific HDX experiments. Some of the key criteria include rapid incorporation of the deuterium label, precise control over the labelling/quenching times, accessible timescale for HDX labelling, rapid workup, and protein sequence coverage. The mixing chamber volume of the capillary-based mixer is between approximately 8 and 12 nL, depending on the diameter of the capillaries used, enabling an effective mixing to be achieved in as little as 5 ms (28,35,63,88). The deuterium labelling time is controlled by the positioning of the inner capillary, which could be done with a precision of at least 0.5 mm, translating in the current system, with a total flow rate of 4 μL min^{-1}, into 185 ms increments. In the present study, D_2O labelling pulses ranged from 179 ms and up to 7.56 s, effectively capturing HDX pre-equilibrium kinetics on a broad millisecond to second range (Fig. 10B). In contrast, the accessible timescale of the typical LC-HDX setup extends down to a minimum labelling time of 10 s (103). Millisecond pulses enabled by the HDX microfluidic device are particularly useful in interrogating the rapid evolution of protein dynamics of weakly-structured protein regions (35), inaccessible to other HDX-based techniques. Residence time of the protein in the proteolytic chamber is estimated at only approximately 4 s. This enables sufficient digestion to occur while further minimizing contribution from back-exchange that plagues conventional LC-HDX methods with post-labelling workup times that are at least an order of magnitude longer (104).

Another important performance indicator of HDX experiments is sequence coverage, which is influenced mainly by digestion efficiency. In a ‘bottom-up’ workup, the

backbone amides of the first two amino acid of each peptic peptide will back-exchange rapidly and would always be missed from the analyses, reducing sequence coverage (105). However, pepsin's tendency to miss cleavage sites results in the generation of overlapping peptides, compensating for this (79). Thus, sequence coverage is highly dependent on the amino acid sequence, secondary and tertiary structure, and residence (digestion) time on the chip, generally yielding sequence coverage of anywhere between 50% and 98% (29). In the current GST system, we achieved sequence coverage of 68% (based on 30 peptides analyzed, Fig. 12) and an average spatial resolution of 5.6 amino acids. Most of the observed GST peptic peptides were derived from the low-structured regions of the protein (Fig. 11). Using a cut-predictor PeptideMass tool on the ExPASy proteomic server (Swiss Institute of Bioinformatics, Basel, Switzerland) (106), one can predict expected cleavage sites, and the resulting peptides. Such an analysis of the GST sequence revealed that, in order to generate peptic peptides observed in the current experiments, an average of 1-2 missed cleavage events were required for most peptides. However, analysis of the regions for which we did not obtain sequence coverage reveals that more frequent missed cleavages (3 or more on average) would have been required to generate useful coverage. Furthermore, the majority of sequence coverage encompassed low-structured regions of GST, suggesting that the protein could have retained a degree of residual secondary/tertiary structure after acidification.

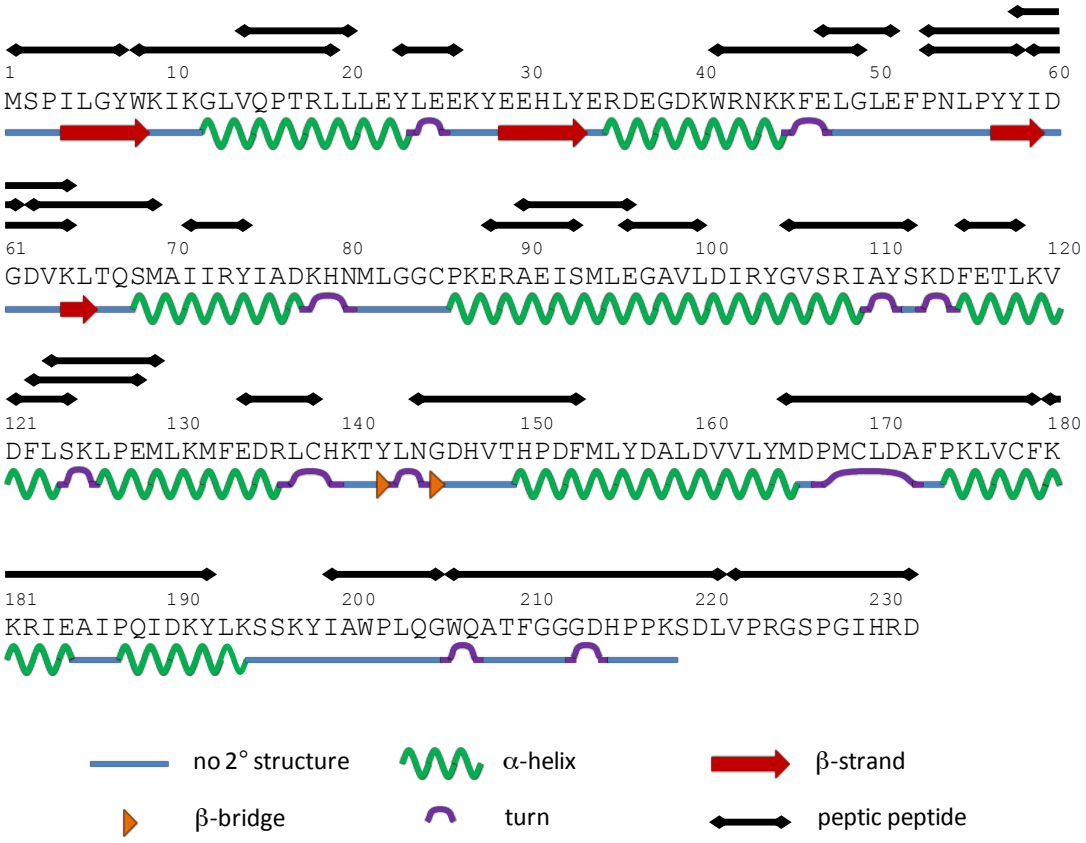

Fig. 12 Primary Protein Sequence and Secondary Structure Assignment (based on the Dictionary of Protein Secondary Structure (DSSP) Assignment (107))) of GST (PDB ID: 1GTA). Peptic peptides resolved and analyzed in the HDX experiments are indicated above the primary sequence. Total GST sequence coverage is 68%.

The GST sequence coverage obtained was sufficient to observe peptic fragments of major interest, corresponding to the GSH binding site at the N-terminus of the protein (Fig. 13A). Peptides from this region exhibit the most pronounced decreases in HDX upon complexation of GST with GSH, as apparent from the analysis of fold deuterium uptake changes throughout the protein sequence (Fig. 13B). While the GSH binding pocket is known in this case, these results show unambiguously that time-resolved HDX is a promising tool for de novo identification of ligand binding sites.

2.4.3 Evolution of GST Dynamics upon Complexation with GSH

In time-resolved HDX-based protein dynamics experiments, the degree of deuterium incorporation into the backbone amides of a peptic fragment provides information on the extent of solvent accessibility and/or hydrogen bonding that this region experiences within the population ensemble of the native protein species in solution. This information can ultimately be interpreted to document changes in secondary structure, rearrangement of the hydrogen bonding network, or the binding of ligands, where backbone amides are directly involved. With the application of our microfluidic device, we were able to generate a dynamic structure of GST that reflects the rearrangements of the hydrogen bonding network of the GST backbone to accommodate GSH binding to the active site.

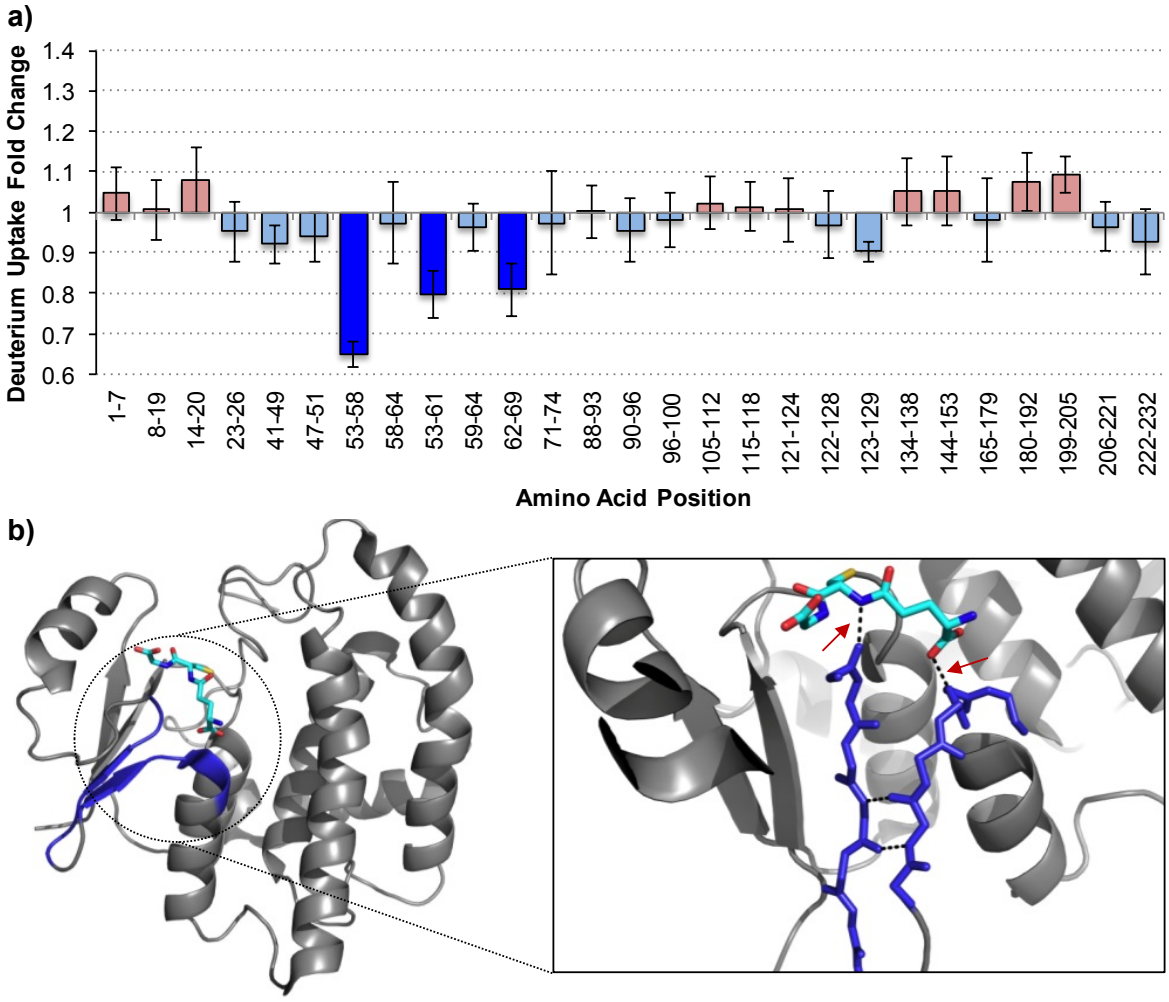

Fig. 13 Fold Change in Deuterium Uptake Between GST apoenzyme and GST Complexed with GSH. A) Fold change in deuterium uptake mapped onto the GST amino acid sequence as compiled from the detected peptic fragments. B) Hotspots of differential deuterium uptake (blue shading) mapped onto the crystal structure of GST complexed with GSH (modelled with GSH based on PDB ID: 1M9A). Hydrogen bonds forming between the backbone amides of the highlighted peptides and GSH are indicated by red arrows. Backbone amide of Leu55 in peptides 53-58 & 53-61 forms a hydrogen bond to the cysteinyl carbonyl of GSH. Backbone amide of Ser68 in peptide 62-69 forms a hydrogen bond to the γ-glutamyl carboxylate of GSH.

The three residues of γ-GSH make a specific contact with GST primarily through hydrogen bonding either to the side-chain or backbone (102). Residues Trp41 and Lys45 of GST stabilize the glycyl carboxylate group of GSH by side-chain hydrogen bonding, while glycyl amino group forms a hydrogen bond with Asn54. Trp8 forms a side-chain hydrogen bond with the cysteinyl carbonyl of GSH, while the amino portion of the GSH cysteinyl region forms hydrogen bonds with backbone of Asn54 and Leu55 residues. Amino group of the γ-glutamyl of GSH also forms hydrogen bonds with the side-chains of Asp101 and Gln67. Ser68 forms a hydrogen bond with the carboxylate group of the γ-glutamyl of GSH to both its backbone and side-chain. Thus, Asn54, Leu55, and Ser68 of GST all form hydrogen bonds with GSH via their backbone amides and are residues of interest in investigating GSH binding by GST by HDX labelling.

Newly created hydrogen bonds are indicated in the GST-GSH complex in Fig. 13B (red arrows), consistent with a significant decrease in deuterium uptake in peptides spanning residues 53-58/53-61 and 62-69 (coloured blue), mapping to the GSH binding site. Backbone amide of Leu55 in peptides 53-58/53-61 and Ser68 in peptide 62-69 form hydrogen bonds to the cysteinyl carbonyl and γ-glutamyl carboxylate of GSH, respectively. Independently detected and analyzed overlapping peptides 53-58 and 53-61, both containing Leu55 that hydrogen bonds with GSH, demonstrate equivalent decrease in magnitude of deuterium uptake (by approximately 11%), underscoring the high reproducibility of the microfluidic device and the HDX technique. We do not observe Asn54, since the backbone amide of this residue (second amino acid in peptides 53-58 and 53-61) back-exchanges rapidly. To get around the coverage

sequence limitation of the HDX experiments, alternative proteases could be employed in parallel analyses, such as nepenthesin (108).

In the current model complex, the dynamics of the highly specific binding of the GSH cofactor by the GST G-site are expected to be dominated by a relatively rigid lock-and-key mechanism (unlike the binding of GST substrates to the hydrophobic H-site, which enjoys considerable substrate flexibility) (109). This is consistent with the observation of minute (largely negligible) changes in deuterium uptake outside the binding pocket between the GST apoenzyme and GST-GSH complex (Fig. 13A), indicating a lack of allosteric transitions in the dynamics accompanying GSH binding. The active dimer of the mu-class GST enzymes does not normally experience catalytic cooperativity between the active sites of the two subunits (98,110). This is also consistent with the lack of dramatic HDX changes throughout the protein globally, and the dimer interface in particular (peptides 96-100, 105-112).

2.5 Conclusions

In this work, we describe a new application of our microfluidic device for millisecond-timescale continuous labelling HDX. We conducted site-specific HDX experiments to interrogate the dynamics of protein-ligand interactions and identify ligand binding site using a model system of GST complexed with its cofactor, GSH. The microfluidic device yielded a broad range of precise HDX labelling pulses and reproducible site-specific deuterium uptake measurements. Comparison of the differential deuterium uptake between the GST apoenzyme and the GSH-complexed protein successfully revealed an HDX hotspot that mapped to the GSH binding site. This data represents the first practical implementation of the microfluidic HDX device for rapid identification of a

ligand binding site in a protein. This fully integrated device reduces the entire HDX workup time down to less than 10 s per labelling cycle, enabling future automation for applications requiring high sample throughput, such as a compound library screening assay (111). We now extend the already broad array of applications of this microfluidic HDX device and establish it as a powerful tool for the study of protein-ligand complexes and mapping of ligand binding sites.

Chapter 3

3 Allosteric Changes in STAT3 Induced by Complexation with Pharmacological Inhibitors of SH2 Domain Dimerization

A version of this chapter was submitted for publication as Resetca, D., Haftchenary, S., Gunning, P.T., and Wilson, D.J. “Allosteric Changes in STAT3 Induced by Complexation with Pharmacological Inhibitors of SH2 Domain Dimerization”.

3.1 Summary

The activity of the transcription factor STAT3 is dysregulated in a number of hematological and solid malignancies. Development of pharmacological STAT3 SH2 domain inhibitors holds great promise for cancer therapy, and a novel class of salicylic acid-based STAT3 dimerization inhibitors has been recently developed that includes orally-bioavailable drug candidates. The compounds SF-1-066 and BP-1-102 are predicted to bind to the STAT3 SH2 domain. However, given the highly unstructured and dynamic nature of the SH2 domain, experimental confirmation of this prediction was elusive. We have interrogated the protein-ligand interaction of STAT3 with these small-molecule inhibitors by means of time-resolved hydrogen-deuterium exchange mass spectrometry (TRESI-MS/HDX). Analysis of site-specific evolution of deuterium uptake induced by the complexation of STAT3 with SF-1-066 or BP-1-102 under physiological conditions enabled the mapping of the *in silico*-predicted inhibitor-binding site to the STAT3 SH2 domain. The binding of both inhibitors to the SH2 domain resulted in significant local and global decreases in dynamics, consistent with solvent exclusion at the inhibitor binding site and increased rigidity of the inhibitor-complexed SH2 domain. Interestingly, inhibitor binding revealed hotspots of allosteric perturbations outside of the SH2 domain, manifesting mainly as increased deuterium uptake, in regions of STAT3 protein important for DNA binding and nuclear localization of the protein. Understanding how pharmacological inhibitors of STAT3 dimerization interact with its SH2 domain and affect the dynamics of the entire protein is critical to the development of next-generation STAT3 inhibitors.

3.2 Introduction

Signal Transducer and Activator of Transcription 3 (STAT3), an SH2 domain-containing protein (MW 88kDa), mediates intracellular signaling downstream of a number of cytokine and growth factor receptors and is involved in regulating cell proliferation, survival, differentiation, angiogenesis, cell migration, and inflammatory signaling (112). Dysregulated STAT3 activity promotes the progression of a multitude of hematological and solid malignancies (113). STAT3 is a transcription factor, whose activation is modulated by tyrosine phosphorylation. Activating phosphorylation at Tyr705 drives STAT3 homo-dimerization or hetero-dimerization with other STAT family members mediated by its Src Homology 2 (SH2) domain (114), which binds the phosphotyrosine peptide with nanomolar affinity (115). Inhibition of SH2 domain function is thus a robust strategy to antagonize its biological activity (116).

The SH2 domain is a structurally conserved feature of many intracellular signaling transducers and is capable of recognizing and binding to phosphorylated tyrosine residues presented in the context of specific protein sequences (117). Comprising minimal secondary structure, the SH2 domain and the phosphopeptide-binding interface are highly unstructured and dynamic (118) – a property that makes the development of small molecule inhibitors targeted at this important domain class a challenge. Gunning and co-workers have recently developed a number of pharmacological, orally-bioavailable inhibitors of STAT3 based on the salicylic acid pharmacophore through a series of QSAR studies (119,120). Two such inhibitors, SF-1-066 and BP-1-102, demonstrate an IC50 of 35 μM and 19.7 μM, respectively, for the inhibition of STAT3 DNA binding activity *in vitro*, and inhibit STAT3 dimerization (121). Additionally, BP-1-

102 has demonstrated potent anti-tumor effects *in vivo* in human breast and lung cancer xenograft studies in mice (119). *In silico* docking studies identified a putative binding site for the two inhibitors comprising all three phosphopeptide-binding sub-pockets of the SH2 domain (121). However, little experimental evidence exists corroborating that the putative binding site of SF-1-066 and BP-1-102 is indeed in the SH2 domain and the mechanism of action of these molecules is not yet fully understood.

While a number of X-ray crystal structures of STAT3 are available (122,123), including that of the phosphorylated STAT3 dimer (124), derivation of X-ray crystal structures of STAT3 complexed with SF-1-066 and BP-1-102 is laborious and is expected to be limited in utility to binding site identification. Unlike these static images, dynamic representations of protein structures can offer mechanistic insights into biological processes and interactions by depicting the time-evolution of protein conformational ensembles (87). Hydrogen-deuterium exchange (HDX) mass spectrometry (MS), when coupled with microfluidic sample processing, enables the interrogation of protein dynamics of the native protein structures in solution, permitting the *in situ* observation of enzyme-catalyzed reactions (63) and protein-ligand interactions (88). HDX, implemented on a microfluidic device for rapid mixing, quenching and proteolytic digestion of the protein analyte, offers substantial advantages over other techniques, including: easy implementation, unlimited protein analyte size, timescales compatible with protein breathing motions, and site-specific resolution of up to few amino acids (35).

We have extended the application of time-resolved MS HDX (TRESI-MS/HDX) to the study of protein-ligand interactions involving the highly unstructured SH2 ligand-binding

domain in the context of the near full-length STAT3 protein. In the present work, TRESI-MS/HDX was applied to (i) experimentally identify the STAT3 binding site of the salicylic acid-based inhibitors, SF-1-066 and BP-1-102, and (ii) probe the changes in protein dynamics induced in STAT3 upon complexation with these inhibitors.

3.3 Experimental Procedures

3.3.1 Reagents

SF-1-066 and BP-1-102 were synthesized as described previously (121) and were dissolved in DMSO. Deuterium oxide (D2O – 99.99%), ammonium acetate (99.99%), acetic acid (99.7%), and pepsin agarose beads were purchased form Sigma Aldrich (St. Louis, MO). Dialysis cassettes (30kDa MWCO) were purchased from Fisher Scientific (Ottawa, ON). Vivaspin 20 (30kDa MWCO) columns were purchased from GE Healthcare (Baie d'Urfe, QC).

3.3.2 Cloning, Expression and Purification of the STAT3 Fusion Protein

A plasmid containing mouse His-tagged STAT3 was provided by Dr. Rob C. Laister (Toronto, ON). STAT3, residues 127-688 (100% sequence identity on the protein level between mouse and human), was excised with NdeI and BamHI and subcloned directly into the pMAL-c5X plasmid digested with the same restriction enzymes to generate an N-terminal MBP (Maltose-Binding Protein)-tagged fusion of STAT3. The resulting pMAL-c5X- STAT3 plasmid was transformed into *E. coli* BL21(DE3) for inducible expression. The resulting MBP-human STAT3 fusion was purified on the Amylose Resin affinity-chromatography resin (New England Biolabs Inc. Ipswich, MA). Purified STAT3 was further concentrated to 80 μM and buffer exchanged into 100 mM ammonium

acetate buffer pH 7.4 using the Vivaspin 20 filtration column (GE Healthcare). Purity was confirmed by SDS-PAGE and absorbance at 280 nm to be above 95%.

3.3.3 Microfluidic Device Construction

Microfluidic device for HDX workup was constructed as described previously (35). Briefly, a standard PMMA block (8.9 cm × 3.8 cm × 0.6 cm) was laser-ablated to incorporate two input channels for introduction of reactants, a proteolytic digestion chamber and a third output channel using the VersaLaser engraver (Universal Laser, Scottsdale, AZ). The rapid-mixing device, described previously (28), was embedded into the first input channel to supply the protein solution and D_2O for labelling. The second channel supplied the quenching solution (5% acetic acid pH 2.4). A proteolytic-digestion chamber was edged in a rectangular shape (30 mm × 5 mm × 0.05 mm) onto the device and filled with pepsin-agarose beads (average diameter 20-50 μm). The output channel fed directly into the MS. A blank PMMA block was used as a cover to seal the device, lined with a silicon-rubber gasket for liquid-tight seal. A custom-build pressure-clamp was used to secure the device seal (LAC Machine & Tooling Limited, Toronto, ON). Metal capillaries were melted into the etched PMMA chip in order to connect automated supply syringes to the device and provide an outlet for direct coupling to the MS. Reactants were supplied into the device with gas-tight Hamilton syringes through PTFE tubing using automated infusion pumps (Harvard, Holliston, MA).

3.3.4 Hydrogen-Deuterium Exchange Mass Spectrometry

HDX experiments were carried out in triplicate with an 80 μM solution of STAT3 pre-incubated with 400 μM SF-1-066, 400 μM BP-1-102, or a DMSO only control for 2 hours on ice. The microfluidic device was directly coupled to the front-end of a modified QStar

Elite hybrid quadrupole time-of-flight (Q-TOF) mass spectrometer (AB Sciex, Framingham, MA). A bypass switch was introduced to simulate the presence of a commercial ESI source. STAT3 solutions were infused through a polyamide-coated glass capillary into the rapid mixing device at a flow rate of 1 μL min^{-1}. Deuterium was supplied through the outer metal capillary at a flow rate of 3 μL min^{-1}. The resulting maximum deuteration was 75%. Deuteration pulse length was controlled by the withdrawal of the inner capillary and was calculated by measuring the position of the inner capillary in reference to the outer capillary in the rapid mixing device. Pulse lengths ranged from 179 ms and up to 7.56 s. 5% acetic acid solution was supplied to quench the exchange through the second input channel at a flow rate of 15 μL min^{-1}. ESI-MS acquisition was carried out in a positive ion mode, with an electrospray voltage of +4700 V to +4900 V, 60 V declustering potential and 250 V focusing potential. Spectra were acquired over the range of 300-1600 m/z with a scanning rate of 1 s^{-1}.

3.3.5 *In Silico* Docking of SF-1-066 and BP-1-102 to STAT3 SH2 Domain Crystal Structure

Structures of SF-1-066 and BP-1-102 were docked into the STAT3 SH2 domain structure (derived from PDB ID: 1BG1) using the GOLD software package (Cambridge Crystallographic Data Centre, Cambridge, UK) as described previously (120).

3.3.6 Data and Statistical Analyses

All MS spectra analyses were performed on the mMass software, version 5.5 (99). Peptic peptide identification was performed using a FindPept tool on the ExPASy proteomic server (Swiss Institute of Bioinformatics, Basel, Switzerland) and confirmed by CID where needed. Deuterium incorporation was computed using software for

isotopic distribution analysis developed in-house. HDX data was fitted using single exponential non-linear regression and normalized in SigmaPlot (Systat Software, San Jose, CA). Protein structures were rendered using PyMOL (The PyMOL Molecular Graphics System, Version 1.5.0.4 Schrödinger, LLC.).

3.4 Results

3.4.1 TRESI-MS Analyses of STAT3 and STAT3-Inhibitor Complexes

STAT3 was pre-incubated with 400 μM or a 1:5 molar excess of SF-1-066 or BP-1-102 inhibitors (inhibitor structures are shown in Fig. 14A and B). This concentration was expected to have saturated STAT3, given the experimentally determined Kd for SF-1-066 and BP-1-102 of 2.74 μM and 504 nM, respectively (119,125). Fig. 14C shows how SF-1-066 (yellow) and BP-1-102 (green) are predicted to bind to the SH2 domain of STAT3, based on *in silico* docking simulations. In these models, residues Lys591, Arg609, Ser611, and Ser613 are predicted to make direct contact with the pTyr-mimetic portion of the scaffold, *ortho*-hydroxybenzoic acid, via hydrogen bonding and electrostatic interactions in the pTyr-binding sub-pocket. The hydrophobic cyclohexyl-benzyl moiety is predicted to form van der Waals' contacts with the distal, hydrophobic sub-pocket of the SH2 domain, lined by residues Trp623, Val637 and Ile659. The Sulfonamide-substituted group of the inhibitors is predicted to access an additional sub-pocket of the SH2 domain and are predicted to interact with Lys591, Glu594, Arg595 and Ile634 (119,121).

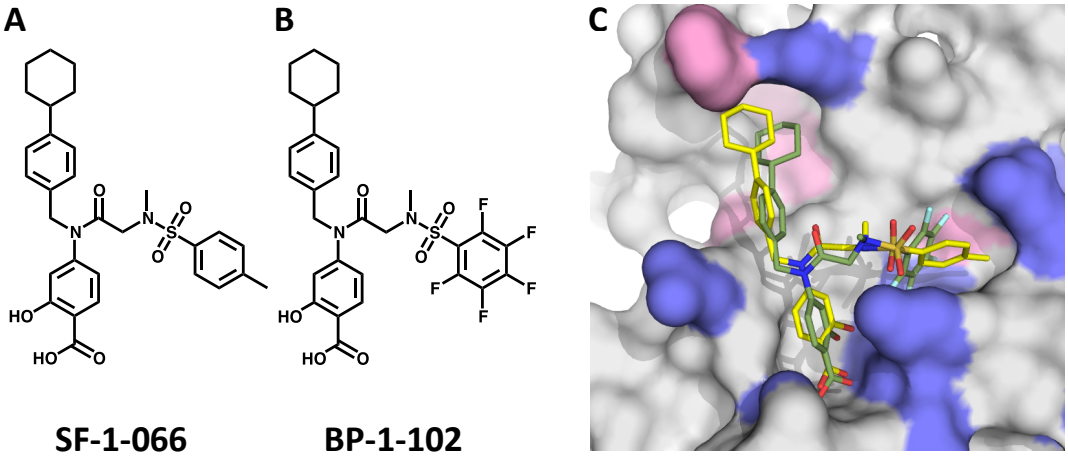

Fig. 14 Structure of the Salicylic Acid-Based Inhibitors, A) SF-1-066 and B) BP-1-102, are depicted. C) Representation of the results of *in silico* docking of SF-1066 (yellow) and BP-1-102 (green) inhibitors to the phosphotyrosine peptide-binding pocket of the STAT3 SH2 domain.

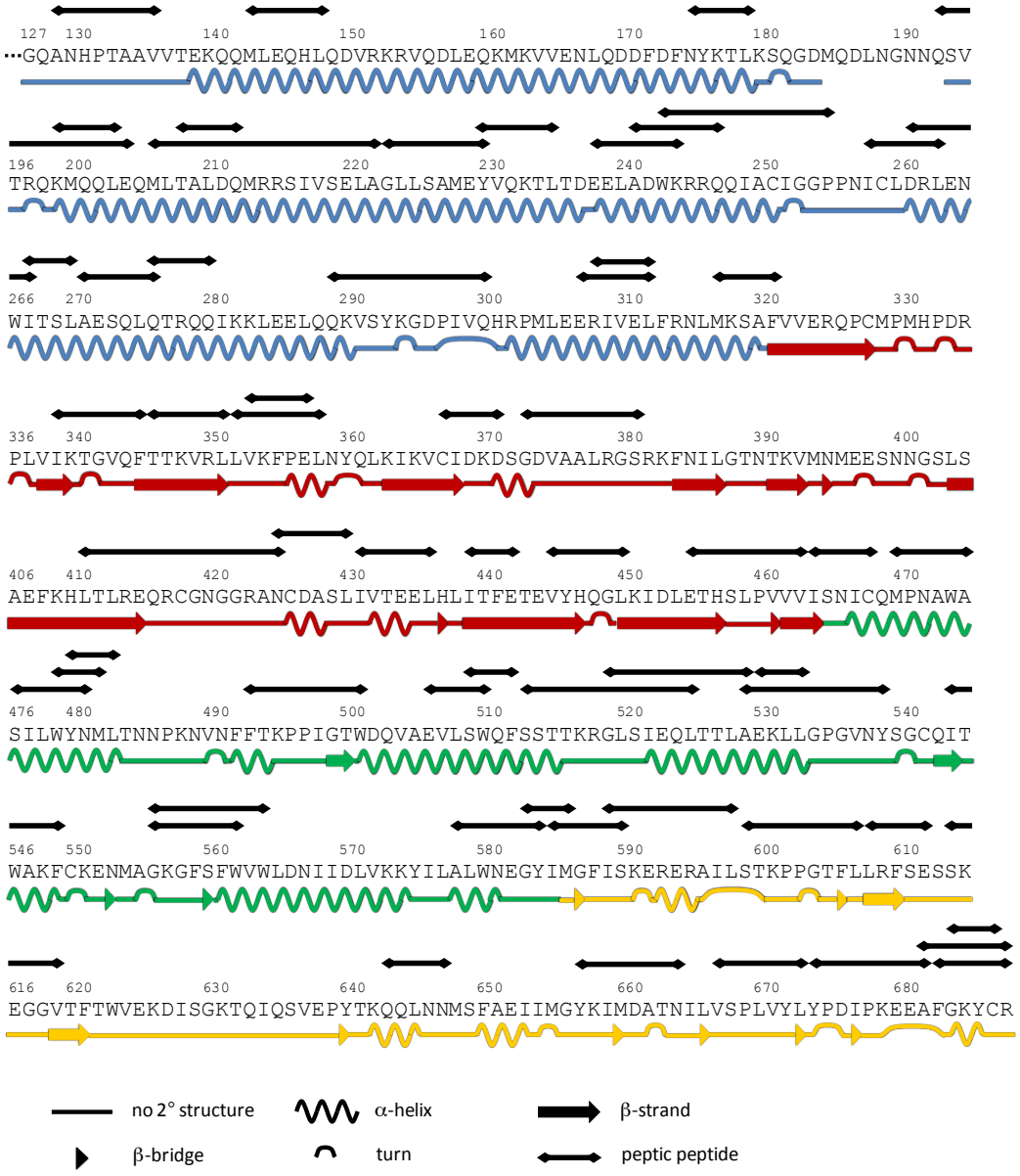

Fig. 15 Primary Protein Sequence and Secondary Structure Assignment (based on the Dictionary of Protein Secondary Structure (DSSP) assignment (107)) of the human STAT3 (PDB ID: 1BG1) segment of the MBP-STAT3 fusion protein. Peptic peptide resolved and analyzed in the HDX experiments are indicated above the primary sequence. Total STAT3 sequence coverage is 71%.

TRESI-HDX was carried out on a microfluidic device that facilitates variable HDX labeling times from 179 ms to 7.56 s, with on-chip digestion and electrospray ionization. Digestion of STAT3 was reasonably efficient in our system, resulting in sequence coverage of 71% corresponding to 53 unique peptides and an average spatial resolution of 5.1 amino acids (Fig. 15). Typical HDX MS data is depicted in Fig. 16A for STAT3 peptides that experienced no change in deuteration, increased deuteration or decreased deuteration as a result of complexation with SF-1-066 and BP-1-102 STAT3 inhibitors. Kinetic profiles, depicting the change in peptide deuteration as a function of labeling time, are shown in Fig. 16B. Data were normalized fit to a single exponential, and the amplitude parameter was used to calculate deuterium uptake. In Fig. 17, deuterium uptake is mapped onto the crystal structure of STAT3 (PDB ID: 1BG1), giving a broad picture of the dynamic nature of the free SH2 domain and the changes in dynamics that occur upon complexation with inhibitors (Fig. 17A-C). Fig. 18 contains the HDX kinetic plots for all the observed peptic peptides in this study.

3.4.2 Mapping the inhibitor binding site in STAT3

Mapping the fold-change in deuterium uptake for inhibitor-bound vs. free STAT3 to the crystal structure (Fig. 19A and B) enables the visualization of regions exhibiting pronounced changes in local backbone dynamics. Decreases in deuterium uptake may indicate the steric exclusion of solvent molecules or, alternatively, reorganization of the local backbone hydrogen bonding network resulting in a net increase in hydrogen bonding. Increases in deuterium uptake typically result from a disruption of secondary structure or increased local accessibility to solvent. The STAT3 SH2 domain (Fig. 17A and B, insets) exclusively experienced significant, large decreases in deuterium uptake upon complexation with both SF-1-066 and BP-1-102 inhibitors, in 5 and 6 unique

peptides, respectively. This observation was consistent with the occlusion of the SH2 phosphotyrosine-binding sub-pockets where the inhibitors are predicted to bind, resulting in decreased solvent accessibility. Peptides ISKERERAIL (589-598), LRFSE (608-612), and YKIMDATN (657-664), lining the surface of the putative inhibitor binding pocket predicted by docking studies, all exhibited a 2-3-fold reduction in deuterium uptake when inhibitors were present (Fig. 19A and B).

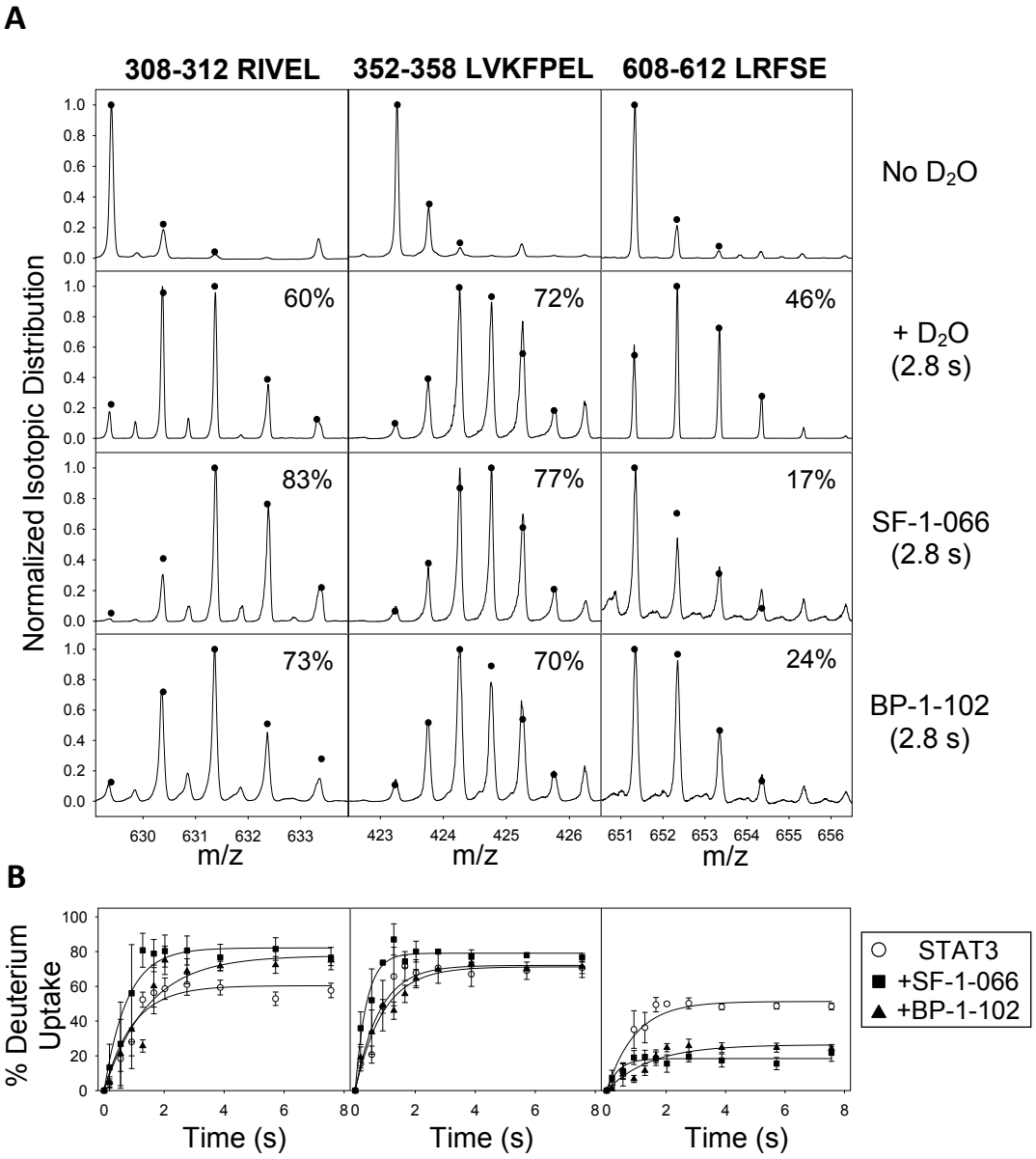

Fig. 16 Analysis of Site-Specific HDX in STAT3. A) Representative spectra of peptic peptides derived from STAT3 for non-deuterated STAT3 (top row), STAT3 labeled with a 2.8 s HDX pulse (second row), and STAT3 complexed with SF-1-066 (third row) or BP-1-102 (bottom row) labeled by a 2.8 s HDX pulse (bottom row). Raw spectra depict the observed shifts in isotopic distribution following HDX. Peptides that exhibited an

increase (left column), a decrease (right column) or no change (middle column) in deuterium uptake are represented. Percent deuterium uptake is indicated on each spectrum. B) Normalized HDX kinetic plots of representative peptides in (A) for the free STAT3 (open circles), and STAT3 complexed with SF-1-066 (filled squares) or BP-1-102 (filled triangles). Data represent an average of triplicate runs (error bars represent SEM).

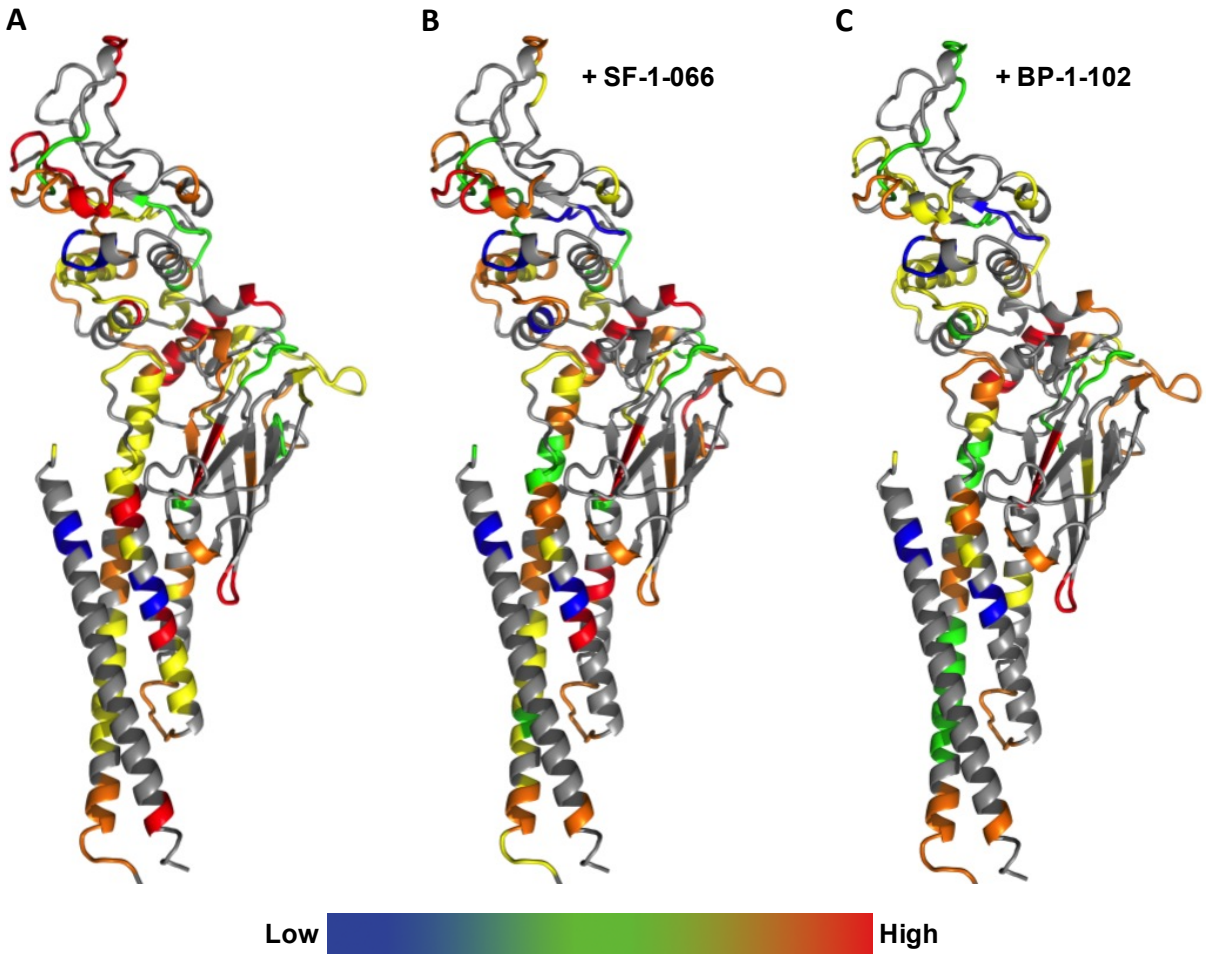

Fig. 17 Deuterium Uptake Mapped onto the Crystal Structure of STAT3. Average deuterium uptake mapped and color-coded onto the crystal structure of STAT3 (PDB ID: 1BG1) for A) free STAT3, B) STAT3 complexed with SF-1-066, and C) STAT3 complexed with BP1-102. STAT3 protein is depicted as a stick representation colored by element. Low (blue shading) represents 0-20% deuterium uptake, followed by green (20-40%), yellow (40-60%), orange (60-80%), and then high (red shading) representing 80-100% deuterium uptake.

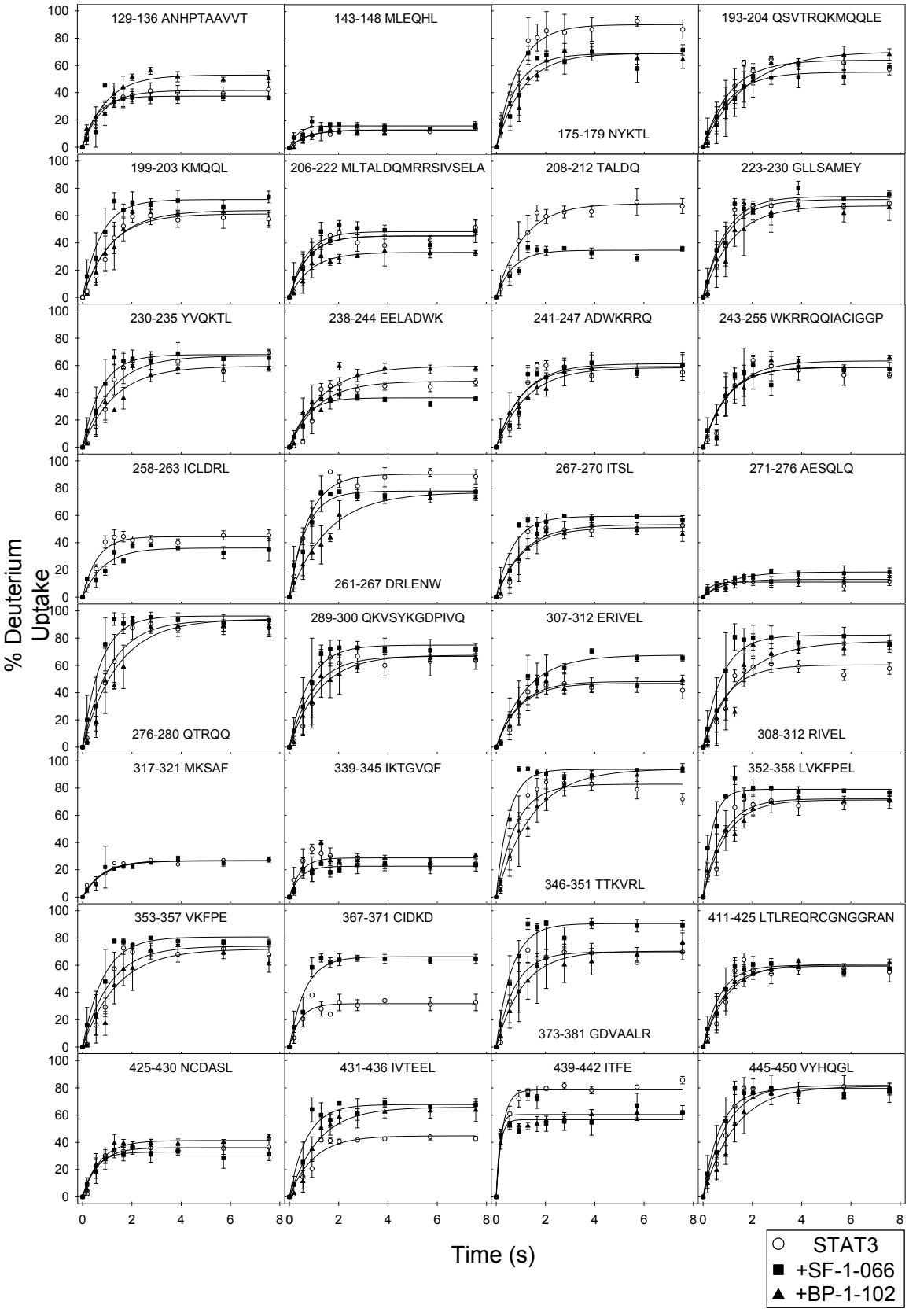
129-136 ANHPTAAVVT
143-148 MLEQHL
175-179 NYKTL
193-204 QSVTRQKMQQLE
199-203 KMQQL
206-222 MLTALDQMRRSIVSELA
208-212 TALDQ
223-230 GLLSAMEY
230-235 YVQKTL
238-244 EELADWK
241-247 ADWKRRQ
243-255 WKRRQQIACIGGP
258-263 ICLDRL
261-267 DRLENW
267-270 ITSL
271-276 AESQLQ
276-280 QTRQQ
289-300 QKVSYKGDPIVQ
307-312 ERIVEL
308-312 RIVEL
317-321 MKSAF
339-345 IKTGVQF
346-351 TTKVRL
352-358 LVKFPEL
353-357 VKFPE
367-371 CIDKD
373-381 GDVAALR
411-425 LTLREQRCGNGGRAN
425-430 NCDASL
431-436 IVTEEL
439-442 ITFE
445-450 VYHQGL
% Deuterium Uptake
Time (s)
STAT3
+SF-1-066
+BP-1-102

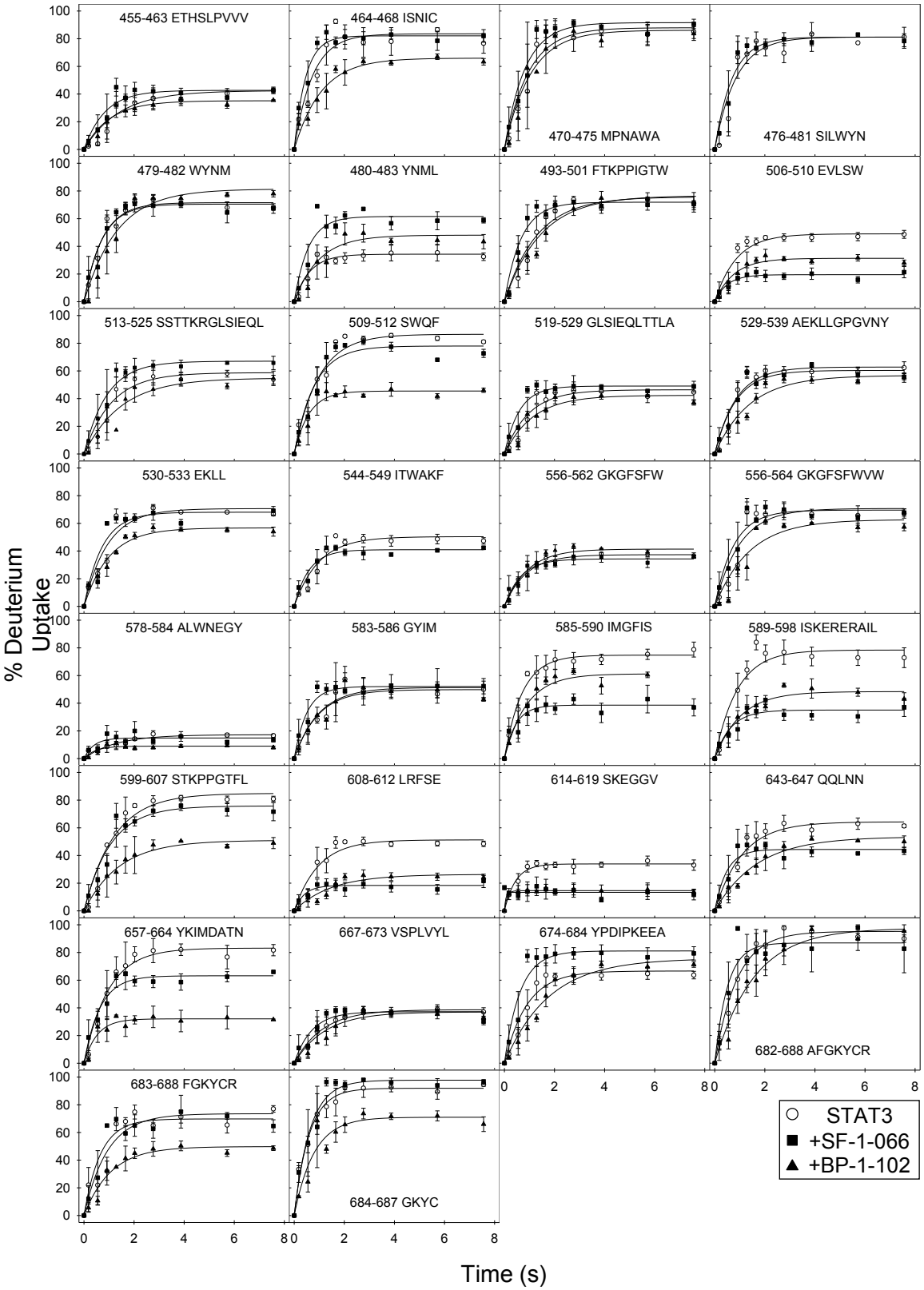
455-463 ETHSLPVVV
464-468 ISNIC
470-475 MPNAWA
476-481 SILWYN
479-482 WYNM
480-483 YNML
493-501 FTKPPIGTW
506-510 EVLSW
513-525 SSTTKRGLSIEQL
509-512 SWQF
519-529 GLSIEQLTTLA
529-539 AEKLLGPGVNY
530-533 EKLL
544-549 ITWAKF
556-562 GKGFSFW
556-564 GKGFSFWVW
578-584 ALWNEGY
583-586 GYIM
585-590 IMGFIS
589-598 ISKERERAIL
599-607 STKPPGTFL
608-612 LRFSE
614-619 SKEGGV
643-647 QQLNN
657-664 YKIMDATN
667-673 VSPLVYL
674-684 YPDIPKEEA
682-688 AFGKYCR
683-688 FGKYCR
684-687 GKYC
% Deuterium Uptake
Time (s)
STAT3
+SF-1-066
+BP-1-102

Fig. 18 Kinetic Plots of Deuterium Uptake in Peptic Peptides Derived From STAT3 and STAT3-Inhibitor Complexes. For each of the 62 peptic peptides identified, calculated percent deuterium uptake is plotted as a function of deuterium labeling time (from 179 ms to 7.59 s) for the digested STAT3 (open circles), STAT3:SF-1-066 (filled squares) and STAT3:BP-1-102 (filled triangles) complexes. Data represent an average of triplicate runs (error bars represent SEM).

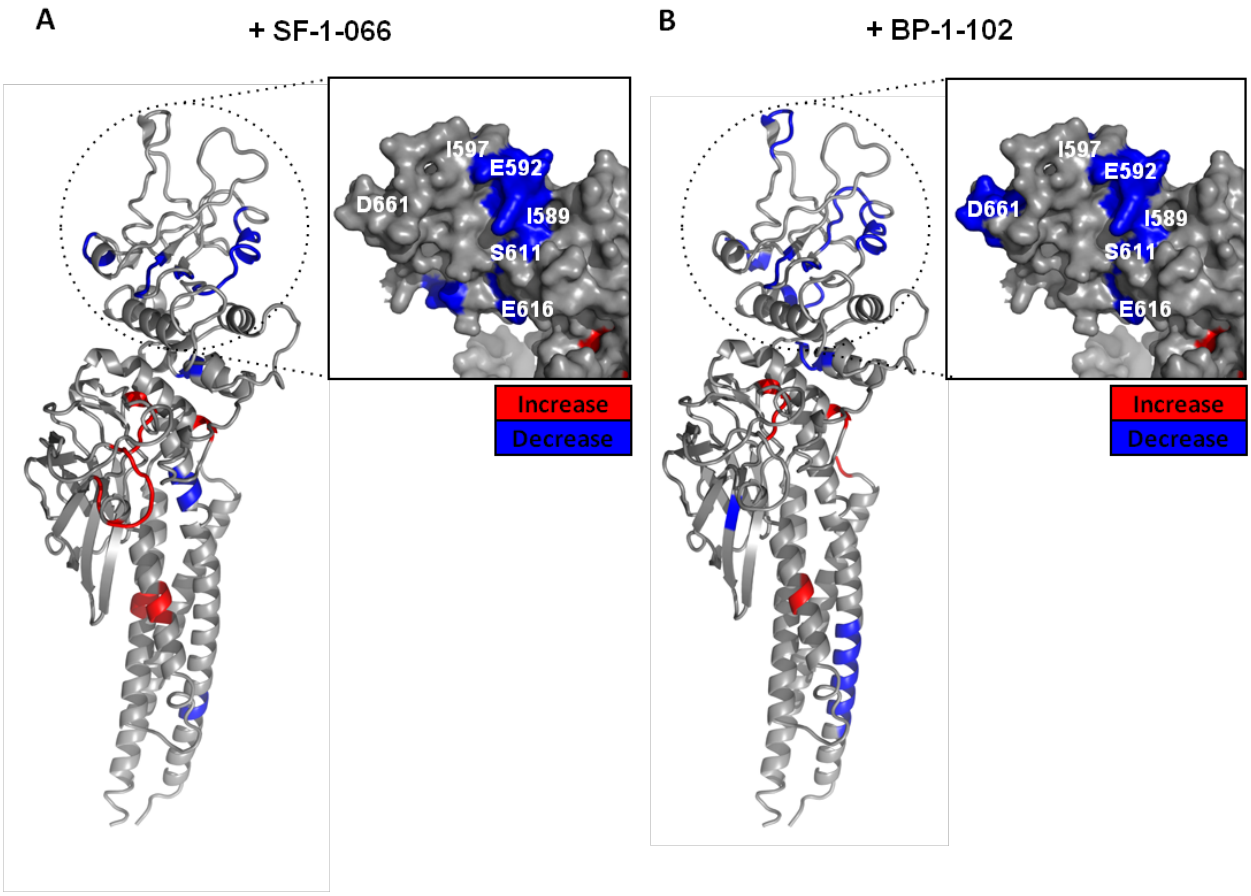

Fig. 19 Fold Changes in Deuterium Uptake of STAT3. Fold changes in deuterium uptake are shown for A) STAT3 complexed with SF-1-066 and B) STAT3 complexed with BP1-102 are shown. Hotspots of differential deuterium uptake, mapped onto the crystal structure of STAT3 (PDB ID: 1BG1), are color-coded as decreases (blue shading) or increases (red shading) in uptake. Insets show a magnified view of the SH2 domain, depicted from the face of the predicted inhibitor-binding pocket.

3.4.3 Allosteric Changes Induced in STAT3 by the SH2 Dimerization Inhibitors

Multiple peptides from outside of the SH2 domain exhibited pronounced changes in relative deuterium uptake upon complexation with inhibitor (Fig. 19A and B, and Fig. 20A and B). The majority of these conformational disturbances manifested as significant increases in deuterium uptake, and were largely localized to regions of α-helical secondary structure. The profile of allosteric differences induced by SF-1-066 versus BP-1-102 was somewhat different. Fig. 20C highlights the regions that exhibited relative changes in HDX that were significantly different between the SF-1-066 (orange) and BP-1-102 (purple) STAT3 complexes.

A +SF-1-066

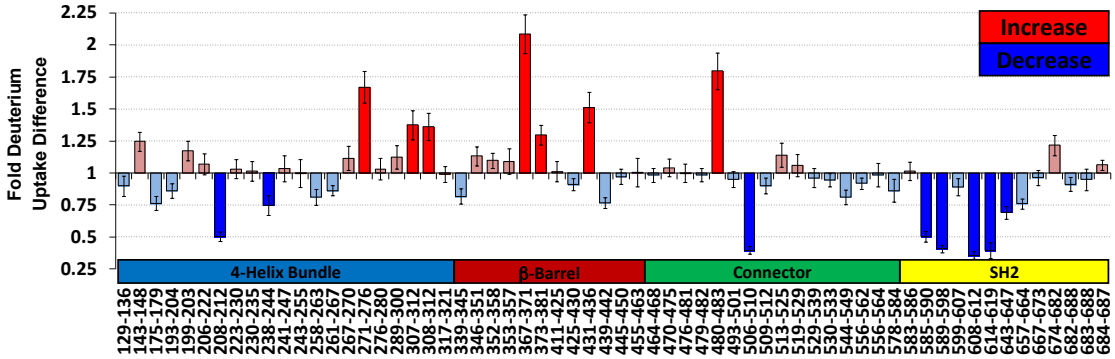

B +BP-1-102

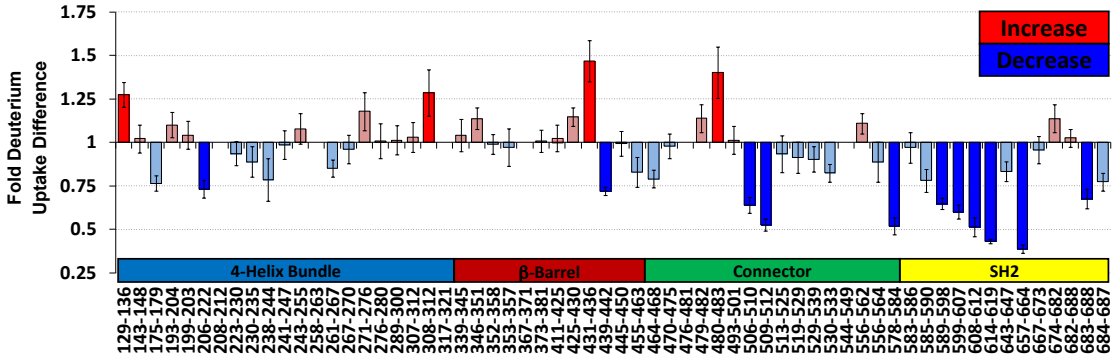

C Significant Differences between SF-1-066 and BP-1-102

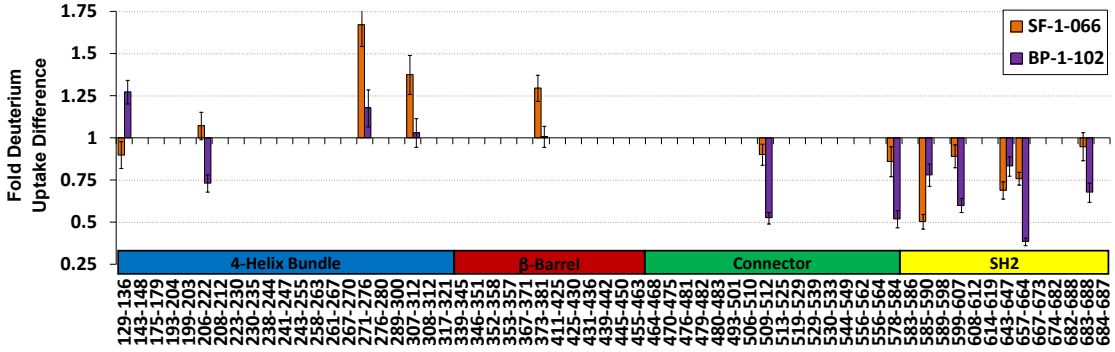

Fig. 20 Fold Changes in Deuterium Uptake for All Peptic Peptides Comprising the STAT3 Primary Sequence Coverage in the HDX Experiments. Fold changes in deuterium uptake from free STAT3 are shown for A) STAT3 complexed with SF-1-066 and B) STAT3 complexed with BP1-102. C) Significant differences in relative deuterium uptake between the STAT3:SF-1-066 (orange) and STAT3:BP-1-102 (purple) complexes are highlighted. Data represent an average of triplicate runs (error bars represent SEM).

3.5 Discussion

This study highlights the utility of structural mass spectrometry based on TRESI-MS/HDX in probing protein-ligand interactions and understanding dynamic changes and mechanisms associated with ligand binding. The “bottom-up” HDX approach, as implemented here, enables one to generate accurate, sub-second timescale kinetic profiles of site-specific exchange in the native protein structures. This structural technique is particularly useful for interrogating protein domains with minimal secondary structure or high degree of intrinsic disorder. While NMR has been used to probe disordered proteins to a degree, it is highly limited by protein size in applications involving protein-ligand interactions (19,87).

Here we applied the microfluidic-integrated TRESI-MS/HDX workflow to derive averaged dynamic structures of free and inhibitor-bound STAT3. Our examination of the dynamic changes in this protein largely confirmed *in silico* predictions with respect to the inhibitor binding regions, as well as revealed additional regions inside the STAT3 SH2 domain that exhibit strong protection from exchange due to the interaction with the inhibitors. SF-1-066 and BP-1-102 represent a novel, state-of-the-art class of salicylic acid-based SH2-targeted STAT3 inhibitors with low micromolar- and nanomolar-range affinity for STAT3, yet no experimental evidence directly describes their interaction with the SH2 domain (119,121). Additionally, our data reveal a series of increases in HDX outside the STAT3 SH2 domain due to inhibitor binding, suggesting allosteric effects that are potentially destabilizing to the protein.

Peptides ISKERERAIL (589-598), LRFSE (608-612), and YKIMDATN (657-664), which exhibit significant decreases in deuterium uptake upon inhibitor binding, map to the

surface of the inhibitor binding pocket predicted by docking studies (Fig. 20A and B). The side-chain of Arg609, mapping near the peptide LRFSE (608-612), was predicted to hydrogen bond with the salicylic acid moiety common to both inhibitors, greatly stabilizing the binding energy of the molecules (119,120). This is consistent with large decreases in backbone deuteration observed in the LRFSE (608-612) peptide given the tight predicted occupancy of this sub-pocket by the salicylic acid moiety for both inhibitors.

The peptide YKIMDATN (657-664), lining the cyclohexylbenzyl-binding sub-pocket, only experienced a significant decrease in deuterium uptake in the case of the higher affinity inhibitor BP-1-102 (Fig. 20A and B). The binding of the cyclohexylbenzyl moiety to the predicted sub-pocket is dominated by relatively weak van der Waals interactions (121). This observation with respect to the YKIMDATN (657-664) peptide, which lines the deepest end of the cyclohexylbenzyl sub-pocket, are consistent with the tighter binding of the cyclohexylbenzyl moiety of BP-1-102 compared to SF-1-066 as predicted by *in silico* docking (Fig. 14C). The only structural difference between the two inhibitors is the substituent at the sulfonamide end of the molecule, being a tosyl sulfonamide for SF-1-066 and a pentafluorobenzyl sulfonamide for BP-1-102. Despite this, in the peptide lining the relevant sub-pocket, ISKERERAIL (589-598), a significant but similar decrease in deuteration was observed, not reflective of any differential effect on the backbone amides in this region.

Other regions of the SH2 domain not immediately lining the surface of the predicted inhibitor-binding site also exhibited significant decreases in deuterium uptake upon inhibitor binding. Some of these segments interact directly with specific regions of the

binding pocket. For example, the peptide SKEGGV (614-619) is located in proximity to LRFSE (608-612) peptide that lines the salicylic acid moiety binding sub-pocket, with the backbone amide of the Ser 611 making a hydrogen bond with the backbone carbonyl of Gly618. Both inhibitors induce a significant decrease in deuterium uptake in the SKEGGV (614-619) peptide.

Overall, the higher-affinity inhibitor, BP-1-102, induced more decreases in deuterium uptake compared to SF-1-066 (Fig. 20C). This and other observations of significant decreases in deuterium uptake in the SH2 domain suggest that either (i) the inhibitors are able to bind to regions of the SH2 domain outside of the *in silico* predicted binding pocket, or (ii) the binding of the inhibitors to the predicted binding pocket results in an overall stabilization of and, possibly, the induction of additional secondary structure in a large portion of the SH2 domain. We tend to favour the latter possibility given the lack of clustered HDX decreases elsewhere in the molecule outside of the SH2 domain that would point to non-specific binding by the inhibitors to STAT3.

Our data suggest that the core of the STAT3 SH2 domain represents a highly dynamic network, potentially able to transmit local perturbations in dynamics to distal regions of the domain. Indeed, studies of dynamics of SH2 domains of other proteins reveal a general, global reduction or stabilization in dynamics in a large portion of the SH2 domain upon peptide ligand binding resulting in increased rigidity that propagates throughout the entire domain (59,126). Overall, the clustering of significant decreases in deuterium uptake in the SH2 domain of inhibitor-complexed STAT3 provides experimental evidence supporting the SH2 domain being the target site of the salicylic acid-based inhibitors, SF-1-066 and BP-1-102. This finding corroborates *in silico*

docking predictions, as well as other experimental evidence. In fluorescence polarization assays with STAT3 and a fluorescently labeled phosphotyrosine peptide (5-carboxyfluorescein-GpYLPQTV-NH2) that mimics the natural SH2 domain target substrate, both SF-1-066 and BP-1-102 inhibitors competed strongly with substrate binding with an IC50 of 20 μM and 4.1 μM, respectively (119,125).

Interestingly, both inhibitors induced a burst of dynamic changes, mainly manifesting as significant relative increases in deuterium uptake, outside of the SH2 domain of STAT3 (Fig. 20A and B). These allosteric changes, induced in the inhibitor-complexed structures, propagate into STAT3 domains and regions involved in DNA binding (β-barrel and connector domains) and nuclear localization of the protein (4-helix bundle and β-barrel domains) (124,127). Interestingly, the majority of allosteric changes mapped to (or near) regions important to the DNA binding activity of STAT3 (DNA binding domain, residues 406-514) (76). The backbone amide of Val432, for instance, is directly involved in DNA binding and Glu435 forms a hydrogen bond that is important for the maintaining the structural rigidity of one of the DNA binding loops (124). We observe a significant increase in deuterium uptake in the peptide IVTEEL (431-436) with both inhibitors. This suggests the possibility that the salicylic acid-based inhibitors SF-1-066 and BP-1-102 could also be acting via an allosteric mechanism to modulate DNA binding of STAT3 – a prediction that will need to be explored experimentally with the use of STAT3 mutants.

The vast majority of allosteric changes induced by inhibitor binding (Fig. 20A and B) mapped to regions predicted to have α-helical secondary structure (Fig. 15). Increases in HDX in α-helical regions are most likely to result from the loss or

remodelling of secondary structure affecting the hydrogen bonding network. STAT3 complexed with SF-1-066 exhibited more allosteric effects (Fig. 20C) compared to the BP-1-102 complex. Allosteric changes were not observed in any peptides derived from the MBP protein that was fused via a poly-asparagine (Asn) linker to the N-terminus of the STAT3 in our construct (data not shown). This confirms that changes induced by the binding of SF-1-066 and BP-1-102 inhibitors to STAT3 outside the SH2 domain are not a result of experimental error.

Allosteric modulation is an important mechanism of communication between distinct domains within the protein and exactly how the information is transmitted between domains is an area of active investigation (128). The ability of the SH2 domain to induce conformational changes in other domains in the same protein has been demonstrated for the C-terminal Src (Csk) kinase (129), a protein tyrosine kinase that phosphorylates other kinases of the Src family. In Csk, the binding of the SH2 domain target peptide, Csk-binding protein (Cbp), appears to induce conformational changes that are transmitted through the SH2 linker to the active site and other regions of the protein. Conversely, binding of Csk nucleotide substrates to the kinase domain was shown to impact HDX protection in other region of the protein, including the SH2 domain, depending on the nature of the nucleotide present (130). Our study adds to the work of others examining allosteric modulation by HDX MS (83,131,132), highlighting the vast utility of this structural technique in probing the evolution of allosteric changes in intact proteins under physiological conditions.

3.6 Conclusions

In summary, *in silico*-predicted interactions of SF-1-066 and BP-1-102 inhibitors with regions of the STAT3 SH2 domain were experimentally confirmed by analyzing changes in site-specific deuterium uptake upon STAT3 complexation with the inhibitors. Showing a large contiguous decrease in deuterium uptake around the putative SH2 domain-binding site, our data support a mechanism of inhibition driven by 'pacification' of the SH2 domain through complexation. This compliments prior biochemical evidence that points to disruption of STAT3 dimerization as the primary inhibitory mechanism.

Significant allosteric changes in deuterium uptake were also observed in other STAT3 domains. Our study highlights the incremental benefits of dynamic structure analysis to understanding protein-ligand interactions via the examination of conformational ensembles rather than static representations of the protein complex structures. The specific findings provide structure-activity insights that would facilitate the design of more potent next-generation dimerization inhibitors of STAT3, for instance by amplifying desirable allosteric effects. Our methodology could be extended to the study of other protein-drug complexes and paves a new avenue for a rapid, sensitive, and affordable analysis to support drug development efforts in medicinal chemistry.

3.7 TRESI-MS HDX Analysis of the STAT3 Complex with a New Tetrapodal Salicylic Acid-Based Inhibitor, BP-5-087

(This section was adapted from Eiring, A.M., Page, B.G., Kraft, I.L., Mason, C.C., Vellore, N.M., Resetca, D., Zabriskie, M.S., Zhang, T.Y., Khorashad, J.S., Engar, A.J., Reynolds, K.R., Anderson, D.J., Senina, A., Pomicter, A.D., Arpin, C.C., Ahmad, S., Heaton, W.L., Tantravahi, S., Moriggl, R., Wilson, D.J., Baron, R., O'Hare, T., Gunning, P.T., and Deininger, M.W. "Combined STAT3 and BCR-ABL1 Inhibition Induces Synthetic Lethality in Therapy-Resistant Chronic Myeloid Leukemia" submitted to Leukemia.)

Analogously to the studies described above, the interaction of STAT3 with a novel, tetrapodal STAT3 inhibitor, BP-5-087, was probed by TRESI-MS HDX. BP-5-087 is a derivative of SF-1-066, with the addition of an *ortho*-methyl benzyl and trifluoro-methyl functional groups (Fig. 21). To map the amino acid residues that are important for BP-5-087 activity, interactions of BP-5-087 with the STAT3 SH2 domain were experimentally confirmed by analyzing changes in site-specific deuterium uptake upon inhibitor binding. The structural transitions that occur in STAT3 upon its association with BP-5-087 were examined by graphing fold changes in deuterium exchange for each peptic peptide detected in STAT3 and the STAT3:BP-5-07 complex (Fig. 22). In three independent replicates, the data confirmed that the binding epitope for BP-5-087 is located within the STAT3 SH2 domain of the protein (Fig. 22). Fold changes in deuterium uptake were analyzed for 68 peptic peptides of STAT3 mapped onto the X-ray crystal structure of STAT3 (Fig. 22A). Significant decreases in deuterium uptake clustered almost exclusively to the STAT3 SH2 domain, indicating exclusion of solvent molecules or the formation of new backbone hydrogen bonds in this region (Fig. 22B). The most pronounced decreases in deuterium uptake were observed in peptic peptides that line the BP-5-087 salicylic acid-binding and trifluoro-methyl-benzene-binding sub-pockets of

the SH2 domain. However, the HDX experiment sequence coverage did not extend to peptides lining the BP-5-087 cyclohexylbenzyl-binding sub-pocket. A number of significant decreases in deuterium uptake were observed in SH2 domain regions proximal to the predicted BP-5-087 sub-pockets, which may be a result of propagating, allosteric changes in STAT3 dynamics induced by drug binding. These data provide additional support for the putative binding site of salicylic acid-based STAT3 inhibitors of dimerization being located in the SH2 domain of the protein, and highlight the robust and reproducible nature of HDX experiments in application to binding-epitope mapping in protein-ligand interactions.

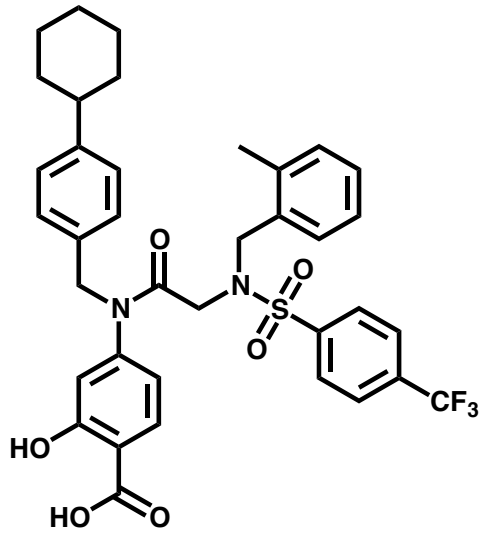

Fig. 21 BP-5-087 Chemical Structure.

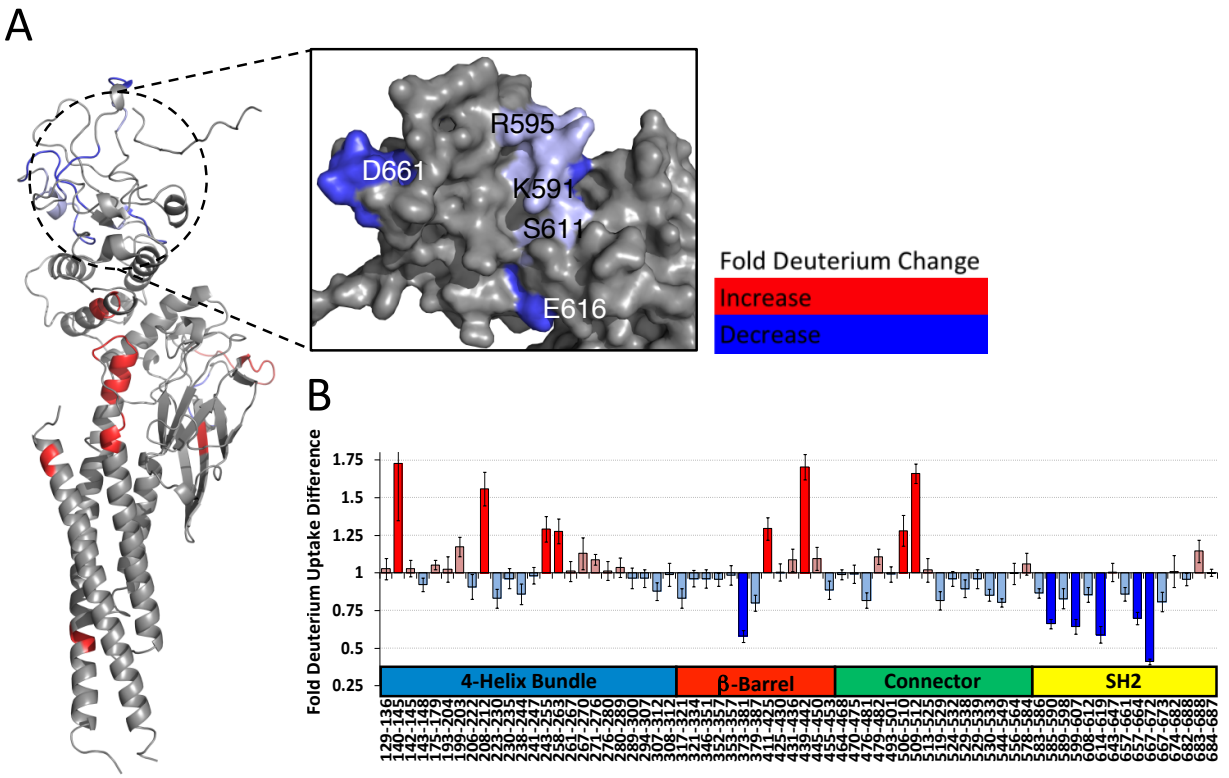

Fig. 22 Fold Changes in Deuterium Uptake of STAT3 and STAT3:BP-5-087 Complex. A) Fold changes in deuterium uptake observed by site-specific TRESI-MS/HDX following complexation of STAT3 with BP-5-087 (1:7 molar ratio) color-coded onto the STAT3 X-ray crystal structure (PDB ID: 1BG1). Select surface-exposed residues mapping to peptic peptides that experience a significant decrease in HDX are indicated on the enlarged region that depicts the SH2 domain on the surface of the predicted BP-5-087 binding site. B) Relative changes in deuterium uptake observed by TRESI-MS/HDX following complexation of STAT3 protein with BP-5-087 mapped onto the primary sequence of STAT3 and grouped by domain. Changes considered significant (>25%) are highlighted by darker colors. Site-specific TRESI-MS/HDX data from three independent repeats. Error bars represent SEM.

Chapter 4

4 Conclusions and Future Directions

4.1 Conclusions

The body of work summarized in this thesis extends the application of site-specific TRESI-MS HDX implemented on a microfluidic device to the study of the dynamics of protein-ligand interactions and binding epitope mapping on native protein complexes in solution. The implementation of TRESI-MS HDX based on a rapid-mixer on the microfluidic device, described in this work, enables the entire HDX “bottom-up” workflow to be carried out continuously with online coupling directly to the ESI-MS ionization source. The introduction to this thesis (Chapter 1) reviews the construction and operation of the HDX microfluidic device, and its existing applications in the investigation of dynamics of protein unfolding, enzyme catalysis, allosteric regulation in enzyme turnover, and characterization of weakly structured regions. In Chapter 2, the HDX microfluidic device was utilized to map and characterize the GSH ligand-binding site of GST. In the context of the predominantly “lock-and-key” type binding in this model, comparative HDX analyses of free GST and GST complexed to GSH readily and clearly revealed the GSH binding region, supporting the totality of X-ray crystallography data on this protein system. Two of the peptic peptides of GST are predicted to make new backbone hydrogen bonds with GSH upon its binding to the protein, and were readily visible in HDX experiments, manifesting in pronounced decreases in deuterium uptake that imply the exclusion of solvent molecules and stabilization of the binding site. In Chapter 3, the ligand-binding site of a much larger protein, STAT3 (~ 66 kDa), was mapped by HDX for a number of STAT3-inhibitor complexes. Data generated from

these HDX experiments supported the *in silico* predictions localizing the binding site of the novel salicylic acid-based inhibitors, SF-1-066, BP-1-102, and BP-5-087, to the SH2 domain of STAT3. TRESI-MS HDX successfully characterized the dynamics of inhibitor binding to STAT3 and revealed a series of allosteric changes propagating form the SH2 domain to other STAT3 domains important for this protein's function. The HDX data form STAT3 support a more complex, "induced-fit" type ligand binding, with major and minors structural reorganization in the protein. This study highlights the general utility of HDX in medicinal chemistry for facilitating lead screening and SAR studies.

The types of applications of microfluidic device-implemented TRESI-MS HDX, detailed in this thesis, highlight the universal applicability and versatility of this technique to probing the sub-second timescale dynamics of protein-ligand interactions. Compared to the previous implementations of HDX in this context, the microfluidic device-based technique that permits the integration of the entire HDX workflow, labelling, quenching and digestion, for continuous-mode operation is highly accurate and reproducible. HDX MS experiments are seeing a steep increase in popularity in applications in both structural biology research and industry, for quality assurance of therapeutic biologicals and biosimilars, and drug development. In the study of protein-ligand interactions in particular, HDX MS experiments are very attractive owing to their favorable speed of implementation and universal adaptability to different model systems, compared to other structural biology techniques.

4.2 Future Directions

Time resolved HDX MS is a highly versatile and universally applicable technique. In this thesis, the application of TRESI-MS HDX for site-specific analysis of protein dynamics to the interrogation of protein ligand interactions was comprehensively described. Given the increasing interest in understanding complex protein-protein interactions in molecular and structural biology and proteomics research, the extension of site-specific TRESI-MS HDX implementation to the interrogation of protein-protein interaction dynamics is highly desired and imminent. The current work lays the foundation for protein-protein interaction studies by TRESI-MS HDX, and is a challenge that scales linearly in difficulty. The major hurdle in extending this technique as described to the study of complexes consisting of two or more distinct proteins lies in the ability to accurately identify the correct peptic peptides, once the MS spectra increases in complexity, crowded by the presence of peptic peptides derived form multiple species. An additional dimension of peptide separation to decrease spectrum complexity could be provided by integration with IMS. Furthermore, the microfluidic device can be integrated online to HPLC, which would greatly enhance peptide separation, but has been shown to significantly increase in back-exchange of the labile deuterated backbone amides.

Another clear advantage of HDX MS implemented on a microfluidic device lies in the ability to utilize it for high-throughput screening (HTS) applications. Compared to the current experimental applications of other structural biology techniques, such as NMR, where HTS is difficult to implement, the microfluidic set-up of TRESI-MS HDX enables high-throughput and multiplexing. The ability of HDX to simultaneously probe changes

in protein dynamics globally could be utilized in the study and further development of molecular chaperons, which has applications in a multitude of disease indications where protein misfolding causes pathology, such as lysosomal storage disorders and CNS disorders and diseases. TRESI-MS HDX can be a great tool for examining changes in the conformational ensembles of the target protein as it interacts with a chaperon, providing an additional level of structural resolution not readily available with other biophysical and bioanalytical techniques currently utilized for such studies. Improvements to the time-resolution of HDX will further facilitate the detection of molecular chaperons that induce very subtle effects in the target proteins.

In summary, the study of protein-ligand and protein-protein interactions by HDX is a new and vastly unexplored paradigm. Advances in the development of techniques, instrumentation, and computational tools for streamlined HDX analysis will fuel an increased interest in the application of HDX to expand on the enormous amount of knowledge and structural data derived by X-ray crystallography and NMR with the protein dynamics-based interpretation of biological interactions, mechanisms, and function.

References

1. Ringe, D., and Petsko, G. A. (1986) Study of protein dynamics by X-ray diffraction. *Methods in enzymology* **131**, 389-433

2. Vallurupalli, P., Bouvignies, G., and Kay, L. E. (2011) Increasing the exchange time-scale that can be probed by CPMG relaxation dispersion NMR. *The journal of physical chemistry. B* **115**, 14891-14900

3. Westenhoff, S., Nazarenko, E., Malmerberg, E., Davidsson, J., Katona, G., and Neutze, R. (2010) Time-resolved structural studies of protein reaction dynamics: a smorgasbord of X-ray approaches. *Acta crystallographica. Section A, Foundations of crystallography* **66**, 207-219

4. Lindorff-Larsen, K., Best, R. B., Depristo, M. A., Dobson, C. M., and Vendruscolo, M. (2005) Simultaneous determination of protein structure and dynamics. *Nature* **433**, 128-132

5. Chen, E., Goldbeck, R. A., and Kliger, D. S. (2009) Probing early events in ferrous cytochrome c folding with time-resolved natural and magnetic circular dichroism spectroscopies. *Current protein & peptide science* **10**, 464-475

6. Lendrihas, T., Zhang, J., Hunter, G. A., and Ferreira, G. C. (2009) Arg-85 and Thr-430 in murine 5-aminolevulinate synthase coordinate acyl-CoA-binding and contribute to substrate specificity. *Protein science : a publication of the Protein Society* **18**, 1847-1859

7. Kolygo, K., Ranjan, N., Kress, W., Striebel, F., Hollenstein, K., Neelsen, K., Steiner, M., Summer, H., and Weber-Ban, E. (2009) Studying chaperone-proteases using a real-time approach based on FRET. *Journal of structural biology* **168**, 267-277

8. Udgaonkar, J. B., and Baldwin, R. L. (1988) NMR evidence for an early framework intermediate on the folding pathway of ribonuclease A. *Nature* **335**, 694-699

9. Schlepckow, K., Wirmer, J., Bachmann, A., Kiefhaber, T., and Schwalbe, H. (2008) Conserved folding pathways of alpha-lactalbumin and lysozyme revealed by kinetic CD, fluorescence, NMR, and interrupted refolding experiments. *Journal of molecular biology* **378**, 686-698

10. Smith, L. J. (2004) Computational methods for generating models of denatured and partially folded proteins. *Methods* **34**, 144-150

11. Bowman, G. R., Beauchamp, K. A., Boxer, G., and Pande, V. S. (2009) Progress and challenges in the automated construction of Markov state models for full protein systems. *The Journal of chemical physics* **131**, 124101

12. Li, Y. (2006) Numerical solutions of a master equation for protein folding kinetics. *International journal of bioinformatics research and applications* **2**, 420-429

13. Greenfield, N. J. (1999) Biomacromolecular Applications of Circular Dichroism and ORD. in *Encyclopedia of Spectroscopy and Spectrometry* (Lindon, J. C. ed.), Elsevier, Oxford. pp 117-130

14. Greenfield, N. J. (2004) Circular dichroism analysis for protein-protein interactions. *Methods in molecular biology* **261**, 55-78

15. Bienert, R., Zimmermann, B., Rombach-Riegraf, V., and Graber, P. (2011) Time-dependent FRET with single enzymes: domain motions and catalysis in H(+)-ATP synthases. *Chemphyschem : a European journal of chemical physics and physical chemistry* **12**, 510-517

16. Rindermann, J. J., Akhtman, Y., Richardson, J., Brown, T., and Lagoudakis, P. G. (2011) Gauging the flexibility of fluorescent markers for the interpretation of fluorescence resonance energy transfer. *Journal of the American Chemical Society* **133**, 279-285

17. Kaltashov, I. A., and Eyles, S. J. (2012) *Mass spectrometry in structural biology and biophysics : architecture, dynamics, and interaction of biomolecules*, 2nd ed., Wiley, Hoboken, N.J.

18. Yoder, C. H., and Schaeffer, C. D. (1987) *Introduction to multinuclear NMR : theory and application*, Benjamin/Cummings Pub. Co., Menlo Park, Calif.

19. Montelione, G. T., Zheng, D., Huang, Y. J., Gunsalus, K. C., and Szyperski, T. (2000) Protein NMR spectroscopy in structural genomics. *Nature structural biology* **7 Suppl**, 982-985

20. Buck, J., Furtig, B., Noeske, J., Wohnert, J., and Schwalbe, H. (2007) Time-resolved NMR methods resolving ligand-induced RNA folding at atomic resolution. *Proceedings of the National Academy of Sciences of the United States of America* **104**, 15699-15704

21. Boehr, D. D., Dyson, H. J., and Wright, P. E. (2006) An NMR perspective on enzyme dynamics. *Chemical reviews* **106**, 3055-3079

22. Jensen, K. S., Winther, J. R., and Teilum, K. (2011) Millisecond dynamics in glutaredoxin during catalytic turnover is dependent on substrate binding and absent in the resting states. *Journal of the American Chemical Society* **133**, 3034-3042

23. Korzhnev, D. M., Neudecker, P., Mittermaier, A., Orekhov, V. Y., and Kay, L. E. (2005) Multiple-site exchange in proteins studied with a suite of six NMR relaxation dispersion experiments: an application to the folding of a Fyn SH3 domain mutant. *Journal of the American Chemical Society* **127**, 15602-15611

24. Chowdhury, S. K., Katta, V., and Chait, B. T. (1990) Probing conformational changes in proteins by mass spectrometry. *Journal of the American Chemical Society* **112**, 9012-9013

25. Koeniger, S. L., Merenbloom, S. I., Valentine, S. J., Jarrold, M. F., Udseth, H. R., Smith, R. D., and Clemmer, D. E. (2006) An IMS-IMS analogue of MS-MS. *Analytical chemistry* **78**, 4161-4174

26. Clemmer, D. E., and Jarrold, M. F. (1997) Ion Mobility Measurements and their Applications to Clusters and Biomolecules. *Journal of Mass Spectrometry* **32**, 577-592

27. Pantazatos, D., Kim, J. S., Klock, H. E., Stevens, R. C., Wilson, I. A., Lesley, S. A., and Woods, V. L., Jr. (2004) Rapid refinement of crystallographic protein construct definition employing enhanced hydrogen/deuterium exchange MS. *Proceedings of the National Academy of Sciences of the United States of America* **101**, 751-756

28. Wilson, D. J., and Konermann, L. (2003) A capillary mixer with adjustable reaction chamber volume for millisecond time-resolved studies by electrospray mass spectrometry. *Analytical chemistry* **75**, 6408-6414

29. Liuni, P., Rob, T., and Wilson, D. J. (2010) A microfluidic reactor for rapid, low-pressure proteolysis with on-chip electrospray ionization. *Rapid communications in mass spectrometry : RCM* **24**, 315-320

30. Rob, T., and Wilson, D. J. (2009) A versatile microfluidic chip for millisecond time-scale kinetic studies by electrospray mass spectrometry. *Journal of the American Society for Mass Spectrometry* **20**, 124-130

31. Rob, T., and Wilson, D. J. (2012) Time-resolved mass spectrometry for monitoring millisecond time-scale solution-phase processes. *European journal of mass spectrometry* **18**, 205-214

32. Franck, J., Longuespee, R., Wisztorski, M., Van Remoortere, A., Van Zeijl, R., Deelder, A., Salzet, M., McDonnell, L., and Fournier, I. (2010) MALDI mass spectrometry imaging of proteins exceeding 30,000 daltons. *Medical science monitor : international medical journal of experimental and clinical research* **16**, BR293-299

33. Zhou, M., Morgner, N., Barrera, N. P., Politis, A., Isaacson, S. C., Matak-Vinkovic, D., Murata, T., Bernal, R. A., Stock, D., and Robinson, C. V. (2011) Mass spectrometry of intact V-type ATPases reveals bound lipids and the effects of nucleotide binding. *Science* **334**, 380-385

34. Simmons, D. A., Wilson, D. J., Lajoie, G. A., Doherty-Kirby, A., and Konermann, L. (2004) Subunit disassembly and unfolding kinetics of hemoglobin studied by time-resolved electrospray mass spectrometry. *Biochemistry* **43**, 14792-14801

35. Rob, T., Liuni, P., Gill, P. K., Zhu, S., Balachandran, N., Berti, P. J., and Wilson, D. J. (2012) Measuring dynamics in weakly structured regions of proteins using microfluidics-enabled subsecond H/D exchange mass spectrometry. *Analytical chemistry* **84**, 3771-3779

36. Pan, J., Han, J., Borchers, C. H., and Konermann, L. (2009) Hydrogen/deuterium exchange mass spectrometry with top-down electron capture dissociation for characterizing structural transitions of a 17 kDa protein. *Journal of the American Chemical Society* **131**, 12801-12808

37. Katta, V., Chait, B. T., and Carr, S. (1991) Conformational changes in proteins probed by hydrogen-exchange electrospray-ionization mass spectrometry. *Rapid Communications in Mass Spectrometry* **5**, 214-217

38. Engen, J. R. (2009) Analysis of protein conformation and dynamics by hydrogen/deuterium exchange MS. *Analytical chemistry* **81**, 7870-7875

39. Campbell, S., Rodgers, M. T., Marzluff, E. M., and Beauchamp, J. L. (1995) Deuterium Exchange Reactions as a Probe of Biomolecule Structure. Fundamental Studies of Gas Phase H/D Exchange Reactions of Protonated Glycine Oligomers with D2O, CD3OD, CD3CO2D, and ND3. *Journal of the American Chemical Society* **117**, 12840-12854

40. Eigen, M. (1964) Proton Transfer, Acid-Base Catalysis, and Enzymatic Hydrolysis. Part I: ELEMENTARY PROCESSES. *Angewandte Chemie International Edition in English* **3**, 1-19

41. Englander, S. W., Downer, N. W., and Teitelbaum, H. (1972) Hydrogen exchange. *Annual review of biochemistry* **41**, 903-924

42. Englander, S. W., Sosnick, T. R., Englander, J. J., and Mayne, L. (1996) Mechanisms and uses of hydrogen exchange. *Current opinion in structural biology* **6**, 18-23

43. Berger, A., Loewenstein, A., and Meiboom, S. (1959) Nuclear Magnetic Resonance Study of the Protolysis and Ionization of N-Methylacetamide1. *Journal of the American Chemical Society* **81**, 62-67

44. Berger, A., and Linderstrom-Lang, K. (1957) Deuterium exchange of poly-DL-alanine in aqueous solution. *Archives of biochemistry and biophysics* **69**, 106-118

45. Bai, Y., Milne, J. S., Mayne, L., and Englander, S. W. (1993) Primary structure effects on peptide group hydrogen exchange. *Proteins* **17**, 75-86

46. Woodward, C. K., and Hilton, B. D. (1980) Hydrogen isotope exchange kinetics of single protons in bovine pancreatic trypsin inhibitor. *Biophysical journal* **32**, 561-575

47. Gregory, R. B., Crabo, L., Percy, A. J., and Rosenberg, A. (1983) Water catalysis of peptide hydrogen isotope exchange. *Biochemistry* **22**, 910-917

48. Dempsey, C. E. (2001) Hydrogen exchange in peptides and proteins using NMR spectroscopy. *Progress in Nuclear Magnetic Resonance Spectroscopy* **39**, 135-170

49. Englander, S. W., and Poulsen, A. (1969) Hydrogen-tritium exchange of the random chain polypeptide. *Biopolymers* **7**, 379-393

50. Leichtling, B. H., and Klotz, I. M. (1966) Catalysis of Hydrogen-Deuterium Exchange in Polypeptides*. *Biochemistry* **5**, 4026-4037

51. Maier, C. S., and Deinzer, M. L. (2005) Protein conformations, interactions, and H/D exchange. *Methods in enzymology* **402**, 312-360

52. Englander, J. J., Rogero, J. R., and Englander, S. W. (1985) Protein hydrogen exchange studied by the fragment separation method. *Analytical biochemistry* **147**, 234-244

53. Woodward, C., Simon, I., and Tuchsen, E. (1982) Hydrogen exchange and the dynamic structure of proteins. *Molecular and cellular biochemistry* **48**, 135-160

54. Li, R., and Woodward, C. (1999) The hydrogen exchange core and protein folding. *Protein science : a publication of the Protein Society* **8**, 1571-1590

55. Tuchsen, E., and Woodward, C. (1985) Mechanism of surface peptide proton exchange in bovine pancreatic trypsin inhibitor. Salt effects and O-protonation. *Journal of molecular biology* **185**, 421-430

56. Tuchsen, E., and Woodward, C. (1985) Hydrogen kinetics of peptide amide protons at the bovine pancreatic trypsin inhibitor protein-solvent interface. *Journal of molecular biology* **185**, 405-419

57. Hvidt, A., and Nielsen, S. O. (1966) Hydrogen exchange in proteins. *Advances in protein chemistry* **21**, 287-386

58. Miller, D. W., and Dill, K. A. (1995) A statistical mechanical model for hydrogen exchange in globular proteins. *Protein science : a publication of the Protein Society* **4**, 1860-1873

59. Engen, J. R., Gmeiner, W. H., Smithgall, T. E., and Smith, D. L. (1999) Hydrogen exchange shows peptide binding stabilizes motions in Hck SH2. *Biochemistry* **38**, 8926-8935

60. Wilson, D. J., and Konermann, L. (2004) Mechanistic studies on enzymatic reactions by electrospray ionization MS using a capillary mixer with adjustable reaction chamber volume for time-resolved measurements. *Analytical chemistry* **76**, 2537-2543

61. Sterling, H. J., and Williams, E. R. (2010) Real-time hydrogen/deuterium exchange kinetics via supercharged electrospray ionization tandem mass spectrometry. *Analytical chemistry* **82**, 9050-9057

62. Alonso, A., Zaidi, T., Novak, M., Grundke-Iqbal, I., and Iqbal, K. (2001) Hyperphosphorylation induces self-assembly of tau into tangles of paired helical filaments/straight filaments. *Proceedings of the National Academy of Sciences of the United States of America* **98**, 6923-6928

63. Liuni, P., Jeganathan, A., and Wilson, D. J. (2012) Conformer selection and intensified dynamics during catalytic turnover in chymotrypsin. *Angewandte Chemie* **51**, 9666-9669

64. Konermann, L., Pan, J., and Wilson, D. J. (2006) Protein folding mechanisms studied by time-resolved electrospray mass spectrometry. *BioTechniques* **40**, 135, 137, 139 passim

65. Roder, H., Elove, G. A., and Englander, S. W. (1988) Structural characterization of folding intermediates in cytochrome c by H-exchange labelling and proton NMR. *Nature* **335**, 700-704

66. Bhuyan, A. K., and Udgaonkar, J. B. (1998) Stopped-flow NMR measurement of hydrogen exchange rates in reduced horse cytochrome c under strongly destabilizing conditions. *Proteins* **32**, 241-247

67. Korzhnev, D. M., Salvatella, X., Vendruscolo, M., Di Nardo, A. A., Davidson, A. R., Dobson, C. M., and Kay, L. E. (2004) Low-populated folding intermediates of Fyn SH3 characterized by relaxation dispersion NMR. *Nature* **430**, 586-590

68. Paiva, A. A., Tilton, R. F., Jr., Crooks, G. P., Huang, L. Q., and Anderson, K. S. (1997) Detection and identification of transient enzyme intermediates using rapid mixing, pulsed-flow electrospray mass spectrometry. *Biochemistry* **36**, 15472-15476

69. Gross, J. W., Hegeman, A. D., Vestling, M. M., and Frey, P. A. (2000) Characterization of enzymatic processes by rapid mix-quench mass spectrometry: the case of dTDP-glucose 4,6-dehydratase. *Biochemistry* **39**, 13633-13640

70. Kolakowski, B. M., Simmons, D. A., and Konermann, L. (2000) Stopped-flow electrospray ionization mass spectrometry: a new method for studying chemical reaction kinetics in solution. *Rapid communications in mass spectrometry : RCM* **14**, 772-776

71. Rojsajjakul, T., Wintrode, P., Vadrevu, R., Robert Matthews, C., and Smith, D. L. (2004) Multi-state unfolding of the alpha subunit of tryptophan synthase, a TIM barrel protein: insights into the secondary structure of the stable equilibrium intermediates by hydrogen exchange mass spectrometry. *Journal of molecular biology* **341**, 241-253

72. Konermann, L., Pan, Y., and Stocks, B. B. (2011) Protein folding mechanisms studied by pulsed oxidative labeling and mass spectrometry. *Current opinion in structural biology* **21**, 634-640

73. Konermann, L., Stocks, B. B., Pan, Y., and Tong, X. (2010) Mass spectrometry combined with oxidative labeling for exploring protein structure and folding. *Mass spectrometry reviews* **29**, 651-667

74. Pan, J., Wilson, D. J., and Konermann, L. (2005) Pulsed hydrogen exchange and electrospray charge-state distribution as complementary probes of protein structure in kinetic experiments: implications for ubiquitin folding. *Biochemistry* **44**, 8627-8633

75. Keppel, T. R., Howard, B. A., and Weis, D. D. (2011) Mapping unstructured regions and synergistic folding in intrinsically disordered proteins with amide H/D exchange mass spectrometry. *Biochemistry* **50**, 8722-8732

76. Horvath, C. M., Wen, Z., and Darnell, J. E., Jr. (1995) A STAT protein domain that determines DNA sequence recognition suggests a novel DNA-binding domain. *Genes & development* **9**, 984-994

77. Banci, L., Bertini, I., Gray, H. B., Luchinat, C., Reddig, T., Rosato, A., and Turano, P. (1997) Solution structure of oxidized horse heart cytochrome c. *Biochemistry* **36**, 9867-9877

78. Li, S., Tsalkova, T., White, M. A., Mei, F. C., Liu, T., Wang, D., Woods, V. L., Jr., and Cheng, X. (2011) Mechanism of intracellular cAMP sensor Epac2 activation: cAMP-induced conformational changes identified by amide hydrogen/deuterium exchange mass spectrometry (DXMS). *The Journal of biological chemistry* **286**, 17889-17897

79. Sowole, M. A., Alexopoulos, J. A., Cheng, Y. Q., Ortega, J., and Konermann, L. (2013) Activation of ClpP protease by ADEP antibiotics: insights from hydrogen exchange mass spectrometry. *Journal of molecular biology* **425**, 4508-4519

80. Xiao, H., Verdier-Pinard, P., Fernandez-Fuentes, N., Burd, B., Angeletti, R., Fiser, A., Horwitz, S. B., and Orr, G. A. (2006) Insights into the mechanism of microtubule stabilization by Taxol. *Proceedings of the National Academy of Sciences of the United States of America* **103**, 10166-10173

81. Dai, S. Y., Burris, T. P., Dodge, J. A., Montrose-Rafizadeh, C., Wang, Y., Pascal, B. D., Chalmers, M. J., and Griffin, P. R. (2009) Unique ligand binding patterns between estrogen receptor alpha and beta revealed by hydrogen-deuterium exchange. *Biochemistry* **48**, 9668-9676

82. Bennett, M. J., Barakat, K., Huzil, J. T., Tuszynski, J., and Schriemer, D. C. (2010) Discovery and characterization of the laulimalide-microtubule binding mode by mass shift perturbation mapping. *Chemistry & biology* **17**, 725-734

83. Zhang, J., Adrian, F. J., Jahnke, W., Cowan-Jacob, S. W., Li, A. G., Iacob, R. E., Sim, T., Powers, J., Dierks, C., Sun, F., Guo, G. R., Ding, Q., Okram, B., Choi, Y., Wojciechowski, A., Deng, X., Liu, G., Fendrich, G., Strauss, A., Vajpai, N., Grzesiek, S., Tuntland, T., Liu, Y., Bursulaya, B., Azam, M., Manley, P. W., Engen, J. R., Daley, G. Q., Warmuth, M., and Gray, N. S. (2010) Targeting Bcr-Abl by combining allosteric with ATP-binding-site inhibitors. *Nature* **463**, 501-506

84. Pan, J., Rintala-Dempsey, A. C., Li, Y., Shaw, G. S., and Konermann, L. (2006) Folding kinetics of the S100A11 protein dimer studied by time-resolved electrospray mass spectrometry and pulsed hydrogen-deuterium exchange. *Biochemistry* **45**, 3005-3013

85. Konermann, L., Pan, J., and Liu, Y. H. (2011) Hydrogen exchange mass spectrometry for studying protein structure and dynamics. *Chemical Society reviews* **40**, 1224-1234

86. Jaswal, S. S. (2013) Biological insights from hydrogen exchange mass spectrometry. *Biochimica et biophysica acta* **1834**, 1188-1201

87. Resetca, D., and Wilson, D. J. (2013) Characterizing rapid, activity-linked conformational transitions in proteins via sub-second hydrogen deuterium exchange mass spectrometry. *The FEBS journal* **280**, 5616-5625

88. Rob, T., Gill, P. K., Golemi-Kotra, D., and Wilson, D. J. (2013) An electrospray ms-coupled microfluidic device for sub-second hydrogen/deuterium exchange pulse-labelling reveals allosteric effects in enzyme inhibition. *Lab on a chip* **13**, 2528-2532

89. Sljoka, A., and Wilson, D. (2013) Probing protein ensemble rigidity and hydrogen-deuterium exchange. *Physical biology* **10**, 056013

90. Zhu, M. M., Rempel, D. L., and Gross, M. L. (2004) Modeling data from titration, amide H/D exchange, and mass spectrometry to obtain protein-ligand binding constants. *Journal of the American Society for Mass Spectrometry* **15**, 388-397

91. Abzalimov, R. R., Kaplan, D. A., Easterling, M. L., and Kaltashov, I. A. (2009) Protein conformations can be probed in top-down HDX MS experiments utilizing electron transfer dissociation of protein ions without hydrogen scrambling. *Journal of the American Society for Mass Spectrometry* **20**, 1514-1517

92. Abzalimov, R. R., Bobst, C. E., and Kaltashov, I. A. (2013) A new approach to measuring protein backbone protection with high spatial resolution using H/D exchange and electron capture dissociation. *Analytical chemistry* **85**, 9173-9180

93. Zhang, H. M., Kazazic, S., Schaub, T. M., Tipton, J. D., Emmett, M. R., and Marshall, A. G. (2008) Enhanced digestion efficiency, peptide ionization efficiency, and sequence resolution for protein hydrogen/deuterium exchange monitored by Fourier transform ion cyclotron resonance mass spectrometry. *Analytical chemistry* **80**, 9034-9041

94. Landgraf, R. R., Goswami, D., Rajamohan, F., Harris, M. S., Calabrese, M. F., Hoth, L. R., Magyar, R., Pascal, B. D., Chalmers, M. J., Busby, S. A., Kurumbail, R. G., and Griffin, P. R. (2013) Activation of AMP-activated protein kinase revealed by hydrogen/deuterium exchange mass spectrometry. *Structure* **21**, 1942-1953

95. Karageorgos, I., Wales, T. E., Janero, D. R., Zvonok, N., Vemuri, V. K., Engen, J. R., and Makriyannis, A. (2013) Active-site inhibitors modulate the dynamic properties of human monoacylglycerol lipase: a hydrogen exchange mass spectrometry study. *Biochemistry* **52**, 5016-5026

96. McTigue, M. A., Williams, D. R., and Tainer, J. A. (1995) Crystal structures of a schistosomal drug and vaccine target: glutathione S-transferase from Schistosoma japonica and its complex with the leading antischistosomal drug praziquantel. *Journal of molecular biology* **246**, 21-27

97. Lim, K., Ho, J. X., Keeling, K., Gilliland, G. L., Ji, X., Ruker, F., and Carter, D. C. (1994) Three-dimensional structure of Schistosoma japonicum glutathione S-transferase fused with a six-amino acid conserved neutralizing epitope of gp41 from HIV. *Protein science : a publication of the Protein Society* **3**, 2233-2244

98. Andujar-Sanchez, M., Smith, A. W., Clemente-Jimenez, J. M., Rodriguez-Vico, F., Las Heras-Vazquez, F. J., Jara-Perez, V., and Camara-Artigas, A. (2005) Crystallographic and thermodynamic analysis of the binding of S-octylglutathione to the Tyr 7 to Phe mutant of glutathione S-transferase from Schistosoma japonicum. *Biochemistry* **44**, 1174-1183

99. Strohalm, M., Kavan, D., Novak, P., Volny, M., and Havlicek, V. (2010) mMass 3: a cross-platform software environment for precise analysis of mass spectrometric data. *Analytical chemistry* **82**, 4648-4651

100. Tessema, M., Simons, P. C., Cimino, D. F., Sanchez, L., Waller, A., Posner, R. G., Wandinger-Ness, A., Prossnitz, E. R., and Sklar, L. A. (2006) Glutathione-S-transferase-green fluorescent protein fusion protein reveals slow dissociation from high site density beads and measures free GSH. *Cytometry. Part A : the journal of the International Society for Analytical Cytology* **69**, 326-334

101. Konermann, L., Vahidi, S., and Sowole, M. A. (2014) Mass spectrometry methods for studying structure and dynamics of biological macromolecules. *Analytical chemistry* **86**, 213-232

102. Cardoso, R. M., Daniels, D. S., Bruns, C. M., and Tainer, J. A. (2003) Characterization of the electrophile binding site and substrate binding mode of the 26-kDa glutathione S-transferase from Schistosoma japonicum. *Proteins* **51**, 137-146

103. Shi, X. E., Wales, T. E., Elkin, C., Kawahata, N., Engen, J. R., and Annis, D. A. (2013) Hydrogen exchange-mass spectrometry measures stapled peptide

conformational dynamics and predicts pharmacokinetic properties. *Analytical chemistry* **85**, 11185-11188

104. Hernychova, L., Man, P., Verma, C., Nicholson, J., Sharma, C. A., Ruckova, E., Teo, J. Y., Ball, K., Vojtesek, B., and Hupp, T. R. (2013) Identification of a second Nutlin-3 responsive interaction site in the N-terminal domain of MDM2 using hydrogen/deuterium exchange mass spectrometry. *Proteomics* **13**, 2512-2525

105. Walters, B. T., Ricciuti, A., Mayne, L., and Englander, S. W. (2012) Minimizing back exchange in the hydrogen exchange-mass spectrometry experiment. *Journal of the American Society for Mass Spectrometry* **23**, 2132-2139

106. Wilkins, M. R., Lindskog, I., Gasteiger, E., Bairoch, A., Sanchez, J. C., Hochstrasser, D. F., and Appel, R. D. (1997) Detailed peptide characterization using PEPTIDEMASS--a World-Wide-Web-accessible tool. *Electrophoresis* **18**, 403-408

107. Kabsch, W., and Sander, C. (1983) Dictionary of protein secondary structure: pattern recognition of hydrogen-bonded and geometrical features. *Biopolymers* **22**, 2577-2637

108. Rey, M., Yang, M., Burns, K. M., Yu, Y., Lees-Miller, S. P., and Schriemer, D. C. (2013) Nepenthesin from monkey cups for hydrogen/deuterium exchange mass spectrometry. *Molecular & cellular proteomics : MCP* **12**, 464-472

109. Kaplan, W., Husler, P., Klump, H., Erhardt, J., Sluis-Cremer, N., and Dirr, H. (1997) Conformational stability of pGEX-expressed Schistosoma japonicum glutathione S-transferase: a detoxification enzyme and fusion-protein affinity tag. *Protein science : a publication of the Protein Society* **6**, 399-406

110. Hegazy, U. M., Mannervik, B., and Stenberg, G. (2004) Functional role of the lock and key motif at the subunit interface of glutathione transferase p1-1. *The Journal of biological chemistry* **279**, 9586-9596

111. Pacholarz, K. J., Garlish, R. A., Taylor, R. J., and Barran, P. E. (2012) Mass spectrometry based tools to investigate protein-ligand interactions for drug discovery. *Chemical Society reviews* **41**, 4335-4355

112. Yu, H., Pardoll, D., and Jove, R. (2009) STATs in cancer inflammation and immunity: a leading role for STAT3. *Nature reviews. Cancer* **9**, 798-809

113. Bromberg, J., and Darnell, J. E., Jr. (2000) The role of STATs in transcriptional control and their impact on cellular function. *Oncogene* **19**, 2468-2473

114. Haan, S., Hemmann, U., Hassiepen, U., Schaper, F., Schneider-Mergener, J., Wollmer, A., Heinrich, P. C., and Grotzinger, J. (1999) Characterization and binding specificity of the monomeric STAT3-SH2 domain. *The Journal of biological chemistry* **274**, 1342-1348

115. Ladbury, J. E., Lemmon, M. A., Zhou, M., Green, J., Botfield, M. C., and Schlessinger, J. (1995) Measurement of the binding of tyrosyl phosphopeptides to SH2 domains: a reappraisal. *Proceedings of the National Academy of Sciences of the United States of America* **92**, 3199-3203

116. Miklossy, G., Hilliard, T. S., and Turkson, J. (2013) Therapeutic modulators of STAT signalling for human diseases. *Nature reviews. Drug discovery* **12**, 611-629

117. Moran, M. F., Koch, C. A., Anderson, D., Ellis, C., England, L., Martin, G. S., and Pawson, T. (1990) Src homology region 2 domains direct protein-protein interactions in signal transduction. *Proceedings of the National Academy of Sciences of the United States of America* **87**, 8622-8626

118. Finerty, P. J., Jr., Mittermaier, A. K., Muhandiram, R., Kay, L. E., and Forman-Kay, J. D. (2005) NMR dynamics-derived insights into the binding properties of a peptide interacting with an SH2 domain. *Biochemistry* **44**, 694-703

119. Zhang, X., Yue, P., Page, B. D., Li, T., Zhao, W., Namanja, A. T., Paladino, D., Zhao, J., Chen, Y., Gunning, P. T., and Turkson, J. (2012) Orally bioavailable small-molecule inhibitor of transcription factor Stat3 regresses human breast and lung cancer xenografts. *Proceedings of the National Academy of Sciences of the United States of America* **109**, 9623-9628

120. Fletcher, S., Page, B. D., Zhang, X., Yue, P., Li, Z. H., Sharmeen, S., Singh, J., Zhao, W., Schimmer, A. D., Trudel, S., Turkson, J., and Gunning, P. T. (2011) Antagonism of the Stat3-Stat3 protein dimer with salicylic acid based small molecules. *ChemMedChem* **6**, 1459-1470

121. Page, B. D., Fletcher, S., Yue, P., Li, Z., Zhang, X., Sharmeen, S., Datti, A., Wrana, J. L., Trudel, S., Schimmer, A. D., Turkson, J., and Gunning, P. T. (2011) Identification of a non-phosphorylated, cell permeable, small molecule ligand for the Stat3 SH2 domain. *Bioorganic & medicinal chemistry letters* **21**, 5605-5609

122. Nkansah, E., Shah, R., Collie, G. W., Parkinson, G. N., Palmer, J., Rahman, K. M., Bui, T. T., Drake, A. F., Husby, J., Neidle, S., Zinzalla, G., Thurston, D. E., and Wilderspin, A. F. (2013) Observation of unphosphorylated STAT3 core protein binding to target dsDNA by PEMSA and X-ray crystallography. *FEBS letters* **587**, 833-839

123. Ren, Z., Mao, X., Mertens, C., Krishnaraj, R., Qin, J., Mandal, P. K., Romanowski, M. J., McMurray, J. S., and Chen, X. (2008) Crystal structure of unphosphorylated STAT3 core fragment. *Biochemical and biophysical research communications* **374**, 1-5

124. Becker, S., Groner, B., and Muller, C. W. (1998) Three-dimensional structure of the Stat3beta homodimer bound to DNA. *Nature* **394**, 145-151

125. Zhang, X., Yue, P., Fletcher, S., Zhao, W., Gunning, P. T., and Turkson, J. (2010) A novel small-molecule disrupts Stat3 SH2 domain-phosphotyrosine interactions and Stat3-dependent tumor processes. *Biochemical pharmacology* **79**, 1398-1409

126. Shoelson, S. E., Sivaraja, M., Williams, K. P., Hu, P., Schlessinger, J., and Weiss, M. A. (1993) Specific phosphopeptide binding regulates a conformational change in the PI 3-kinase SH2 domain associated with enzyme activation. *The EMBO journal* **12**, 795-802

127. Ma, J., Zhang, T., Novotny-Diermayr, V., Tan, A. L., and Cao, X. (2003) A novel sequence in the coiled-coil domain of Stat3 essential for its nuclear translocation. *The Journal of biological chemistry* **278**, 29252-29260

128. Ma, B., Tsai, C. J., Haliloglu, T., and Nussinov, R. (2011) Dynamic allostery: linkers are not merely flexible. *Structure* **19**, 907-917

129. Wong, L., Lieser, S. A., Miyashita, O., Miller, M., Tasken, K., Onuchic, J. N., Adams, J. A., Woods, V. L., Jr., and Jennings, P. A. (2005) Coupled motions in the SH2 and kinase domains of Csk control Src phosphorylation. *Journal of molecular biology* **351**, 131-143

130. Hamuro, Y., Wong, L., Shaffer, J., Kim, J. S., Stranz, D. D., Jennings, P. A., Woods, V. L., Jr., and Adams, J. A. (2002) Phosphorylation driven motions in the COOH-terminal Src kinase, CSK, revealed through enhanced hydrogen-deuterium exchange and mass spectrometry (DXMS). *Journal of molecular biology* **323**, 871-881

131. Iacob, R. E., Pene-Dumitrescu, T., Zhang, J., Gray, N. S., Smithgall, T. E., and Engen, J. R. (2009) Conformational disturbance in Abl kinase upon mutation and deregulation. *Proceedings of the National Academy of Sciences of the United States of America* **106**, 1386-1391

132. Panjarian, S., Iacob, R. E., Chen, S., Wales, T. E., Engen, J. R., and Smithgall, T. E. (2013) Enhanced SH3/linker interaction overcomes Abl kinase activation by gatekeeper and myristic acid binding pocket mutations and increases sensitivity to small molecule inhibitors. *The Journal of biological chemistry* **288**, 6116-6129